2021

March

No. 1

ISSN 1453-7303
ISSN-L 1453-7303

HIDRAULICA

HYDRAULICS-PNEUMATICS-TRIBOLOGY-ECOLOGY-SENSORICS-MECHATRONICS

CAD - CAE - CAM

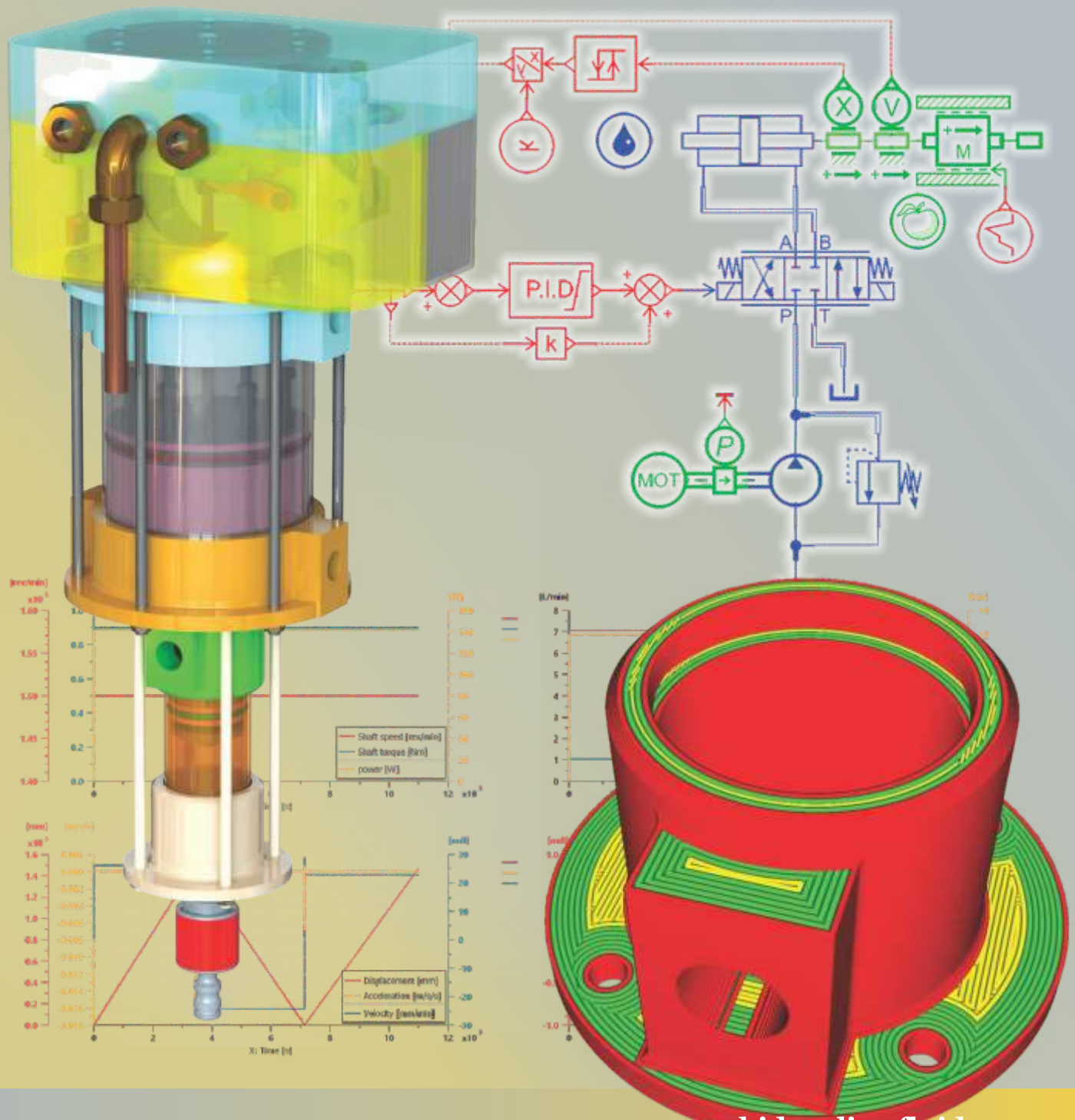

hidraulica.fluidas.ro

CONTENTS

EDITORIAL: Research without young people? 5 - 6
Ph.D. **Petrin DRUMEA**

- **Analysis of the Dynamic Behaviour and Energy Efficiency of an Oscillating Hydraulic Pressure Intensifier** 7 - 16
PhD Stud. Eng. **Alexandru-Polifron CHIRIȚĂ,** Ph.D. Eng. **Teodor Costinel POPESCU,** Eng. **Ioan BĂLAN,** Res. Assist. **Ana-Maria POPESCU,** Assist. Prof. **Fănel Dorel ȘCHEAUA**

- **Energy Loss Reduction in Hydraulic Installations of the Machine Tools Served by Constant Flow Pumps** 17 - 23
Prof. PhD Eng. **Anca BUCUREȘTEANU**, Assoc. Prof. PhD Eng. **Adrian MOTOMANCEA**, Assistant **Alina OVANISOF**

- **Fluid Hammer Phenomenon Aspects on Circular Ducts** 24 - 31
Assistant professor **Fănel Dorel ȘCHEAUA**

- **Choosing an Economical Solution for Water Aeration** 32 - 37
PhD Std. **Nicoleta Dorina ALBU**, Prof. Dr. Eng. **Nicolae BĂRAN**, Șl. Dr. Eng. **Mihaela CONSTANTIN**

- **Hot Water Recirculation in High Rise Buildings to Reduce Water Consumption** 38 - 43
Dipl. Eng. **Paul FRĂSIE**, Assoc. Prof. Dr. Eng. **Adriana TOKAR**

- **A New Type of Fine Bubble Generator Used to Water Aeration** 44 - 49
PhD Std. **Nicoleta Dorina ALBU**, Prof. Dr. Eng. **Nicolae BĂRAN**, Șl. Dr. Eng. **Mihaela CONSTANTIN**

- **Drying of Biomass in an Infrared Tunnel with Conveyor Belt** 50 - 56
PhD Stud. Eng. **Ioan PAVEL**, PhD Eng. **Gheorghe ȘOVĂIALĂ**, Dipl. Eng. **Alina Iolanda POPESCU**, Tech. **Kati PAVEL**, Dipl. Eng. **Dragoș PREDA**, Dipl. Eng. **Bogdan DURAN**

- **A Critical Review of Combustion Noise in Combustion Engines** 57 - 65
Dr. **Sunny NARAYAN**, Dr. **Aman GUPTA**

- **Upgrading a Digital Hydraulic Switching Valve to Become an Intelligent Hydraulic Equipment** 66 - 71
PhD. Stud. Eng. **Bogdan-Alexandru TUDOR**, PhD. Stud. Eng. **Mihai-Alexandru HRISTEA**, PhD. Eng. **Marian BLEJAN**, PhD. Stud. Eng. **Ștefan-Mihai ȘEFU**

- **A Critical Review of Piston Motion Noise in Combustion Engines** 72 - 79
Dr. **Sunny NARAYAN**, Dr. **Aman GUPTA**

Published by:
Hydraulics and Pneumatics Research Institute, Bucharest-Romania
Address: 14 Cuţitul de Argint, district 4, Bucharest, 040558, Romania
Phone: +40 21 336 39 91; Fax: +40 21 337 30 40; e-Mail: ihp@fluidas.ro; Web: www.ihp.ro
with support from:
National Professional Association of Hydraulics and Pneumatics in Romania - FLUIDAS
e-Mail: fluidas@fluidas.ro; Web: www.fluidas.ro

HIDRAULICA Magazine is indexed by international databases

ISSN 1453 – 7303; ISSN – L 1453 – 7303

EDITORIAL

Cercetare fără tineri?

Dr. Ing. Petrin DRUMEA
DIRECTOR PUBLICAȚIE

În zilele noastre, în Romania, se vorbește destul de des despre cercetare, mai ales de către persoane care nu înțeleg fenomenul și, de fapt, nu sunt interesate cu adevărat de acest subiect. Atât de mult sunt interesați că de la bugetul țării se asigură doar câteva salarii, restul ... să se descurce! Să nu ne mirăm că în curând nu vor mai exista institute de cercetare capabile să rezolve chiar și tematici simple. Vorbesc de institute pentru că, tradițional, ele se ocupau de cercetarea aplicativă.

Primul lucru important făcut după 1990 a fost să desființăm ideea de proiectare, cu tot ce implică ea, pentru a ne alinia la ... chiar nu știu la ce. Un alt lucru important făcut de coordonatori a fost să decidă că bazele cercetării, chiar și ale celei aplicative, se vor muta pe lângă universități, fără a le sprijini în preluarea acestei sarcini. Dacă la început lucrurile au mers cât de cât, astăzi constatăm că majoritatea centrelor de cercetare de pe lângă Univesități au personal în vârstă, cu puține abilități de cercetători, iar Institutele se bazează pe foștii specialiști, acum la vârsta pensiei.

E greu de convins un tânăr să devină cercetător când salariile sunt mici, eforturile sunt mari, iar munca este apreciată pe criterii stabilite de oameni care nu au lucrat efectiv în cercetare. Fără să fac o cercetare statistică, constat la o privire generală că numărul de profesori și conferențiari este cam egal cu cel al asistenților și că numărul cercetătorilor de gradele 1 și 2 este cam egal cu cel al asistenților cercetători și cercetătorilor simpli.

Dacă este așa, o fi în regulă? Oare nu ar trebui să urmăm exemplul țărilor într-o creștere rapidă, și nu pe al celor aflate într-un declin pe care nu îl recunosc? Fără aducerea de urgență a tinerilor în zonele de cercetare, indiferent în ce structuri se găsesc acestea, și fără lansarea unor programe naționale de cercetare concrete și cu finalizări utile economiei putem să ne luăm adio de la o dezvoltare rapidă și efectivă.

Poate se va conveni că inginerii trebuie să conceapă echipamente și tehnologii, că trebuie să fie inventatori și că trebuie să transfere o parte din rezultate în economie. Chiar nu putem reduce importanța articolelor teoretice de tip modern, adică cele care tratează probleme neesențiale cu formule la modă, definind aceasta activitate drept cercetare fundamentală?

Experiența ultimilor 10 ani îmi spune că atunci când tinerii sunt implicați în lucruri concrete devin activi și interesati de probleme. Este greu să fie convinși că doar studiile de sertar și articolele fără fond reprezintă cercetarea actuală, motiv pentru care părăsesc această activitate. Totuși, există speranțe atât timp cât încă mulți tineri se interesează de domeniu.

Multă sănătate!

EDITORIAL

Research without young people?

Ph.D.Eng. Petrin DRUMEA
MANAGING EDITOR

Nowadays, in Romania, there is quite often much talk about research, especially by people who do not understand the phenomenon and, in fact, are not really interested in this topic. They are so interested that only a few salaries are provided from the national budget, the rest ... let them provide for themselves! Let us not be surprised that soon there will be no more research institutes capable of solving even simple topics. I am saying 'institutes' because, traditionally, they were the ones to deal with applied research.

The first major thing done after 1990 was to dismantle the idea of design, with all that it entails, in order to align with ... I really don't know what with. Another important thing the coordinators did was to decide that the foundations of research, even applied research would be passed on to universities, without supporting them in taking on this task. While in the beginning things went more or less, nowadays we find that most of the research centers attached to the Universities have elderly staff with little research skills, and the research Institutes rely on former specialists, now at their retirement age.

It is difficult to convince a young person to become a researcher when the salaries are low, the efforts are high, and the work is assessed according to criteria established by people who have not actually worked in research. Without doing a statistical research, I find at a glance that the number of professors and associate professors is about equal to that of assistant professors, and the number of 1st and 2nd rank researchers is about equal to that of research assistants and simple researchers.

If so, is it okay? Shouldn't we follow the example of fast-growing countries, not of those in a decline that they don't recognize? Without urgently bringing young people to research areas, whatever structures they are located in, and without launching realistic national research programmes with useful endings for the economy we can say goodbye to rapid and effective development.

Maybe we will agree upon the fact that engineers need to design equipment and technology, that they need to be inventors, and that they need to transfer some of the results to the economy. Really, can't we reduce the importance of modern theoretical articles - that is, those that address non-essential issues with fashionable formulas, defining this activity as fundamental research?

Experience of the last 10 years tells me that when young people are involved in realistic things, they become active and interested in issues. It is hard for them to be convinced that only record studies and contentless papers are the current research, reason why they leave this activity. However, there is hope as long as yet many young people are interested in the field.

I wish you all good health.

Analysis of the Dynamic Behaviour and Energy Efficiency of an Oscillating Hydraulic Pressure Intensifier

PhD Stud. Eng. **Alexandru-Polifron CHIRIȚĂ*[1],** Ph.D. Eng. **Teodor Costinel POPESCU[1],** Eng. **Ioan BĂLAN[1],** Res. Assist. **Ana-Maria POPESCU[1],** Assist. Prof. **Fănel Dorel ȘCHEAUA[2]**

[1] Hydraulics and Pneumatics Research Institute INOE 2000-IHP, Bucharest, Romania

[2] "Dunărea de Jos" University of Galați, MECMET Research Center

* chirita.ihp@fluidas.ro

Abstract: *This paper presents modeling and numerical simulation of a generic single action oscillating pistons hydraulic pressure intensifier (SAOHPI), the operation mode, the analysis of the dynamic behavior of its parameters as well as the energy efficiency of a high-pressure hydraulic system comprising such an intensifier.*

Keywords: *OHPI, 2000 bar, energy efficiency, dynamic behavior, analysis, numerical simulation*

1. Introduction

There are two ways of obtaining high pressure in hydraulic systems: by using of high-pressure hydraulic pumps or by means of hydraulic pressure intensifiers. The chosen method determines the construction of a hydraulic system. When a high-pressure pump is used, all hydraulic components in the pressure line (e.g., hoses, valves, and actuator) have to be designed for high-pressure working, resulting in an increased cost of the hydraulic system. When the pressure intensifier is used, a single component, the actuator, works with high pressure, making the hydraulic system cheaper. What is more, the system with fewer component/s operating on high pressure is safer, because of lower damage probability. Using hydraulic pressure intensifier is a good solution when only the actuator/s in the system requires high pressure. [1, 2]
SAOHPIs are known in the literature under several names: oscillating hydraulic pressure amplifiers, oscillating pumping units, pressure intensifiers, boosters, mini-boosters.
Usually, these pumping units, fig.1, have in the primary an inlet connection, low pressure **IN** and an outlet connection **R** (tank), and in the secondary, an outlet connection, high pressure **H**. Structurally, they include: two joined pistons, of which one of large diameter, **LP** and another of small diameter, **HP**, the ratio of the areas of the transversal surfaces of the pistons being equal to the amplification ratio; a check valve, **KV1**, for suction of the working fluid into the high pressure chamber; other check valve, **KV2**, for discharging the working fluid from the high pressure chamber to the consumer; a **DV** unlockable check valve (for certain construction types) and a 3/2 bi-stable distribution valve, **BV1**. The position of the pistons will determine, at the end of each stroke, an **S** signal to **BV1**, which will lead to a change in the direction of travel of the piston. This cycle will continue until the final pressure is reached. At this point, the pistons stop. They will move only to maintain the final pressure. [3, 4]
These types of amplifiers operate in two phases: in the first phase, they provide consumers with an almost constant and continuous flow, equal to the maximum flow of the pump, at low pressure, and in the second phase, they provide a small pulsating flow at high pressure.
From the point of view of the pulsations of the high-pressure flow, the amplifiers with oscillating pistons can be with single action (they have higher pulsations), or with double action (they have lower pulsations).
The operating principle of an SAOHPI is as follows: a large volume at a low fluid pressure pushes a large diameter piston, into contact with another small diameter piston; as a result of this action, the small diameter piston will push a small volume of fluid, high pressure, HP, equal to the low pressure amplified with the ratio of the piston surfaces. The high pressure, HP, will always be proportional to the supply pressure of the large LP piston (if there are no internal flow losses).

In phase I of operation, on the H output of the intensifier, almost all the flow (or sheerly all the flow) given by the pump will come out at the pressure at which the safety valve is adjusted and the pistons depending on the position in which they remained previously, will move or not, then, as the load increases in the secondary, the pistons begin to move.
In phase II, the pistons will move with a frequency determined by the pump flow and the primary volume, under the control of BV1, until the maximum pressure of the amplifier is reached, after which they will stop.
If there is a pressure drop on the amplifier secondary, the pistons will restart, in order to restore the pressure to the consumer.

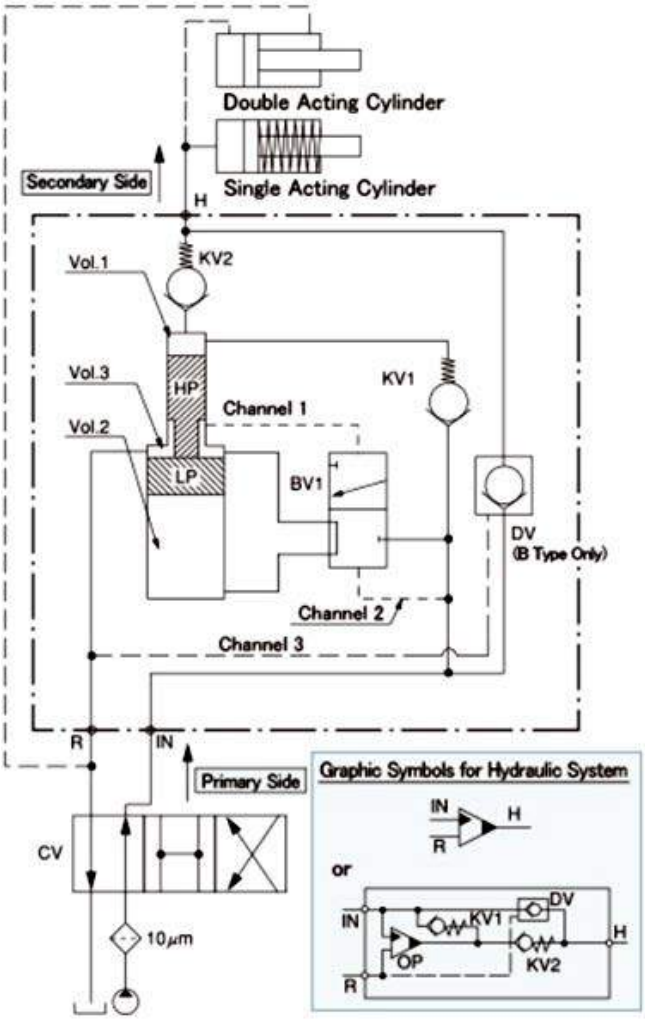

Fig. 1. SAOHPI - hydraulic diagram and functional constructive details [5]

2. Numerical simulation of a generic SAOHPI

With the Simcenter Amesim v2021.1 numerical simulation software, the physical simulation model of an SAOHPI was developed, and it is presented in fig. 2.
In the lower part of the simulation network, the one that supplies the intensifier primary, the following components can be identified: the electric motor that has a speed of 1500 rev/min, a hydraulic pump with gears, with a capacity of 8 cc/rev, a pressure valve, with the role of a safety valve, that opens if the pressure exceeds 200 bar, as well as a power, flow and pressure transducer and a tank from which the hydraulic fluid is absorbed.
In the upper part of the simulation network, which is fed from the secondary of the intensifier, the following components can be identified: a flow, pressure and power transducer, a consumer which in this case is a throttle valve, with variable section, that is controlled by a signal, which at a certain

moment commands the closing of the hydraulic orifice, as well as the tank, where the hydraulic fluid drains.
The dotted line represents a hydraulic block and delimits the hydro-mechanical components of SAOHPI, which has the following parameters: at inlet, a flow of 12 L/min at a maximum pressure of 205 bar, at outlet, an amplification factor i=10, a flow of approx. 0.8 L/min at a maximum pressure of 2000 bar.
Its structure and internal parameters were chosen so that the operating frequency is relatively low (5 Hz), so that the physical phenomena are easy to notice.
Oscillating chamber parameters are: LP diameter 24 mm, HP diameter 7.6 mm, and a stroke length of 80 mm.
Other numerical simulation settings: start time: 0 s, final time: 2 s, print interval: 0.0001 s, number of points: 20001, sampling frequency: 10000 Hz, number of variables: 255, integrator tolerance: $1e^{-07}$.

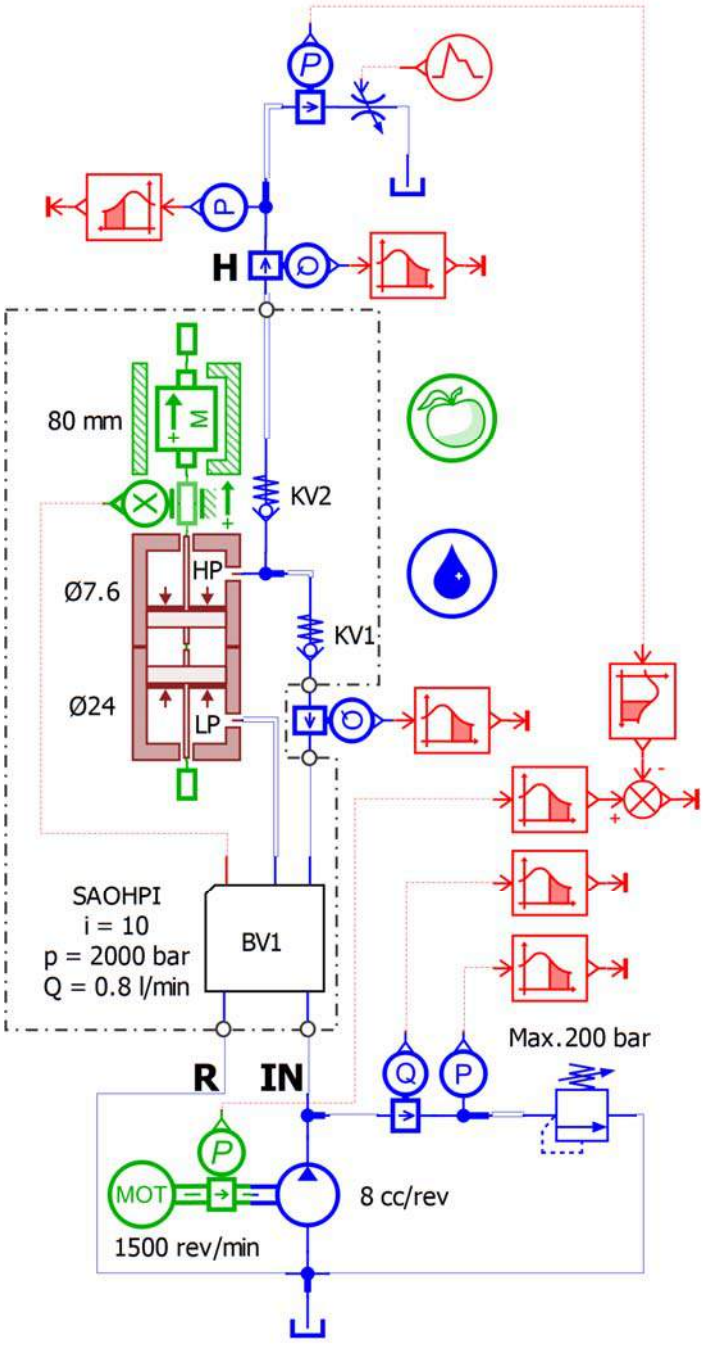

Fig. 2. SAOHPI - simulation network

2.1 Results

In this subchapter the results of the numerical simulation are presented in the form of graphs. Most of them show the evolution in time of two or even three variables on the same graph, first of all to highlight their correspondence and to save space.

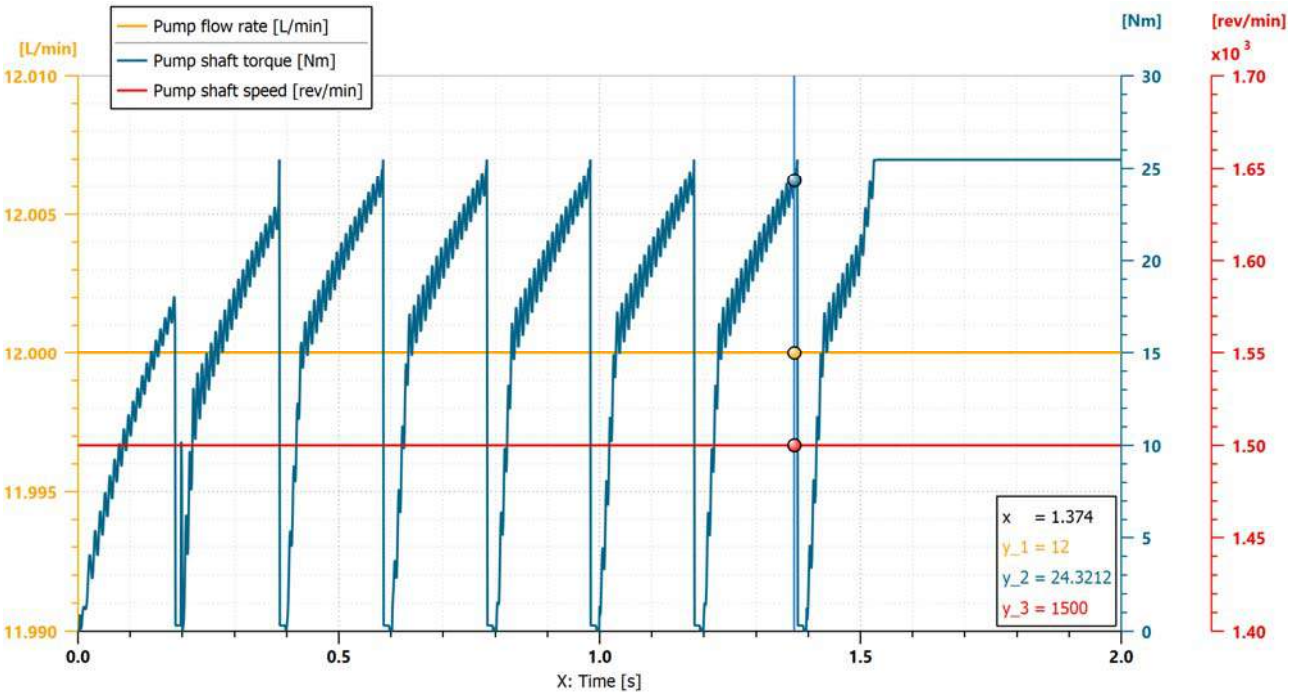

Fig. 3. Pump flow, torque and speed

Figure 3 shows the variation in time of the pump parameters, in which one can see that both speed and flow are constant; the only parameter whose evolution changes over time is torque; its variation depends on the frequency of the oscillator and the pressure of hydraulic orifice (load).

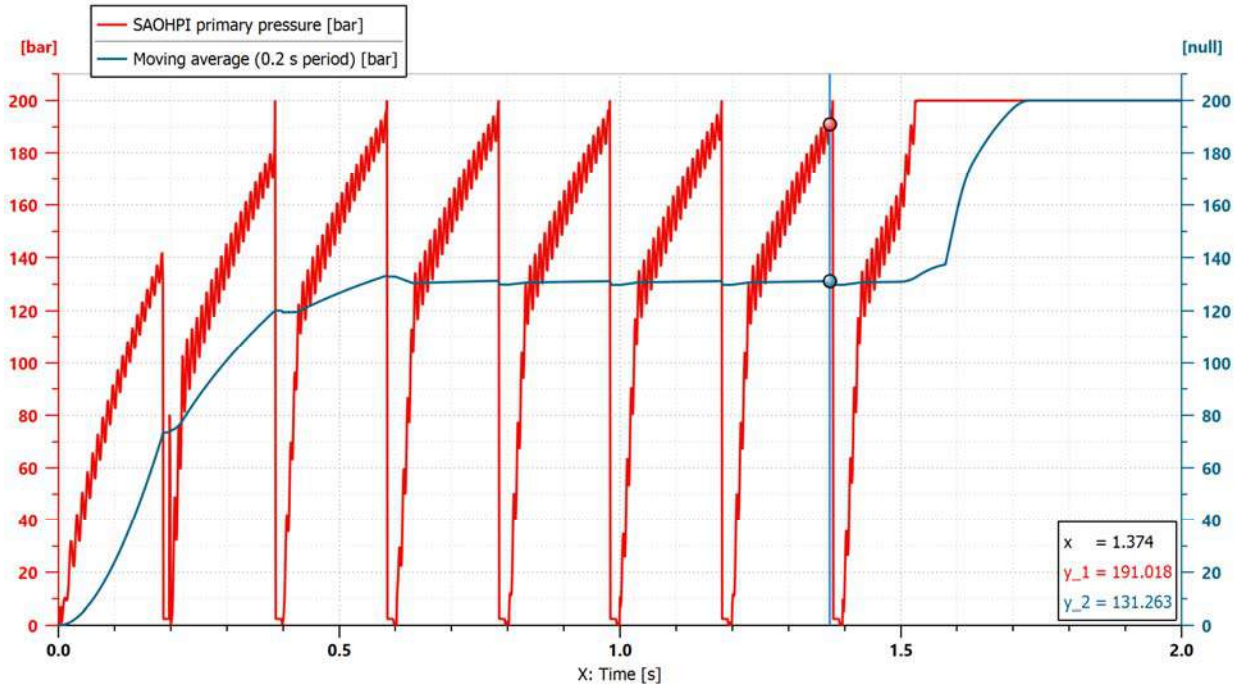

Fig. 4. Pressure in the oscillator primary

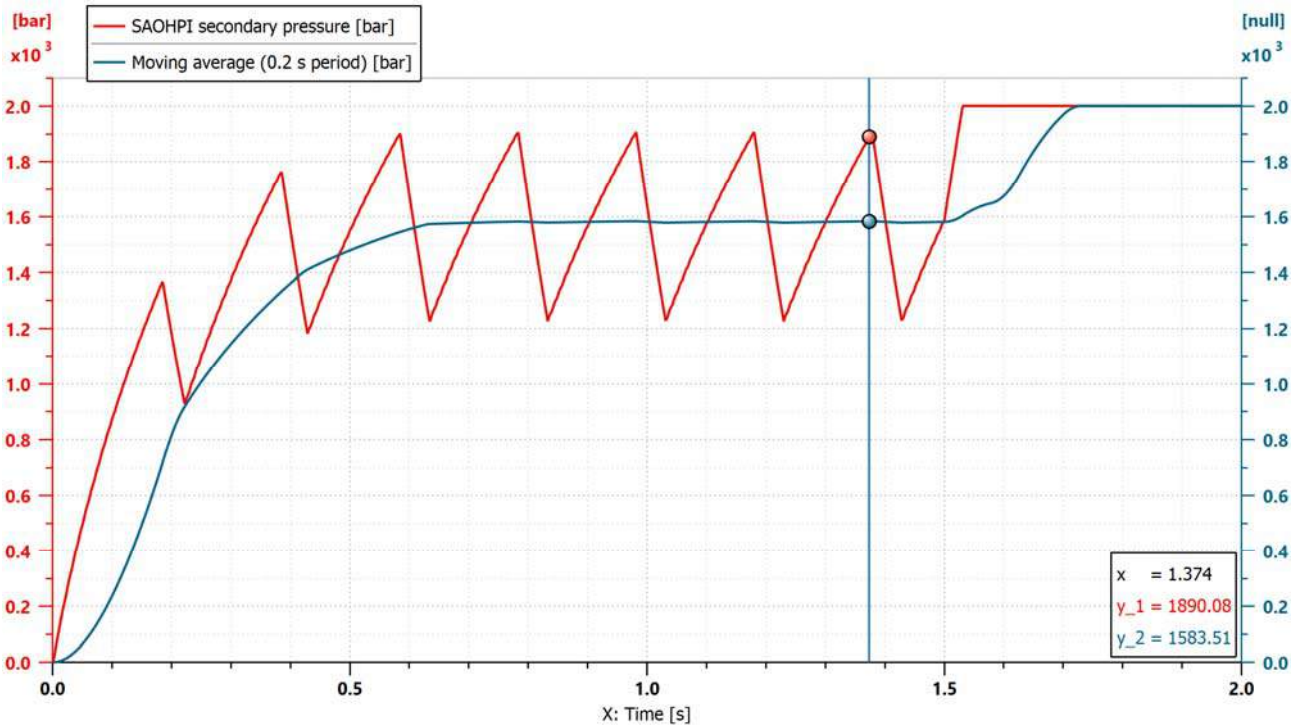

Fig. 5. Pressure in the oscillator secondary

In figure 4 and 5 one can see the evolution over time of the pressure in the oscillator primary and secondary as well as their moving average values. Also, on these graphs, one can notice the frequency of pressure pulsations in the primary and secondary of the intensifier.

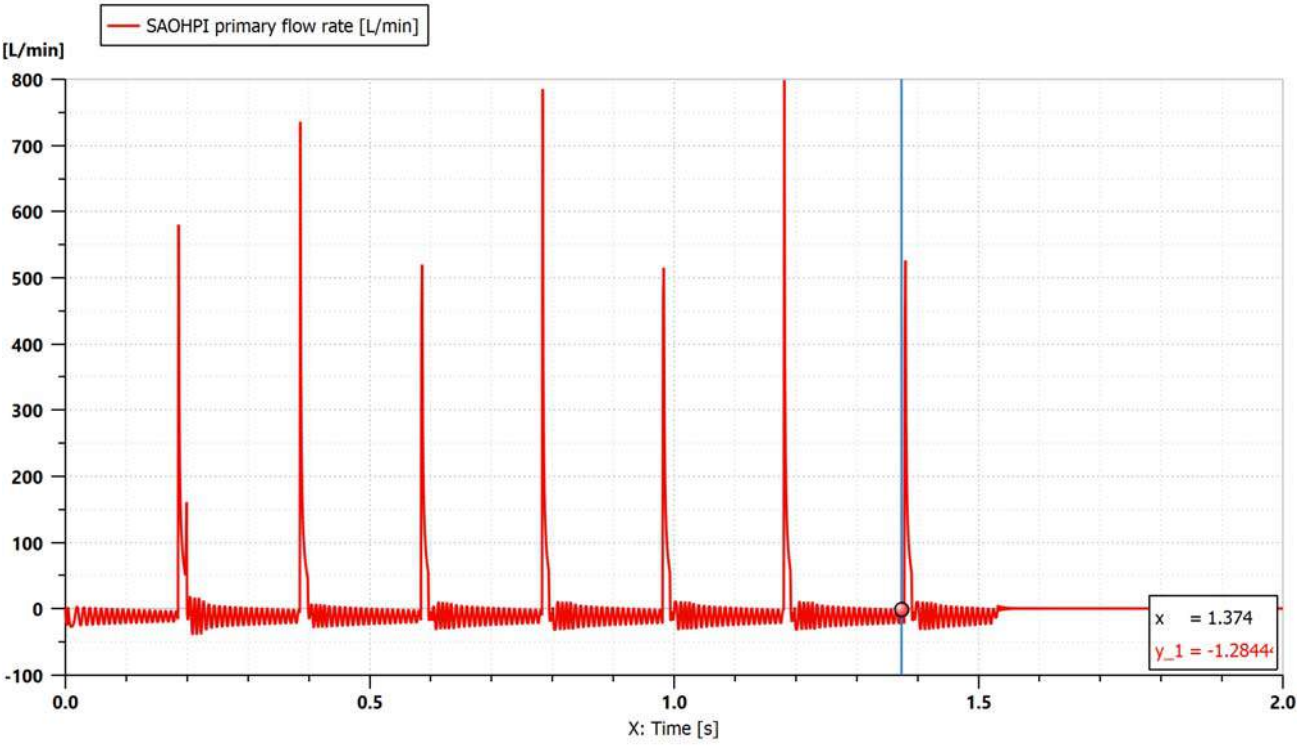

Fig. 6. Flow rate in the oscillator primary

Figure 6 and 7 show the time variation of the instantaneous flow rate values entering and leaving the two chambers of the intensifier.

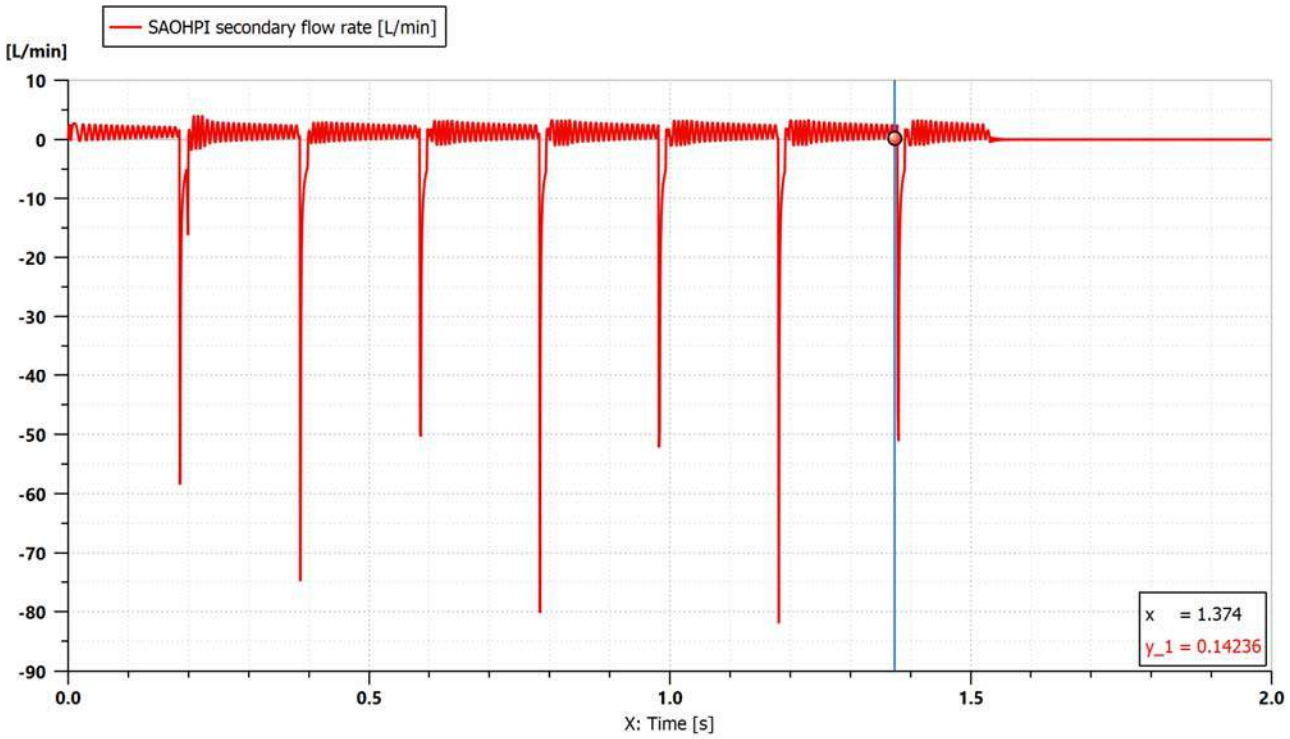

Fig. 7. Flow rate in the oscillator secondary

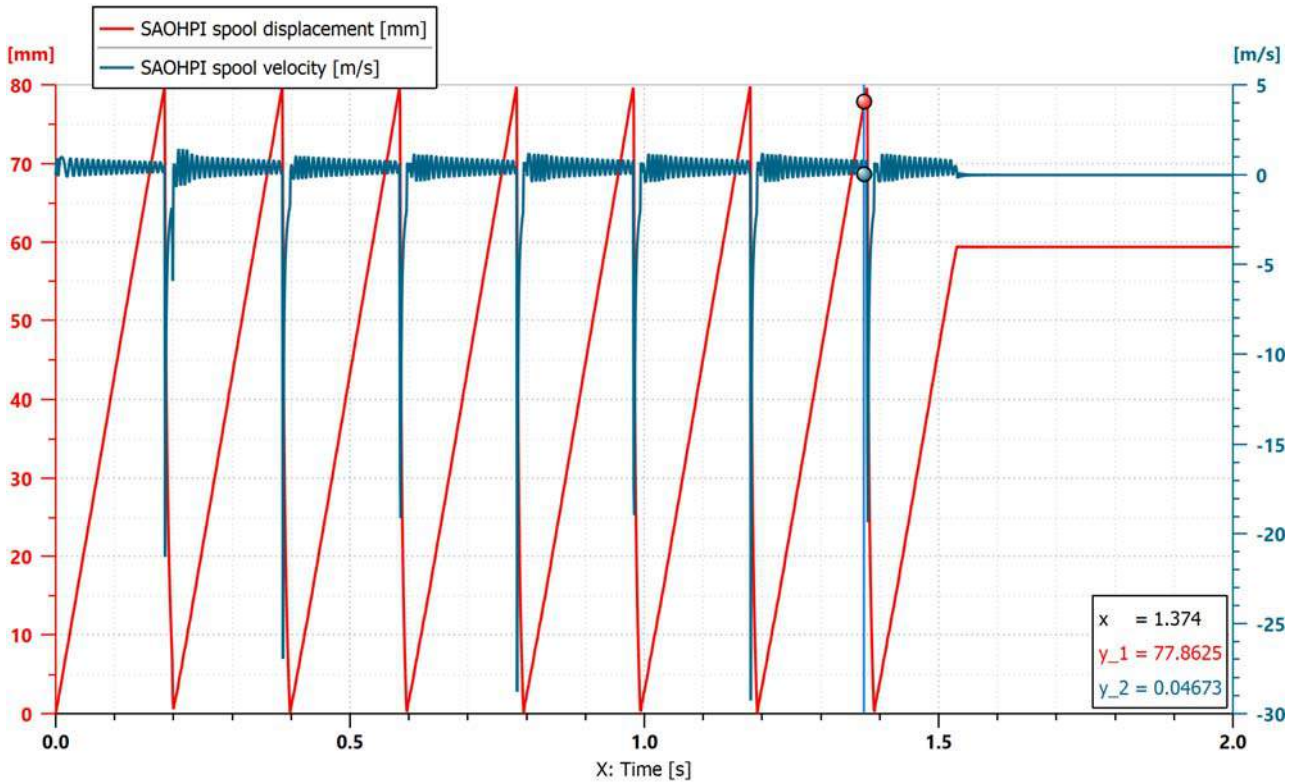

Fig. 8. Displacement and velocity of the intensifier piston

Figure 8 shows the time variation of the displacement and the displacement velocity of the piston. On this graph one can see that the displacement velocity on the active stroke is low, and on the passive stroke it is high, because all the pump flow enters the secondary chamber, which has a considerably smaller volume than the primary chamber.

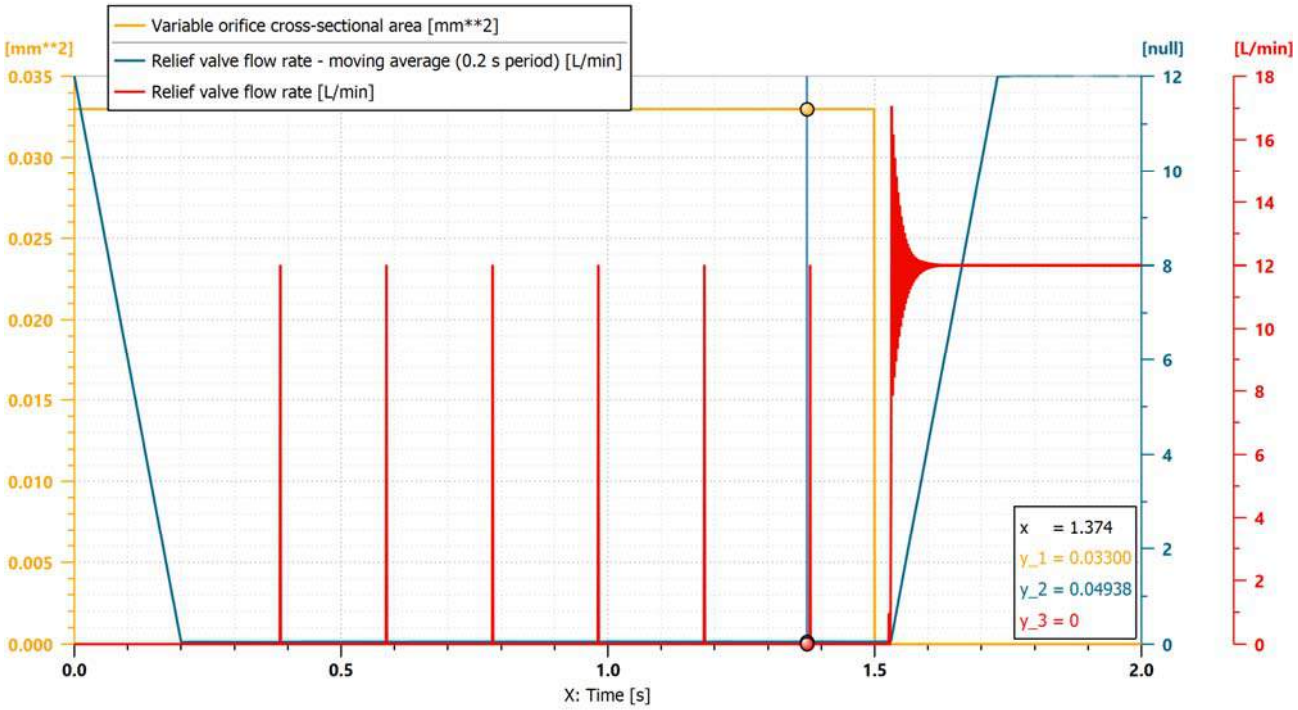

Fig. 9. The variation of the hydraulic orifice section and the flow discharged through the safety valve as well as its moving average

In the graph in figure 9 one can see that the flow section of the hydraulic orifice is open for 1.5 s, and then it is closed so that the pressure reaches 2000 bar. On the same graph one can notice the behavior of the pressure valve: it discharges a very low flow rate every time when the oscillator reaches the upper end of the stroke and changes the direction of travel; this phenomenon occurs due to the delay caused by the inertia of the oscillating piston mass, when the primary pressure reaches 200 bar and the pressure valve discharges.

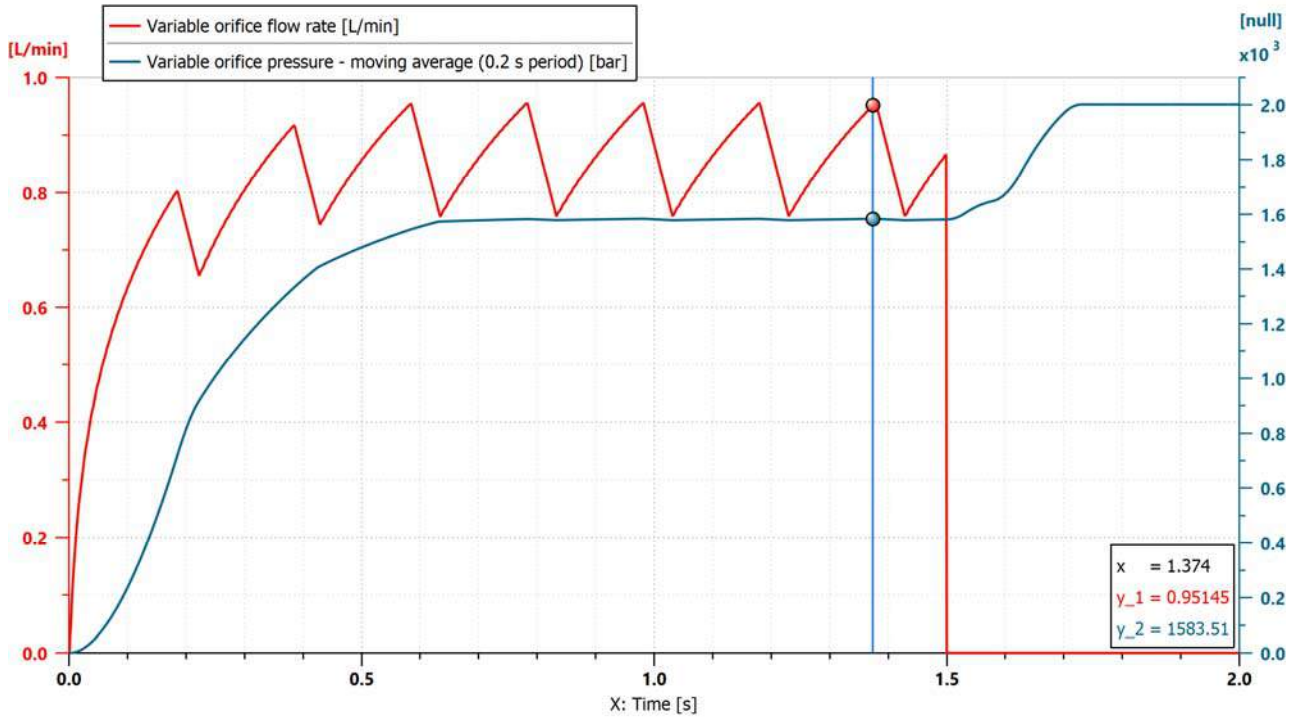

Fig. 10. Variation in time of the pulsating flow at the exit of the hydraulic orifice and the moving average of the upstream pressure

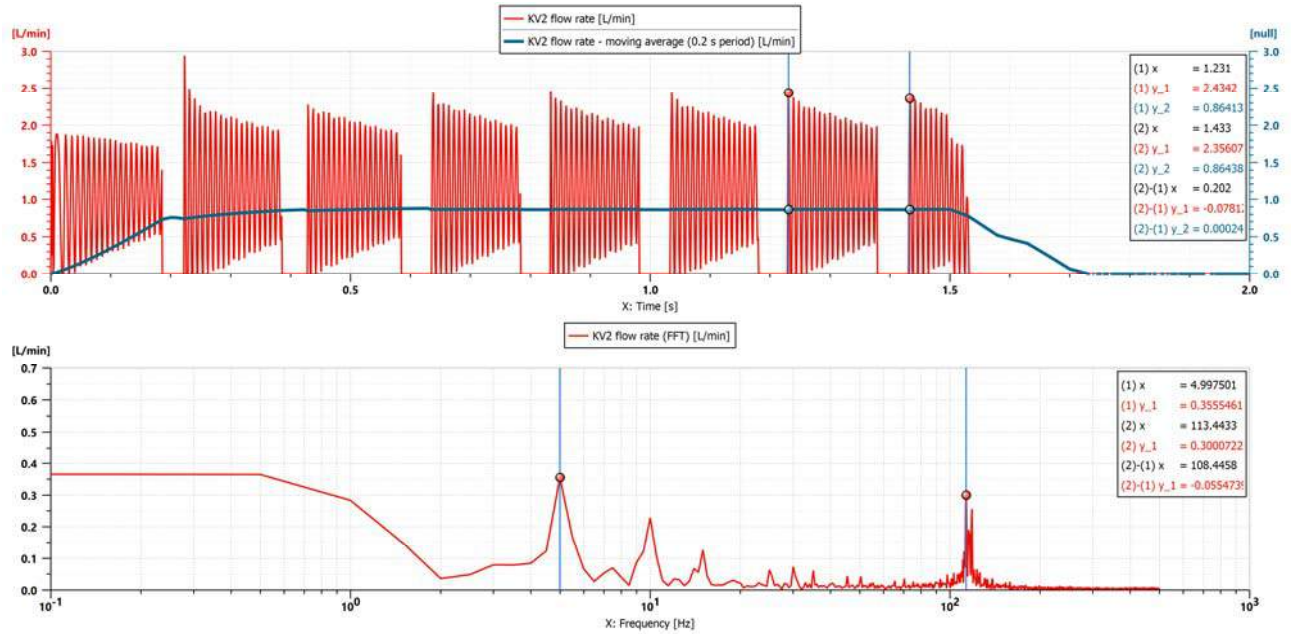

Fig. 11. KV2 flow rate, moving average and its spectrum

In figure 11, in the upper part of it, the variation in time of the flow rate of hydraulic fluid passing through the check valve KV2 is presented; the value of its moving average is 0.86 L/min. In the lower part of the figure the flow rate spectrum is presented; on it the frequencies of flow rate pulses can be identified. On this spectrum there are two notable resonant phenomena. The first phenomenon is the pumping one, with a frequency of 5 Hz and the highest amplitude of 0.35 L/min, and to its right, with a frequency of 10 Hz and 15 Hz, its harmonics can be identified. The second phenomenon, and most interesting, is located in the frequency range between 110 and 120 Hz. This resonant phenomenon is due to the inertia of the piston and the elasticity of the hydraulic system; it appears at the beginning of the piston stroke on its active side, when the value of the piston acceleration fluctuates; the only parameter of the numerical simulation that influences the frequency of this phenomenon is the mass of the piston.

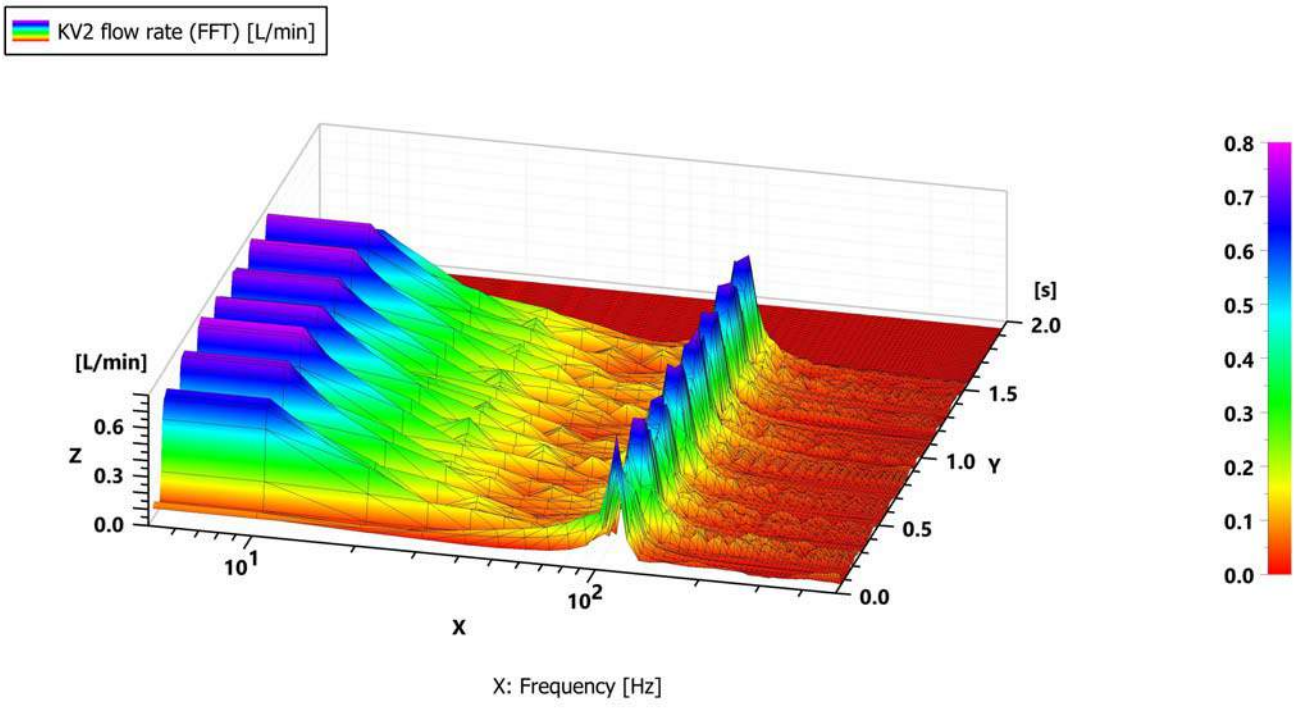

Fig. 12. Variation in time of the flow rate spectrum

The graph in figure 12 shows the variation in time of the flow spectrum; it is the same spectrum as the one in figure 11, adding a new dimension: the time on the Y axis. It was previously mentioned that certain parameters of the simulation were chosen, so that, on such a figure, the physical process is very easy to notice. In this situation, there is the diameter of the primary and the secondary (24 mm and 7.6 mm); in reality, they are much smaller and probably the piston stroke is smaller. The graph in figure 12 shows the flow variations, which can reach the consumer, when certain hydraulic components pass through resonance, when closing, opening, accelerating or decelerating their components. In the lower part of the spectrum, with a frequency of 5, 10 and 15 Hz, one can see the eight flow rates, pumped by the secondary of the intensifier; the last one is partial because the piston does not reach the end of the stroke. Another variation of the flow rate occurs in the frequency range 110-120 Hz, on the active stroke of the piston, of the pressure intensifier, when it accelerates, when leaving the place; a notable aspect is that this phenomenon occurs before the one mentioned above, which indicates that the piston moves, the secondary fluid is compressed, the compressibility of the hydraulic system dampens the piston vibration, and then the secondary flow is sent to the consumer. Other flow variations occur at: pressure safety valve with a frequency of 65, 70 and 75 Hz; KV2 - 45, 50 and 55 Hz; KV1 - 25, 30 and 35.

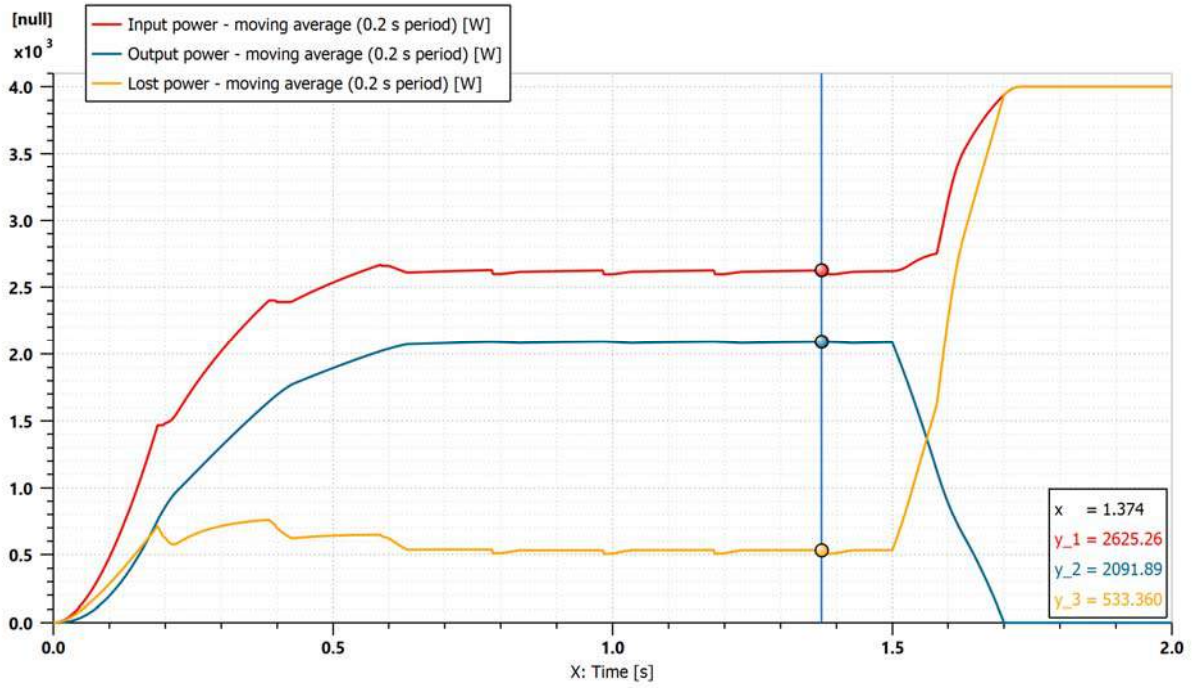

Fig. 13. Moving average of input, output and lost power

Figure 13 shows three curves, whose variation in time depicts: the power that enters the hydro-mechanical system, in red color; the useful power, which leaves the system, in blue color; and the lost power, due to flow losses to the tank, with certain pressure drops and mechanical frictions - depicted in yellow color.

3. Conclusions

- The SAOHPI is used for pressure boosting, low pressure pumping units, feeding hydraulic cylinders that linearly move large loads, anywhere on their stroke, or achieve and maintain high pressure in a closed enclosure. The SAOHPI is mounted between the pump unit and the driven cylinder, as close as possible to the latter.
- The energy efficiency of a pumping system equipped with SAOHPI is about 80%; such efficiency is comparable to that of a high-pressure pump.
- Unlike pumping systems with high pressure hydraulic pumps, SAOHPI has the following advantages: only the hydraulic circuit from the intensifier to the consumer is under high

pressure, which reduces the probability of a failure due to the small number of hydraulic components that are at high pressure; they are relatively cheap and do not require high pressure command and control equipment, and they are small in size and light.

- An important aspect to mention is that the SAOHPIs are not recommended for dynamic hydraulic drives where uniform flow rate is required, at a high pressure; due to the way they work, there are generated flow rate pulses, and between flow rate pulses there is a short time period in which the consumer is not supplied with flow rate and pressure, which causes uneven operation of the consumer.
- The amplitude of the flow rate and pressure pulses can be significantly reduced by decreasing the volume of the secondary chamber of the intensifier, but the smaller the volume of the secondary, the longer it will take the intensifier to reach high pressure.
- In order to further improve the uniformity of flow and pressure, in addition to the constructive recommendations mentioned above, a double-acting oscillating pistons hydraulic pressure intensifier can be used, which has two active strokes in the same operating cycle, unlike the SAOHPI, which has just one active stroke.

Acknowledgments

The research presented in this paper has been developed under Financial Agreement no. 272/24.06.2020, signed by the Ministry of European Funds / Ministry of Education and Research and S.C. HESPER S.A. Bucharest for the Innovative Technological Project titled "Digital mechatronic systems for generating pressure of 1000 bar, using hydraulic pressure intensifiers" (SMGP), which is under implementation from 01.07.2020 to 30.06.2023.

References

[1] Bartnicki, Adam. "The Research of Hydraulic Pressure Intensifier for Use in Electric Drive System." *IEEE ACCESS* 7 (2019): 20172-20177.
[2] Paunescu, Tudor. "A new concept of intensifier for double acting hydraulic power workholding systems." Paper presented at the NNECFSIC'12: 12th WSEAS International Conference on Neural Networks, Fuzzy Systems, Evolutionary Computing & Automation, Brasov, Romania, April 11-13, 2011.
[3] ***. "How does miniBOOSTER work?" Accessed March 3, 2021. https://www.minibooster.com/how-does-minibooster-work/.
[4] ScanWill. "Product Overview". Accessed March 5, 2021. https://www.scanwill.com/products/pressure-intensifiers.html.
[5] P.M.P. Pioneer Machine Tools. "The increase pressure actuation system of hydraulic boosters HC series." Accessed March 5, 2021. http://pmt-pioneer.com/en/product-detail5.html.

Energy Loss Reduction in Hydraulic Installations of the Machine Tools Served by Constant Flow Pumps

Prof. PhD Eng. **Anca BUCUREȘTEANU**[1]*, Assoc. Prof. PhD Eng. **Adrian MOTOMANCEA**[1], Assistant **Alina OVANISOF**[1]

[1] University POLITEHNICA of Bucharest

* ancabucuresteanu@gmail.com; (adrian.motomancea@deltainfo.ro, alinaovanisof@yahoo.com)

Abstract: *In this paper, the authors present an analysis of the adjustment systems related to the flow-pressure type operating parameters in the hydraulic installations of the machine-tools which enable energy consumption to be reduced. Some of the most common basic schemes in the hydraulic installations of the machine-tools are presented, analyzing technically but also economically the opportunity to use them. In order to support possible options, the authors also present the results of the simulations carried out.*

Keywords: *Machine-tools, hydraulic installations, energy loss reduction, simulations*

1. Introduction

The transfer of power in any hydraulic installation is carried out as shown in the diagram in Figure 1 [1].

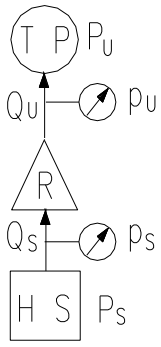

Fig. 1. Transfer of power in a hydraulic installation

The power of the P_S source is developed at the HS hydraulic source. The components are: Q_S flow rate and p_S source working pressure. Among these sizes, we have the relation:

$$P_S = p_S Q_S \tag{1}$$

The flow rate and pressure can be adjusted, as necessary, by means of the adjustment equipment R. Finally, the technology process served by TP includes: the effective flow Q_U, the effective pressure P_U and the effective power P_U:

$$P_U = p_U Q_U \tag{2}$$

The efficiency of the installations of the type shown in Figure 1 is:

$$\eta = \frac{P_U}{P_S} \tag{3}$$

The value of the required power results from the specific process. In this case, to increase the efficiency value, the only solution is to reduce the power of the source. However, the actual

operating conditions must also be taken into account in the presence of local losses and on hydraulic flow and/or pressure routing [2, 3, 4]:

$$Q_U < Q_S \tag{4}$$

$$p_U < p_S \tag{5}$$

If the process requires multiple flow rates and/or working pressures, then the hydraulic system may provide much higher powers than the effective one in some phases. In addition to the low efficiency of the installation, there is another drawback: the lost power is converted into heat which can lead to the installation malfunctioning or even to its destruction [2, 3]. The difference between the OABC and OXYZ triangle areas, shown in Figure 2, is the power lost in any operation phase of the installation.

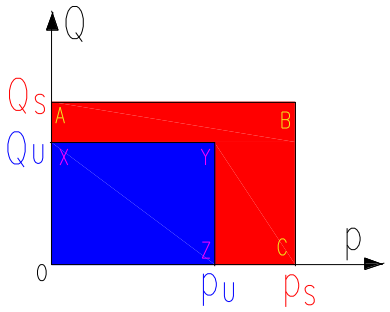

Fig. 2. Effective power and lost power

The hydraulic source (HS) is usually made up of [1]: the electric drive motor of the pump(s), the pump(s) and the pressure regulation system p_S. Under these conditions, the flow Q_S with a certain characteristic represented by the closed curve C_1 in Figure 3 shall be provided.

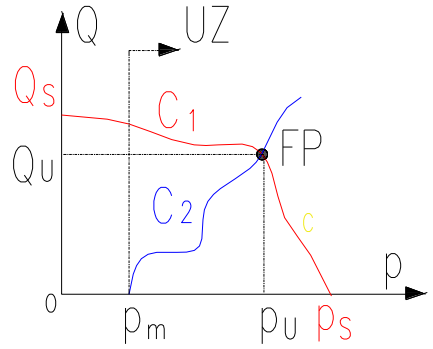

Fig. 3. Establishing the operating point

At the level of the technological process (TP), a minimum p_m pressure and flow rate are required represented by the open curve C_2. The intersection of the two curves represents the "operating point" of the FP installation [1]. This is where the Q_U effective flow and the p_U pressure get. Any adjustments may only be carried out in the feature's useful area (UZ), as shown in Figure 3.

2. Hydraulic Sources

The simplest hydraulic source is shown in Figure 4 and includes: the EM electric motor, the PC constant flow pump which sucks oil from the T tank and the PV pressure regulating valve. The source pressure is displayed on the M_1 pressure gauge.

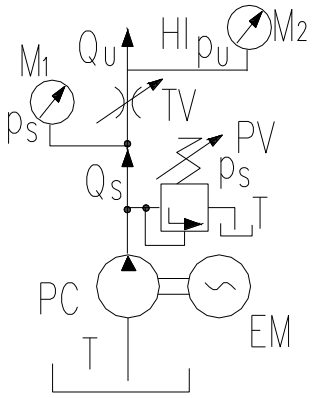

Fig. 4. The source with a constant flow pump

The hydraulic installation (HI) served is supplied by the Q_U flow-rate source regulated by the hydraulic installation represented by the TV hydraulic throttle. Under these conditions, an instantaneous p_U pressure develops in the installation and can be seen on the M_2 pressure gauge. Such pressure must check the relation:

$$p_m \leq p_U \leq p_S \tag{6}$$

If the pressure valve is considered to open instantaneously, the characteristic of this source and the method of determining the operating point in this case are shown in Figure 5.

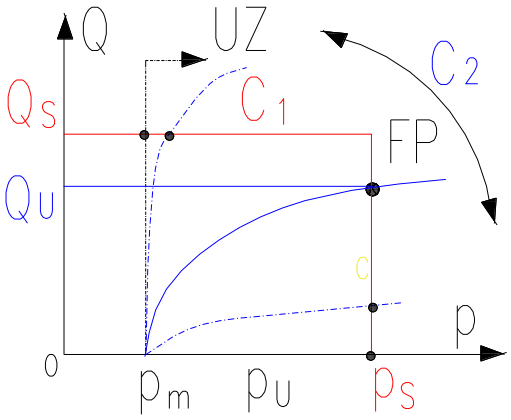

Fig. 5. The characteristic of the hydraulic source with a pump

According to the characteristic in Figure 5, the Q_U effective flow is:

$$Q_U = \begin{bmatrix} 0, p \leq p_m \\ Q_S, p_m < p < p_S \\ \in (0, Q_S), p = p_S \\ 0, p \geq p_S \end{bmatrix} \tag{7}$$

In this case, if the installation works with significantly different flow rates and in a restricted pressure range close to the p_S value, the source sizing shall be carried out for the maximum flow required and p_S pressure.
Let us assume that the served installation works in two phases:
Phase1: Q_{U1} = 30 l/min, p_{U1} = 15 bar, p_m = 10 bar;
Phase2: Q_{U2} = 3 l/min, p_{U2} = 70 bar, p_m = 10 bar.
Under these conditions, a pump with a flow rate of 30 l/min has been selected and the pressure valve will be adjusted to 70 bar.

The source power shall be, in this case, P_S = 3.5 KW. The effective power in the first phase is P_{U1} = 0.75 KW and, in the second phase, P_{U2} = 0.35 KW. The outputs in these two cases shall be: η_1 = 21.5% and η_2 = 10%.
The operating characteristics for the two phases are shown in Figure 6.

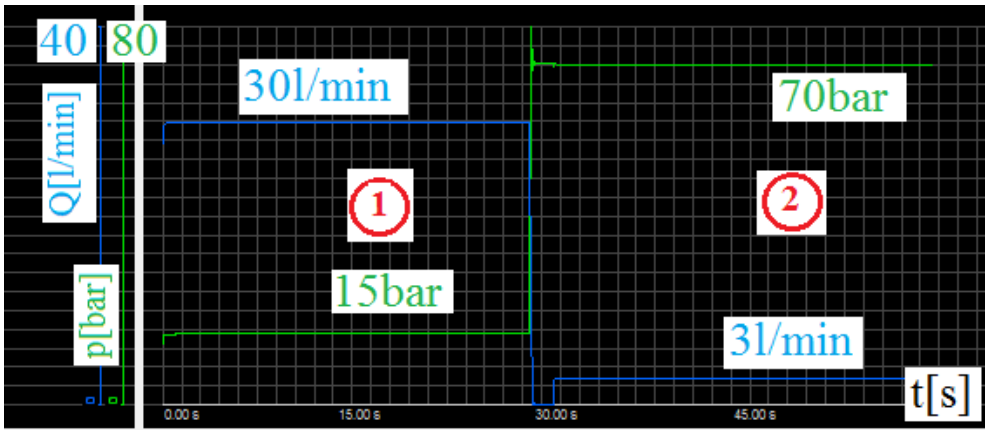

Fig. 6. Operating characteristics

This solution, with a single pump and a single pressure valve, is characterized by the fact that the outputs in both working phases are low, but also by the fact that it is the cheapest solution.
A solution which even exceeds twice the previous price is the one which uses two pumps and two pressure valves, as shown in Figure 7.

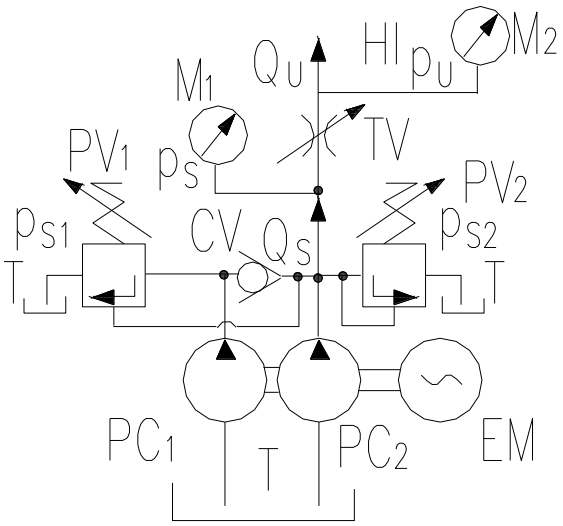

Fig. 7. The hydraulic source with two pumps

In this case, the EM electric motor drives two constant flow pumps PC_1 and PC_2. Their flows are Q_{S1} = 24 l/min and Q_{S2} = 6 l/min. The two pumps are coupled in the installation via the CV non-return valve. The PV_1 and PV_2 pressure valves are adjusted at pressures p_{S1} = 20 bar and p_{S2} = 70 bar. The same working conditions as in the previous case are considered.
If the pressure valves are considered to open instantaneously, the characteristic of this source and the method of determining the operating point in this case are shown in Figure 8.

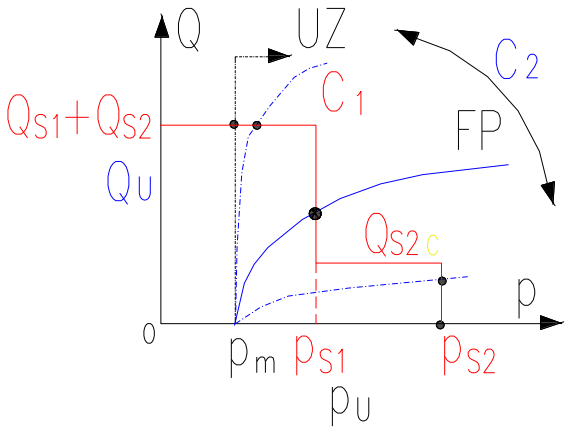

Fig. 8. The characteristic of the source with two pumps

According to the characteristic in Figure 8, the Q_U effective flow is:

$$Q_U = \begin{bmatrix} 0, p \le p_m \\ Q_{S1} + Q_{S2}, p_m < p < p_{S1} \\ \in (Q_{S2}, Q_{S1} + Q_{S2}), p = p_{S1} \\ Q_{S2}, p_{S1} < p < p_{S2} \\ \in (0, Q_{S2}), p = p_{S2} \\ 0, p \ge p_{S2} \end{bmatrix} \quad (8)$$

The source power shall be, in this case for the first phase P_{S1} = 1 kW, and on phase two it becomes P_{S2} = 0.7 KW. The effective power in the first phase is P_{U1} = 0.75 KW, and in the second phase P_{U2} = 0.35 KW. The outputs in these two cases shall be: η_1 = 75% and η_2 = 50%. There is a significant increase in outputs for each phase.
Even if the solution seems to be more complicated and expensive, cost reductions are being made for other reasons. In the first case, an electric drive motor was required with the power P_{EM} = 4 KW. For the second option, a motor having the power P_{EM} = 1.5 KW is sufficient.
In the second case, for the two phases the operating characteristics are as shown in Figure 6. The difference is that, at a pressure of 70 bar, the flow rate of the PC1 pump is fully discharged through the pressure valve PV1 at a pressure of 20 bar.
In fact, in the case of machine tools, type 2 phases (chipping processes) take much longer than type 1 phases (positioning, approach phases etc.) [5]. This meant an even greater energy saving.
Apart from the work phases, hydraulic installations actually have phases in which they do not work. In this case, the oil is discharged through the pressure valves.
In the first case, the 30 l/min flow rate is discharged through the pressure valve PV at a pressure of 70 bar. In the second case, the 24 l/min discharge shall be carried through the pressure valve PV_1 at a pressure of 20 bar and the remaining 6 l/min shall be discharged through valve PV_2 at a pressure of 70 bar.
For such cases, considerable energy savings are achieved without stopping the pump(s) by using pre-control type solutions [1, 6].

3. Pre-control Hydraulic Installations

Pre-control valves require a pressure valve bypass system so that, when the installation is not required, the pumps discharge freely to the tank.
The diagram shown in Figure 4 was supplemented by a pre-control system as shown in Figure 9.
As long as the DV distributor is not driven and is in position 0, the pump will discharge directly to the tank. If coil E is powered, the distributor switches to position 1, which engages the system for the desired phases.

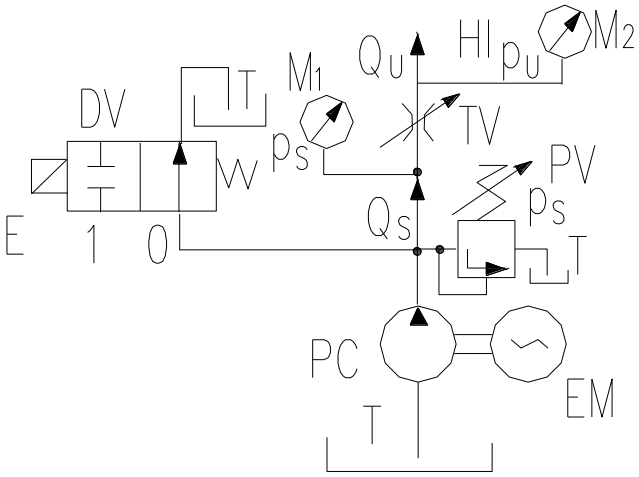

Fig. 9. Pre-control hydraulic source

Figure 10 shows the three operating phases in case there is pre-control.

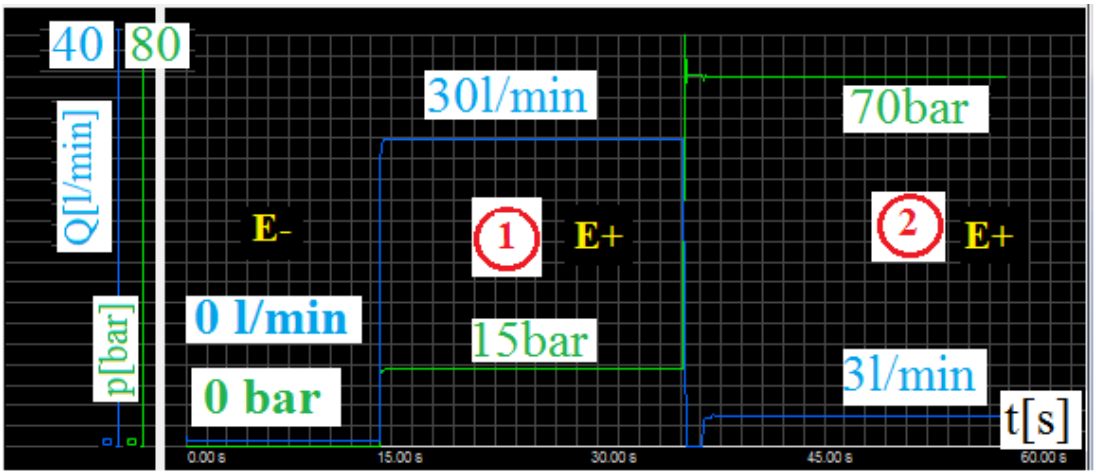

Fig. 10. Operating characteristics

The Q_U effective flow shall be:

$$Q_U = \begin{bmatrix} if\ E- \\ 0 \\ if\ E+ \\ 0, p \le p_m \\ Q_S, p_m < p < p_S \\ (0, Q_S), p = p_S \\ 0, p \ge p_S \end{bmatrix} \quad (9)$$

Theoretically, when the distributor is not driven, the source power is P_S = 0 KW because the pressure is zero (p_S = 0) because the PV pressure valve is closed. In fact, the system must cover the inherent pressure and flow losses.
In the case of machine-tools, there are installations where the pre-control systems are accompanied by hydro pneumatic accumulators [2, 5, 7, 8].

4. Conclusions

Due to multiple power conversions, electrical to mechanical, mechanical to hydraulic and, finally, hydraulic to mechanical, the hydraulic installations are characterized by low outputs. Constant flow or variable flow pumps shall be used as hydraulic power generators. Due to the low price, constant flow pumps (usually gear pumps) are the most commonly used. The design of the hydraulic system when these pumps are used has a particular effect on the efficiency of these installations. The use of two or even three pumps, with or without different flow rates, which together provide the maximum required, can increase the efficiency of these plants. The characteristics of the pumps and of the equipment used must be selected according to the phases and work procedure.
Pre-control systems can bring significant energy savings, especially for high-power installations, if there are working phases where the hydroelectric installation is not required. In this case, it is not recommended to switch electric pump drive motors on/off, the only option being to use the pre-control whether or not the batteries are present.

References

[1] Prodan, Dan. *Machine-Tools Hydraulics/Hidraulica Masinilor-Unelte*. Bucharest, Printech Publishing House, 2004.
[2] Guibert, Ph. *Applied Industrial Hydraulics/Hydraulique industrielle appliquee*. Université de Metz, 1991.
[3] Prodan, Dan, Mircea Duca, Anca Bucureşteanu and Tiberiu Dobrescu. *Hydrostatic drives-machine parts/Acţionări hidrostatice – Organologie*. Bucharest, AGIR Publishing House, 2005.
[4] Totten, George E. and Victor J. De Negri. *Handbook of Hydraulic Fluid Technology*. Boca Raton, U.S.A., CRC Press Taylor & Francis Group, 2012.
[5] Bucuresteanu, Anca. *Pneumatic Hydraulic Accumulators. Use and Modeling/Acumulatoare pneumohidraulice. Utilizare si modelare*. Bucharest, Printech Publishing House, 2001.
[6] Prodan, Dan. *Heavy machine tools. Mechanical and Hydraulic Systems/Maşini-unelte grele. Sisteme mecanice si hidraulice*. Bucharest, Printech Publishing House, 2010.
[7] Prodan, Dan and Anca Bucureşteanu. "Mathematical Modeling of Hydraulic Systems with Pneumohydraulic Accumulators for Machine-Tools Installations/Modelarea matematică a sistemelor hidraulice cu acumulatoare pneumohidraulice utilizate în instalaţiile maşinilor-unelte." *Hidraulica Magazine,* no. 2 (2008): 8-11.
[8] ***. Catalogues and leaflets BOSCH REXROTH and HYDAC.

Fluid Hammer Phenomenon Aspects on Circular Ducts

Assistant professor **Fănel Dorel ȘCHEAUA**[1]

[1] "Dunărea de Jos" University of Galați, MECMET Research Center, fanel.scheaua@ugal.ro

Abstract: *Theoretical aspects related to fluid circulation through circular pipes under pressure with a certain velocity value are presented while the valve is sudden or slow closed at a certain moment. The model represents the non-permanent fluid circulation type through circular pipes frequently encountered in the case of hydraulic applications, in the work installations operation, with a need for stopping and restarting according to the existing operating work body needs. For this purpose, special devices capable to adjust the fluid flow rate are mounted in the circuit represented by valves which by their action have the possibility to interrupt the hydraulic flow stream in the circuit when needed. When the valve closes suddenly there are high overpressure efforts acting on the duct walls that far exceed the registered pressure value in the above permanent fluid circulation regime. This paper describes the theoretical aspects for fluid hammer phenomenon for the case of a rigid circular steel duct. A numerical fluid flow analysis on the virtual model of the pipe with closing element is made and the results are presented in order to highlight the specific fluid pressure and velocity values that occur when closing the valve.*

Keywords*: Fluid flow, fluid hammer, pressure, three-dimensional modelling, CFD*

1. Introduction

The model of non-permanent flow through pressure pipelines is highlighted, which is characteristic for the machines and industry equipment hydraulic installations operation, which depending on the requirements and needs of the working body have the possibility to interrupt and connect the installation to the system pressure source. Due to the intermittent nature of the pressurised fluid flow, high stresses appear on the installation duct walls due to the created overpressures that far exceed the value of the nominal pressure of the installation operating in permanent flow of working fluid forming important stresses on the pipe wall.

Considering the presented aspects, it is necessary a proper dimensioning of the installation pipes that are subjected to important stresses due to the intermittent operation regime and the non-permanent fluid flow regime. [1-5]

2. Fluid hammer characteristics

By abruptly closing the flow section of the hydraulic network pipes, the formation and propagation of specific pressure waves in the fluid region inside the pipe is ensured as a result of the sudden handling of the closing elements that determine the increase of pressure values in the respective fluid area considering the compressibility of the working fluid.

In the case of forced or gradual closing of the hydraulic installation valve, an overpressure is produced first, then an underpressure, the process having a cyclical character until the pressure values are balanced at the nominal value.

This pulsating process has a direct influence on the hydraulic network pipe through cyclic stresses on the pipe wall.

The phenomenon is also observable for the velocity variation case or the the installation pump shutdown when a subpressure is first registered followed then by an fluid overpressure, the process being repeated cyclically along the discharge line of the system pump.

The pipe elasticity coefficient must be taken into account, as well as the load losses that occur during the fluid circulation.

In the case of steel pipe it cannot be considered rigid so that the forced compression of the working fluid causes the elastic deformation of the pipe wall registered with a certain delay time due to the significant difference between the pipe material elasticity modulus and the working fluid and the inertia of the pipe material which cannot instantly follow the cyclic process of compressing and decompressing the liquid.

The pipe material low rigidity has the effect of attenuating in time the propagation velocity characteristic values of the pressure waves appeared as a result of the hammer fluid. 00

3. Theoretical aspects regarding the fluid hammer

The characteristic equations of the fluid hammer phenomenon are necessary for the analytical study in case the non-permanent flow registered within a circular pipe with diameter (D), fed from a tank containing liquid with free surface located at the height given by the dimension (z). The thickness of the pipe wall d is considered, and the elasticity modulus of the pipe material is (E).

The working fluid has the specific gravity range, the density (ρ) and the modulus of elasticity (e).

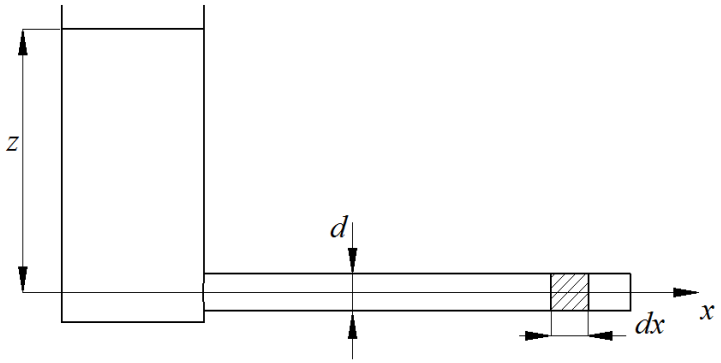

Fig. 1. Fluid particle motion within circular duct 0

For the analytical study of the fluid hammer it is necessary to determine the change of the velocity and the fluid pressure in time along the circular pipe length.
The equation of motion results from applying Newton's law to a fluid particle located within the main fluid stream inside the pipe.
The forces acting on the particle are represented by the mass forces (weight) and the surface forces given by pressure and viscosity. The weight has a vertical component and the viscosity forces are neglected, so the only forces taken into account are the pressure forces between two points on different sections.
The overpressure appears on the duct section from the shut-off valve with a higher value than the nominal flow pressure registered at the moment before the valve shut-off. 0
Together with the pressure waves propagation along the circular pipe length, the relation for the pressure forces resultant can be written as follows: 0

$$F_p = \frac{\pi D_c^2}{4}\left(p + \frac{\partial p}{\partial x}dx\right) - \frac{\pi D_c^2}{4}p = \frac{\pi D_c^2}{4}\frac{\partial p}{\partial x}dx \tag{1}$$

$$\sum F = ma = \rho\frac{\pi D_c^2}{4}dx\frac{\partial v}{\partial t} = \frac{\pi D_c^2}{4}\frac{\partial p}{\partial x}dx \tag{2}$$

The relation for particle fluid motion that describes the connection between the fluid flow velocity and height functions related to space and time can be written as: 0

$$\frac{\partial v}{\partial t} = g\frac{\partial z}{\partial x} \tag{3}$$

Taking into account the pipe wall stresses and the fluid compressibility values, the continuity equation can be written to describe the fluid hammer phenomenon. 0

$$dV = dV_1 - dV_2 \tag{4}$$

It is considered that the working fluid volume is modified with the forced compression that determines the pipe wall deformation by increasing the momentary volume. 0

$$dV = (Q_1 - Q_2)\,dt = \frac{\pi D_c^2}{4}\left[v - \left(v - \frac{\partial v}{\partial x}dx\right)\right]dt = \frac{\pi D_c^2}{4}\frac{\partial v}{\partial x}dxdt \tag{5}$$

Hooke's law describes the increase in the diameter value based on the unit effort depending on the pipe material elasticity modulus. 0

$$dV_1 = \pi d_c \frac{dD_c}{2}dx;\ dD_c = \frac{d\sigma}{E}d_c;\ d\sigma = \frac{D_c dp}{2\delta} \tag{6}$$

$$dV_1 = \pi D_c \frac{dD_c}{2}dx = \frac{\pi}{2}\frac{d\sigma D_c^2}{E}dx = \frac{\pi}{4}\frac{D_c^3}{\delta E}dpdx \tag{7}$$

For the fluid hammer case, the pressure values change in time is more important than the space change and the relation for the conveyed fluid volume variation in the increase direction can be adopted as the following form: 0

$$dp = \frac{\partial p}{\partial x}dx + \frac{\partial p}{\partial t}dt \tag{8}$$

$$\frac{\partial p}{\partial t} >> \frac{\partial p}{\partial x} \Rightarrow dp = \frac{\partial p}{\partial t}dt \tag{9}$$

The change in fluid volume can be calculated as follows with the relation: 0

$$dV_1 = \frac{\pi D_c^3}{4\delta E_c}\frac{\partial p}{\partial t}dtdx \tag{10}$$

Fluid volume compression causes the decrease of the initial volume according with the relation: 0

$$dV_2 = -\frac{1}{\varepsilon}Vdp = -\frac{1}{\varepsilon}\frac{\pi D_c^2}{4}dx\frac{\partial p}{\partial t}dt \tag{11}$$

The continuity equation can be considered that establishes the relationship between the volume functions and the circulated fluid level. 0

$$\frac{\pi D_c^2}{4}\frac{\partial v}{\partial x}dxdt = \frac{\pi D_c^3}{4\delta E_c}\frac{\partial p}{\partial t}dtdx + \frac{1}{\varepsilon}\frac{\pi D_c^2}{4}dx\frac{\partial p}{\partial t}dt \tag{12}$$

Because the pressure can be considered as $p = \gamma z$ and after simplification the continuity equation is obtained as: 0

$$\frac{\partial v}{\partial x} = \left(\frac{1}{\varepsilon} + \frac{1}{E_c}\frac{D_c}{\delta}\right)\gamma\frac{\partial z}{\partial t} \tag{13}$$

Fluid hammer phenomenon determines the pressure waves appearance whose propagation along the circular pipe is described by the specific propagation equation. This equation is obtained from the derivation in relation to space and time of the equation of motion and continuity. With a special notation introduced and derivation in range with space and time the propagation equations are obtained: 0

$$\frac{g}{a^2} = \left(\frac{1}{\varepsilon} + \frac{1}{E_c}\frac{D_c}{\delta}\right)\gamma \tag{14}$$

$$\frac{\partial^2 z}{\partial x^2} = \frac{1}{a^2}\frac{\partial^2 z}{\partial t^2};\ \frac{\partial^2 v}{\partial x^2} = \frac{1}{a^2}\frac{\partial^2 v}{\partial t^2} \tag{15}$$

The disturbances produced as a result of the fluid stopping after JUKOVSCHI are described as follows: 0

$$dp = -\rho\frac{dx}{dt}dv \tag{16}$$

$\frac{dx}{dt}$ = c_p representing the pressure wave propagation velocity.

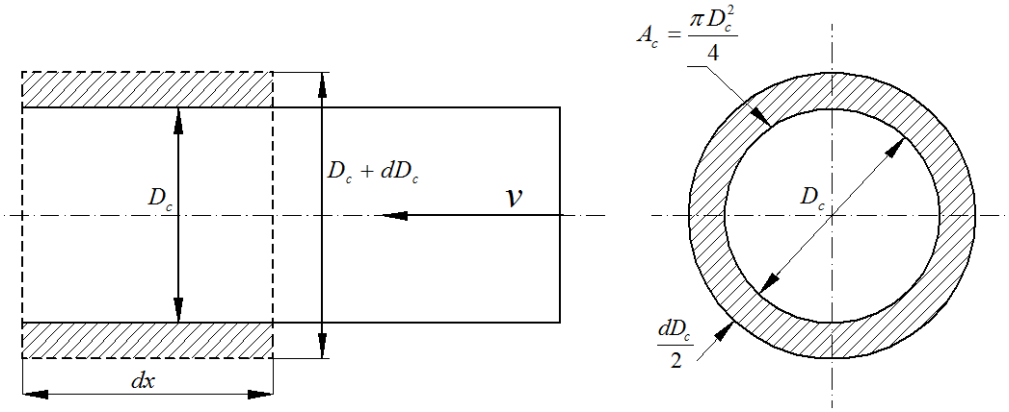

Fig. 2. Pressure disturbances on a circular duct (dx) length and radial deformation (dD_c) 0

The pressure increase maximum value within the pipe is considered at complete valve closing, which means fluid velocity reduction to zero value: 0

$$\Delta p = -\rho c_p v \tag{17}$$

After a time interval (dt) the pressure disturbance has reached a length of pipe (dx) and the fluid mass contained in this space is: 0

$$dm = \rho A_c dx \tag{18}$$

Another fluid amount reaches this region which by braking remains in space (dx): 0

$$d(dm) = \rho A_c dv dt \tag{19}$$

The extra fluid mass acts to change the fluid density (ρ) and for pipe radial deformation (dD_c): 0

$$d(dm) = dx(A_c d\rho + \rho dA_c) \tag{20}$$

By equalizing the relations, it is obtained: 0

$$A_c dv dt = dx(A_c d\rho + \rho dA_c) \tag{21}$$

$$dv = -c_p\left(\frac{d\rho}{\rho} + \frac{dA_c}{A_c}\right) \tag{22}$$

Replacing with the fluid compressibility coefficient $\left(\beta = \frac{1}{\varepsilon}\right)$ is obtained: 0

$$\frac{d\rho}{\rho} = \beta dp = \frac{dp}{\varepsilon} \tag{23}$$

Modification of the pipe section is described by the term $\left(\frac{dA_c}{A_c}\right)$, with $A_c = \frac{\pi D_c^2}{4}$: 0

$$\frac{dA_c}{A_c} = \frac{\frac{\pi D_c dD_c}{2}}{\frac{\pi D_c^2}{4}} = 2\frac{dD_c}{D_c} \tag{24}$$

Considering the Hooke law can be written: 0

$$d\sigma = E_c \frac{dD_c}{D_c} = \frac{D_c dp}{2e} \Rightarrow 2\frac{dD_c}{D_c} = \frac{D_c dp}{eE_c} = \frac{dA_c}{A_c} \tag{25}$$

$$dv = -\frac{dp}{\rho c_p} = -c_p\left(\frac{dp}{\varepsilon} + \frac{D_c dp}{eE_c}\right) \Rightarrow c_p = \sqrt{\frac{1}{\frac{\rho}{\varepsilon} + \frac{\rho D_c}{eE_c}}} \tag{26}$$

It is known that the ratio $\frac{\varepsilon}{\rho} = c_0^2$ represents the sound velocity within the respective fluid, further can be written:

$$c_p = \frac{c_0}{\sqrt{1 + \frac{\varepsilon D_c}{eE_c}}} \tag{27}$$

The obtained relation represents the analytical expression that describes the pressure waves propagation velocity through elastic circular pipes, also called the JUKOVSCHI-ALLIEVI relation.
It can be seen that the propagation velocity depends on the pipe diameter (D_c), the wall thickness (e), the pipe material elasticity modulus (E_c), as well as the elastic properties of the fluid in the pipe (ε). 0

4. Pressure wave propagation

The calculation is performed in order to determine the specific pressure wave propagation velocity values for high density polyethylene pipes, with a diameter of 110 mm, but for different pressure groups, which means different values of the pipe wall thickness.
The specific values of the pipe wall thickness and the pressure groups at which they can be used are presented in Table 1.

Table 1: The pipe wall thickness and pressure values 0

Polyethylene pipes (PE 100)							
Pn=6 bar	Pn=6 bar	Pn=8 bar	Pn=10 bar	Pn=12.5 bar	Pn=16 bar	Pn=20 bar	Pn=25 bar
$e\,[mm]$							
4	4.2	5.3	6.6	8.1	10	12.3	15.1

The specific values of the pressure wave propagation speed were calculated using the JUKOVSCHI-ALLIEVI formula, and the results are presented in the figure 3 diagram.

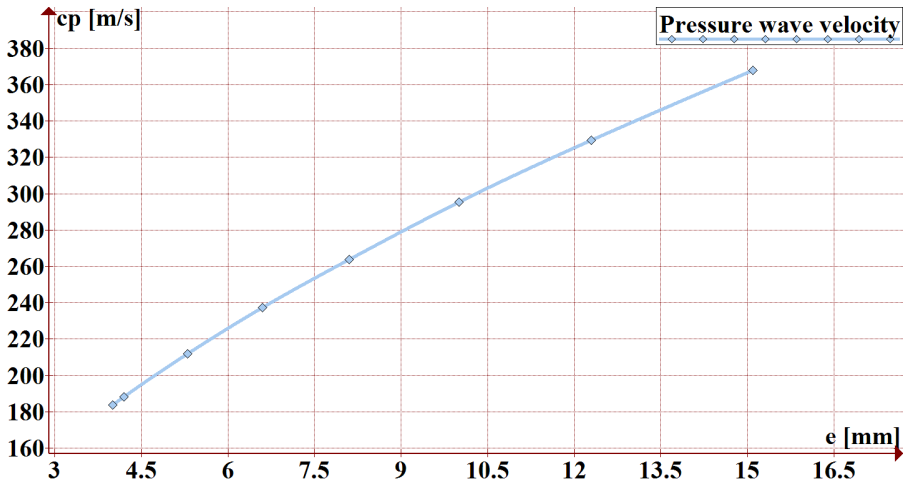

Fig. 3. Pressure wave propagation velocity function of pipe wall thickness

5. Numerical analysis on pipe virtual model

The numerical analysis method performed with ANSYS Fluent is used in order to highlight the fluid hammer effect on the virtual model of a high-density PE pipe with a diameter of 110 mm.
Water inlet with a velocity of 2 m/s is declared, being circulated inside the pipe, and at half distance a valve is placed which is in the half-open position at an angle of 45 degrees to the vertical direction.
The valve position forms a resistance to the fluid flow through the pipe, so that an increase in pressure values is obtained in the valve upstream region, and in the space between the closing element and the pipe wall flow velocity increased rates are obtained (fluid is laminated in the restricted area).
The results are presented in figure 4 in terms of pressure and velocity in the analyzed fluid area, being highlighted the specific values in the valve area which is considered as a resistance in the fluid flow path.

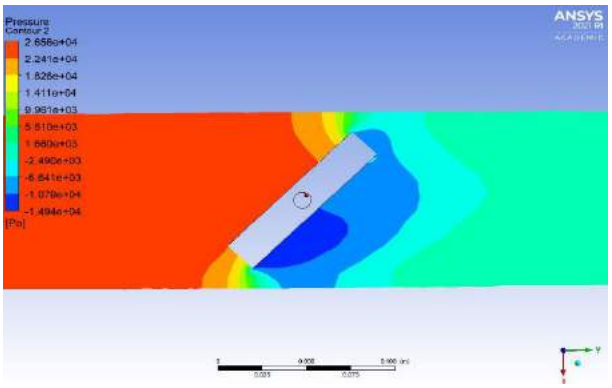

a) pressure values

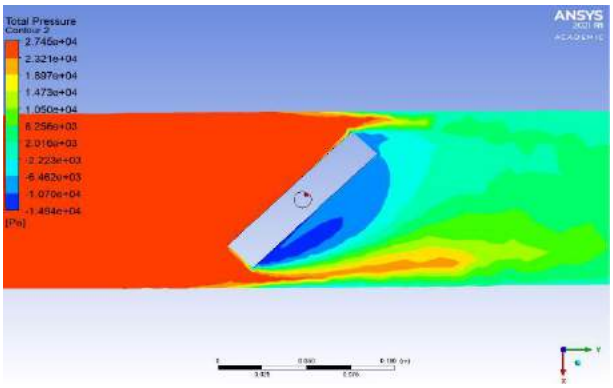

b) total pressure values

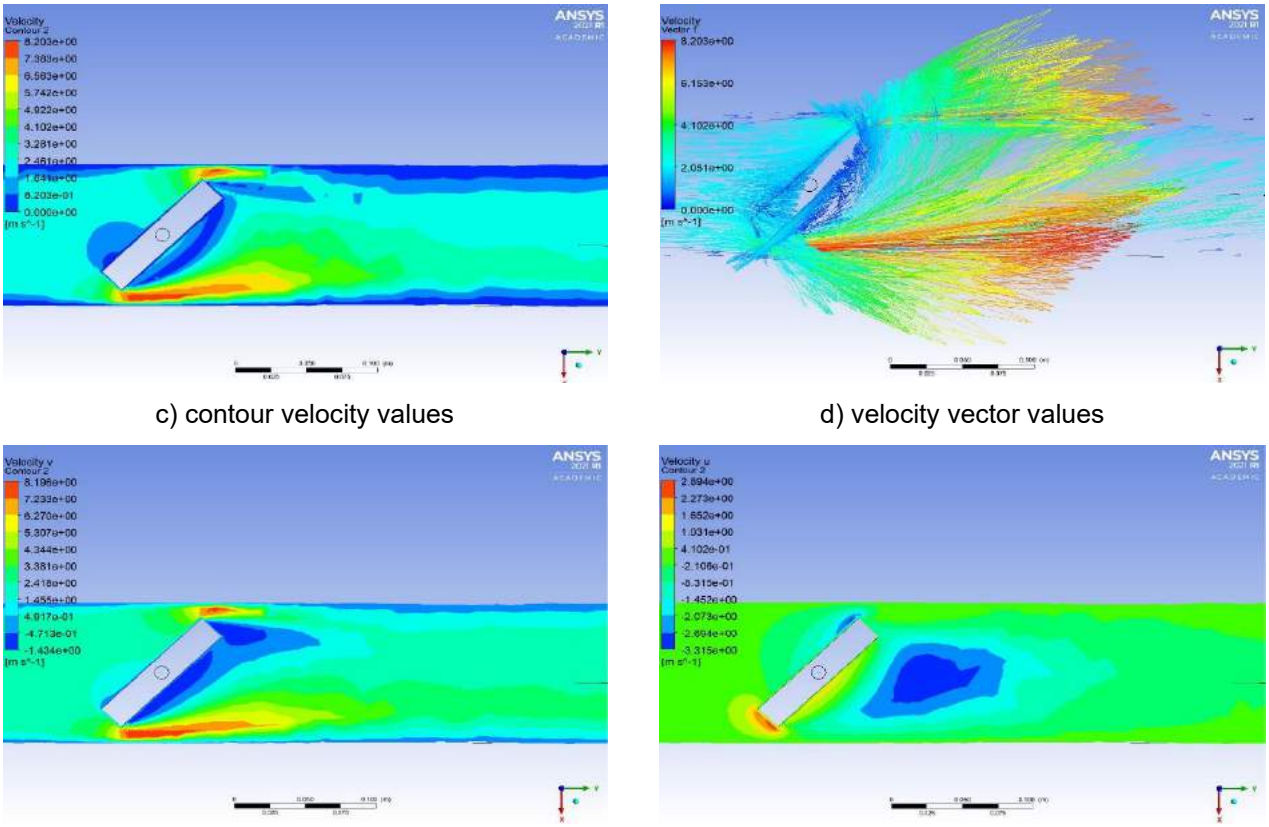

c) contour velocity values

d) velocity vector values

d) contour velocity v values

e) velocity vector u values

Fig. 4. Fluid flow analysis results

It can be seen that when the valve is suddenly closed, a maximum pressure value is obtained in the area upstream of the valve, and the flow velocity values record the maximum in the area between the valve wall and the pipe wall where the fluid is forced to flow.
The results indicate that for this model of pipe is not exceeded the maximum pressure value of 6 bar for which the pipe is designed to withstand, but depending on the values of circulation speed this value can be exceeded, this being an unfavourable case in practice.

6. Conclusion

The theoretical aspects related to the fluid hammer phenomenon were presented in this paper, being highlighted the importance of this phenomenon for the fluid flow through a circular pipe.
The case of high-density polyethylene pipes used for urban water circulation was presented.
The specific values of the pressure wave propagation velocity were calculated for different wall thicknesses corresponding to the working pressure groups for which they are used.
A numerical analysis was also performed for water flow through the 110 mm outer diameter polyethylene pipe.
For a declared value of the circulation speed of 2 m/s, an increase of the total pressure of up to 2.7 atm in the area upstream of the shut-off valve was obtained.
The fluid velocity values are maximum in the area between the pipe wall and the valve wall reaching the values of approx. 8 m/s, which explains the fact that in this area the fluid is forced to circulate through lamination.

References

[1] Axinti, G., and A. S. Axinti. *Hydraulic and pneumatic drives - Components and systems, functions and characteristics / Actionari hidraulice si pneumatice – Componente si sisteme, functii si caracteristici*. Chisinau, Tehnica-Info Publishing House, 2008.
[2] Vasilescu, Al. A. *Fluid mechanics / Mecanica Fluidelor*. Galati, University of Galati, 1979.

[3] Florescu, I. *Fluid mechanics. Course notes for student use / Mecanica fluidelor. Note de curs pentru uzul studentilor*. Bacau, Alma Mater Publishing House, 2007.
[4] Scurtu, I. C., C. Clinci, and A. Popa. ″Water interference effect on ship due to square shaped object shielding.″ *IOP Conference Series: Earth and Environmental Science* 172 (2018): 012030.
[5] Popa, A., and I. C. Scurtu. "CFD Results On Propeller Analysis.″ *“Mircea cel Batran” Naval Academy Scientific Bulletin* 20, no. 2 (2017): 124-131.
[6] Todicescu, Al. *Fluid mechanics and hydropneumatic machines / Mecanica Fluidelor și mașini hidropneumatice*. Bucharest, Didactic and Pedagogical Publishing House, 1974.
[7] https://www.valrom.ro/media/media/Carte_tehnica_PEHD.pdf.
[8] Livescu, S., S. Craig, and B. Aitken. ″Fluid-hammer effects on coiled-tubing friction in extended-reach wells.″ *SPE Journal* 22, no. 01 (August 2018): 365-373.
[9] Han, G., M. Bruno, and T. Grant. "Lab investigations of percussion drilling: from single impact to full scale fluid hammer.″ Paper presented at Golden Rocks 2006, The 41st US Symposium on Rock Mechanics (USRMS), Golden, Colorado, June 17-21, 2006.
[10] Shin, Y. W., and R. A. Valentin. "Numerical analysis of fluid-hammer waves by the method of characteristics.″ *Journal of Computational Physics* 20, no. 2 (1976): 220-237.
[11] Streeter, V. L., and C. Lai. ″Water-hammer analysis including fluid friction.″ *Transactions of the American Society of Civil Engineers* 128, no. 1 (1963): 1491-1524.
[12] Shin, Y. W., and W. L. Chen. "Numerical fluid-hammer analysis by the method of characteristics in complex piping networks.″ *Nuclear Engineering and Design* 33, no. 3 (1975): 357-369.
[13] Staysko, R., B. Francis, and B. Cote. ″Fluid hammer drives down well costs.″ Paper presented at SPE/IADC Drilling Conference and Exhibition, Amsterdam, the Netherlands, March 1 – 3, 2011.
[14] Azhdari, M., A. Riasi, and P. Tazraei. ″Numerical analysis of fluid hammer in helical pipes considering non-Newtonian fluids.″ *International Journal of Pressure Vessels and Piping* 181 (2020): 104068.
[15] Zhang, W., H. Shi, G. Li, and X. Song. "Fluid hammer analysis with unsteady flow friction model in coiled tubing drilling.″ *Journal of Petroleum Science and Engineering* 167 (2018): 168-179.
[16] Oliveira, G. M., A. T. Franco, and C. O. Negrão. ″Mathematical Model for Viscoplastic Fluid Hammer.″ *Journal of Fluids Engineering* 138, no. 1 (January 2016): 011301.
[17] Lema, M., F. L. Peña, P. Rambaud, J. M. Buchlin, and J. Steelant. "Fluid hammer with gas desorption in a liquid-filling tube: experiments with three different liquids.″ *Experiments in Fluids* 56, no. 9 (2015): 1-12.
[18] Pavlou, D. G., and M. C. Ong. "Damping effect on the wave propagation in carbon steel pipelines under fluid hammer conditions.″ *Journal of Offshore Mechanics and Arctic Engineering* 139, no. 4 (August 2017): 041702.
[19] Huang, Z. Y., and Y. J. Liu. ″Characteristics of laminar MHD fluid hammer in pipe.″ *Journal of Magnetism and Magnetic Materials* 397 (2016): 213-224.
[20] Peveroni, L., C. Esposito, J. Pinho, J. Steelant, and J. B. Gouriet. ″Hydro-thermodynamic behavior of a hydraulic restriction in liquid nitrogen in steady-state and fluid-hammer conditions.″ Paper presented at Aerospace Europe Conference, Bordeaux, France, February 25--28, 2020.
[21] Aliabadi, H. K., A. Ahmadi, and A. Keramat. "Frequency response of water hammer with fluid-structure interaction in a visco-elastic pipe.″ *Mechanical Systems and Signal Processing* 144 (2020): 106848.

Choosing an Economical Solution for Water Aeration

PhD Std. **Nicoleta Dorina ALBU**[1], Prof. Dr. Eng. **Nicolae BĂRAN**[1],
Șl. Dr. Eng. **Mihaela CONSTANTIN**[1]*

[1] University Politehnica of Bucharest

* i.mihaelaconstantin@gmail.com

Abstract: *The paper presents four versions for increasing the concentration of dissolved oxygen in water:*
I - Introduction of atmospheric air,
II - Introduction of atmospheric air and oxygen from a cylinder in certain proportions,
III - Introduction of a low nitrogen gas (95% O_2 + 5% N_2),
IV - Introduction of atmospheric air and ozone produced by an ozone generator.
Following some calculations, the most economical version was chosen, namely version III.

Keywords: *Water aeration, water oxygenation, energy consumption, dissolved oxygen concentration.*

1. Introduction

Aeration of water can be achieved by agitation at the surface (generally performed by mechanical aerators) by introducing air at the base of the tank, lake, etc. (aeration by pneumatic installations) or by spraying air with a device to allow the exchange of oxygen at the surface and the release of harmful gases. Thus, the aeration process can be performed, depending on the dispersion mode, with the help of [1] [2]:
a) Mechanical aeration installations;
b) Pneumatic aeration installations;
c) Mixed aeration installations
Initially, the aeration of the waters was ensured by mechanical aeration installations. Atmospheric air was introduced into the liquid mass by agitation at the surface of the water. In recent years, emphasis has been placed on the development of new methods of water aeration [3] [4].
Mechanical aeration systems are mechanical aggregates that provide hydrodynamic movements to disperse water in drops or films, in order to obtain a contact surface, as large as possible, between water and atmospheric air, and which homogenizes dissolved oxygen in the water mass [5] [6].
According to the location of the active organ, mechanical aeration systems are classified in [5]:
a) mechanical surface aeration installations (mechanical aerators with slow or fast rotor and vertical axis, aeration brushes);
b) medium depth mechanical aeration installations at which the active organ is located at a depth of 1 ... 2 m from the static water level in the tank;
c) mechanical deep aeration installations with the rotor located at about 4 ... 6 m from the static water level.

2. Installations for the introduction of gas mixtures into water

2.1 Version I: Installation for the introduction of atmospheric air into water

The installation for blowing atmospheric air into water is shown in Figure 1.

Fig. 1. Overview of the experimental installation for the introduction of atmospheric air

On the left side of figure 1, there is a computer, an electro compressor and a rotameter.

2.2 Version II: Installation for the introduction of a mixture of atmospheric air and oxygen from a cylinder

In figure 2 are distinguished:
- On the left is a computer and the electric compressor with the air tank;
- In the centre one can see the oxygen cylinder provided with pressure reducer and manometer;
- On the right is the transparent plexiglass parallelepiped tank.

Fig. 2. Overview of the experimental installation for the introduction of a mixture of gases (atmospheric air and oxygen)

Two hoses are inserted into the tank through which the microbubble generator (MBG) with a mixture of air and oxygen. The air flow rate and oxygen flow rate are measured separately with a rotameter; the air and oxygen are mixed in a mixing chamber and then the mixture reaches the MBG through two hoses connected at the two ends of the MBG.

2.3 Version III: Installation for the introduction of a low nitrogen gas

In figure 3 two oxygen concentrators are observed on the left side. The gas passes through a rotameter embedded in each oxygen concentrator and then the gas pressure and temperature at the inlet to the MBG.

Fig. 3. Overview of the experimental installation for the introduction of a low nitrogen gas

The atmospheric air aspirated from the atmosphere passes through a filter, is compressed and sent to the zeolite filters; here nitrogen is retained so that at the exit of the device a gas containing 95% oxygen is obtained. Each oxygen concentrator delivers 300 dm^3 / h.

2.4 Version IV: Installation for the introduction of a gas mixture made of atmospheric air and ozone

The TCB-300O3 ozone generator is a complex and controllable automatic device for decontamination of indoor air. The ozone generator TCB - 300O3 has a hard plastic body with degree of protection IP-56, which allows the use of this device in different conditions and spaces - residential, industrial, etc.
In figure 4 the ozone generator connected to the pipes of the water oxygenation installation is presented, and in figure 5, the electronic part of the ozone generator is observed.

Fig. 4. Plan view of the ozone generator connected to the pipelines

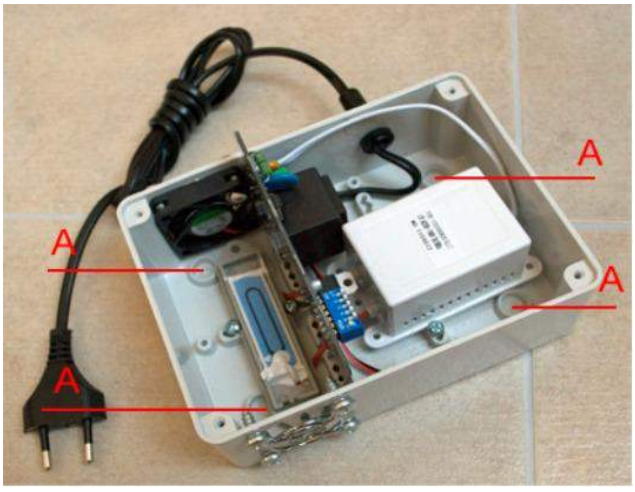

Fig. 5. Ozone generator components

The above installations are equipped with devices for measuring the flow rate and temperature of the conveyed fluids, devices with digital indication.

3. Theoretical determination of energy consumption, for the four studied versions

Problem formulation: what are the energy consumptions and the costs to reach from an initial concentration (C_0) to a saturation concentration (C_s) of dissolved oxygen in water in the case of the four studied versions?

3.1 Version I: Introduction of atmospheric air into water

For version I, 0.6 m^3/h of atmospheric air is introduced into the water. Energy E is the product of the consumed power P_I [kW] and the operating time of the installation τ [h].
For version I one can obtain:

$$E_I = P_I \cdot \tau_I \ \ [kWh] \tag{1}$$

$$P_t = \frac{n}{n-1} \cdot p_1 \cdot \dot{V}_a \cdot \left(\varepsilon^{\frac{n-1}{n}} - 1 \right) \cdot \frac{1}{10^3} \ \ [kW] \tag{2}$$

where:
n is the polytropic exponent n = 1.3;
p_1 - suction pressure of the compressor: p_1 = 1 bar;
$\dot{V}_a$ - volumetric flow rate of air sucked by the compressor: $\dot{V}_a = \frac{0.6}{3600} \ [m^3/s]$;
ε - compression ratio ε = 1.5.

$$P_t = \frac{1.3}{1.3-1} \cdot 1 \cdot 10^5 \cdot \frac{0.6}{3600} \cdot \left(1.5^{\frac{1.3-1}{1.3}} - 1 \right) \cdot \frac{1}{10^3} \ \ [kW]$$

$$P_t = 0.00705 = 7 \cdot 10^{-3} \ \ [kW]$$

Admitting an efficiency of the η_{agr} unit, compressor + electric drive motor, of 0.5, results in the real drive power:

$$P_I = \frac{P_t}{\eta_{agr}} = \frac{7 \cdot 10^{-3}}{0.5} = 14 \cdot 10^{-3} \ \ [kW] \tag{3}$$

The operation time of the installation is two hours, so the mechanical consumed energy to reach from C_0 to C_s will be:

$$E_I = P_I \cdot \tau_I = 14 \cdot 10^{-3} \cdot 2 = 28 \cdot 10^{-3} [kWh] \tag{4}$$

It is known that the average efficiency of a coal-fired power plant is about 30%, as a result of the electricity absorbed from the electricity network in the case of the first version will be:

$$E_{I,el} = \frac{E_I}{\eta_{CTE}} = \frac{0.028}{0.3} = 0.0933 \left[kWh \right] \tag{5}$$

3.2 Version II: Introduction of a mixture of atmospheric air and oxygen from a cylinder

For the four cases from version II the volume of gas aspirated by the compressor will be: $\dot{V}_a$ = 0.6/3600 m^3/s, and the compression ratio is ε = 1.5, the same as in version I.
As a result, the electricity absorbed from the grid will be the same:

$$E_{II,el} = \frac{E_I}{\eta_{CTE}} = \frac{0.028}{0.3} = 0.0933 \left[kWh \right] \tag{6}$$

3.3 Version III: Introduction of a low nitrogen gas

The oxygen concentrator type PLATINUM (2 pieces) used in the installation provides 300 dm^3/h of O_2, so both work with 600 dm^3/h = 0.6 m^3/h.
From the technical data of the oxygen concentrator, it results that the maximum pressure at the outlet of the compressed gas is 0.35 bar, so the compression ratio compared to version I will be:

$$\varepsilon^{\frac{n-1}{n}} \rightarrow \varepsilon = 1.35^{\frac{1.3-1}{1.3}} < 1.5^{\frac{1.3-1}{1.3}} \Leftrightarrow 1.35^{0.23} < 1.5^{0.23} \Leftrightarrow 1.071 < 1.007$$

As a result, the electricity consumed from the network will be lower:

$$E_{III} = \frac{1.071}{1.007} = 0.09756$$

$$E_{III} = 0.0933 \cdot 0.09756 = 0.0900 \left[kWh\right] \tag{7}$$

$$E_{III} < E_I$$

3.4 Version IV: Introduction of a gas mixture made of atmospheric air and ozone

Air + ozone is introduced into the installation; the air flow rate and the air pressure are the same as in version I; here appears an electricity consumption of the ozone generator.
To the $E_{I,el}$ = 0.0933 [kWh] value the electricity consumption of the ozone generator is added; from the package leaflet E_{ozon} = 0.04 [kWh].

$$E_{IV} = E_{I,el} + E_{ozon} = 0.0933 + 0.04 = 0.1333\left[kWh\right] \tag{8}$$

The theoretically calculated values are presented in table 1.

Table 1: Theoretically calculated values

No.	Introduced gas	Operating time $C_0 \rightarrow C_s$ [т]	Value C_s [mg O_2/dm^3]	Time to reach C_s	Consumed electricity [kWh]
I	Atmospheric air	2 h	8.40	2h	0.0933
II	Case I-Air + 25 % O_2	2 h	10.73	15'	0.0933
	Case II-Air + 50 % O_2	2 h	21.46	5'	0.0933
	Case III-Air + 75 % O_2	2 h	32.21	3'	0.0933
	Case IV-Air + 100 % O_2	2 h	43.00	2'	0.0933
III	Atmospheric air with low nitrogen content (95 %)	2 h	34.80	2.5'	0.0900
IV	Air + ozone	2 h	8.98	87'	0.133

From table 1 it is observed that following the theoretical calculations the most advantageous method would be version III.

4. Conclusions

The originality of the paper is reflected in the development of a methodology for performing experimental measurements.
To make a comparison between the four studied versions, the initial data such as: gas flow rate in water, compressed air pressure, initial concentration of dissolved oxygen in water, water temperature and duration of experience are the same; differing in the composition of the gaseous mixture blown from the water.
Following the evaluation of energy consumption, the most favourable version is version III.
In this case there is a short time at which the oxygen concentration from $C_0 \rightarrow C_s$ is reached.

References

[1] Robescu, D. L., S. Lanyi, A. Verestoy, and D. Robescu. *Modeling and simulation of treatment processes*/*Modelarea şi simularea proceselor de epurare*. Bucharest, Technical Publishing House, 2004.
[2] Stenstrom, M. K., and D. Rosso. *Aeration*. Los Angeles, University of California, 2010.
[3] Nistreanu, V. *Unitary processes for water treatment/Procese unitare pentru tratarea apelor*. Bucharest, AGIR Publishing House, 2000.
[4] Oprina, G. *Contributions to the hydro-gas-dynamics of porous diffusers/Contribuţii la hidro-gazo-dinamica difuzoarelor poroase*. Doctoral thesis. University Politehnica of Bucharest, Faculty of Power Engineering, 2007.
[5] Călușaru, I. *The influence of the physical properties of the liquid on the efficiency of the oxygenation processes/Influenţa proprietăţilor fizice ale lichidului asupra eficienţei proceselor de oxigenare*. Doctoral thesis. University Politehnica of Bucharest, Faculty of Mechanical and Mechatronics Engineering, 2014.
[6] Pătulea, Al. S. *The influence of the functional parameters and the architecture of fine bubble generators on the efficiency of aeration installations/Influenţa parametrilor funcţionali şi a arhitecturii generatoarelor de bule fine asupra eficienţei instalaţiilor de aerare*. Doctoral thesis. University Politehnica of Bucharest, 2012.

Hot Water Recirculation in High Rise Buildings to Reduce Water Consumption

Dipl. Eng. **Paul FRĂSIE**[1], Assoc. Prof. Dr. Eng. **Adriana TOKAR**[2]

[1] Pinchin Ltd., Canada, paul.frasie@yahoo.com

[2] Politehnica University Timisoara, Faculty of Civil Engineering, adriana.tokar@upt.ro

Abstract: *In present, water save has become essential in all regions, even where water seems abundant. The most effective way to save hot water from buildings plumbing is recirculation systems, but for high rise buildings the things are more complex. The article approaches an analysis of a 27-storey high-rise building with three recirculation pumps and associated heat exchangers. The lower head zone pumps and smaller local heat exchangers are used successfully. By using a low head pump instead of a high head pump it can be saved the operating cost, even though the initial cost of a small double wall plate heat exchanger and low head pump is comparable to the cost of a high head pump*.

Keywords*: Recirculation, Hot Water, High Rise Buildings, Water Consumption*

1. Introduction

Water is very precious resource being considered at the same time a renewable one; however, the percentage of usable water (fresh water) is decreasing while the population are increasing in number [1]. From the total of usable water available on the Earth, more than 68% is embedded in glaciers, and only 3% is usable water (Figure 1) [2, 3, 4].

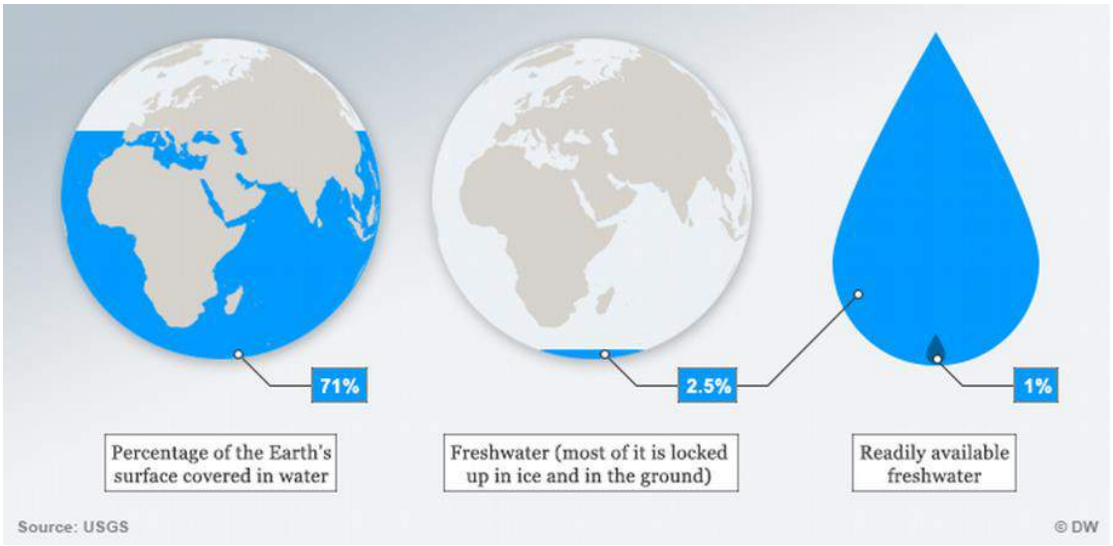

Fig. 1. Percentage of the water on the Earth [3]

Fresh water sources such as aquifers, lakes, and rivers are affected by the increased population, since are used to water supply to the communities. On the other hand, hydrotechnical construction and dams affected the rivers everywhere in the world. World river systems in percent of approximatively 60% were broken by the dams and other constructions, and just a small part of the big rivers in the world are flow freely.

From the above-mentioned reasons, and to reduce the water and energy consumption, it is important that engineers, designers, contractors involved in plumbing systems for residential and nonresidential sector, to optimize the hot water recirculation systems; this specially applies to high rise buildings. Hot water recirculation systems provide comfort and help to reduce the water consumption, ate the same time. In the modern world the human comfort and preservation of the

natural resources, such as water, go hand in hand; these imply the engineers and designers to find solutions.
Technical solution of the domestic hot water recirculation line (Figure2) implies a pipe which is installed parallel with the domestic hot water line which provides a continuous flow of hot water though the pipes and help to maintain warm water in the entire system [5].

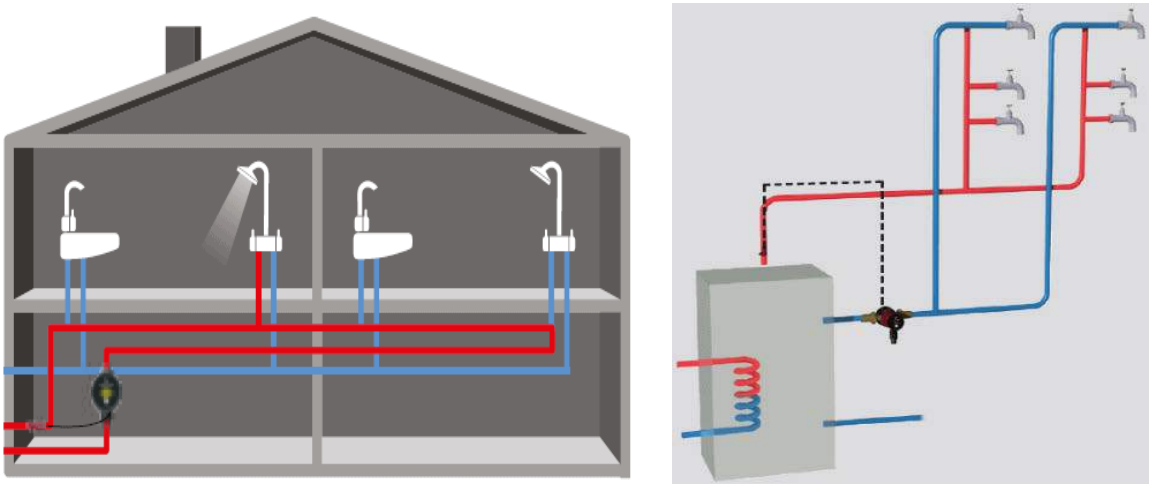

a) b)

Fig. 2. Domestic hot water classical recirculation systems [5]
a) water horizontal distribution, b) water vertical distribution

2. Building Statistics

As building owners evolve, and as building code officials may or may not become more stringent on energy use for new buildings, the actual performance of the base building system will mater more than ever. The performance of the building systems has a direct relationship with the overall operating cost. Operating costs tend to reoccur every month over the life of the building and must align with the owner's portfolio performance expectations.
For example, pumping systems are contributing to the success of performance of the base building system using alternative applications including variable frequency drives or water heaters with minimal or no storage.
On the other hand, pumping systems account for nearly 20% of the world's electrical energy demand and range from 25-50% of the energy usage in certain industrial plant operations [6].

In the World Energy Usage & Consumption (Figure 3):

- 70% of pumps electric motor power is used for pumps, fans, and compressors;
- 20% of the world's electricity is used in pumping;
- 50% of pumping energy is wasted.
-

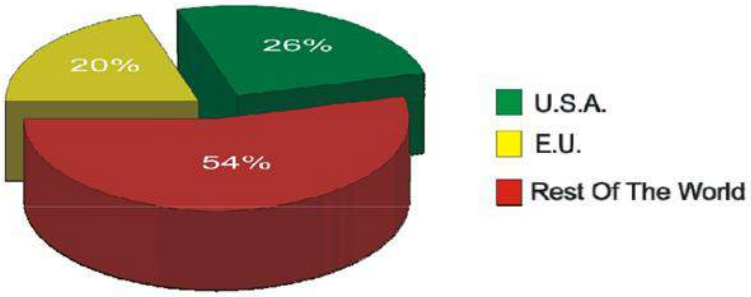

Fig. 3. World Energy Usage & Consumption [6]

3. WHY Recirculation?

The purpose of the domestic hot water recirculation lines is to maintain a minimum flow through the hot water risers at all times. This ensures that hot water is quickly available to all suites, even at times of low hot water use, like late at night.
On the other hand, hot water recirculation pumps are used in order to decrease the unnecessary throwing of cold water, which results in water and energy savings, and more convenience for the owner. Normally, recirculation pumps typically have fractional horsepower motors and run constantly.
For instance, in low rise building cases the recirculation works properly, because the circulators have to overcome friction as closed loop pumps.
In a high-rise building, the things are more complicated and complex. For example, a 27 – story high rise building will have three recirculation pumps and associated heat exchangers. (Note: A double wall plate heat exchanger is a special plate heat exchanger used for heating domestic hot water. It is virtually impossible for boiler water to contaminate the potable water because the plates are separated by air passages leading to the atmosphere. If a plate leaks for any reason, the liquid leaks out of the heat exchanger).
Water is boosted from the basement to the top of the building, and in the illustration shown in Figure 4 a, residual pressure of 275.7KPa (40psi) must be maintained; the total static pressure is 482.6KPa (76psi). This forces the water through the pressure reducing valves (PRVs) in each lower zone in order to avoid excessive pressure at the plumbing fixtures. For instance, the domestic hot water recirculation zone pumps DP-1A&1B&1C would be sized for 9GPM la 117.2KPa (17PSI), and the domestic hot water recirculation zone heat exchanger pumps DP-2A&2B&2C would be sized for 0.57L/S (9GPM) at 48.2 KPa (7PSI); the zone heat exchangers HX-1A&1B&1C is sized for a flow of 0.57L/S (9GPM) at Entering Temperature = 60°C (140°F) and Leaving Temperature = 48.8°C (120°F) (Figure 4 b).

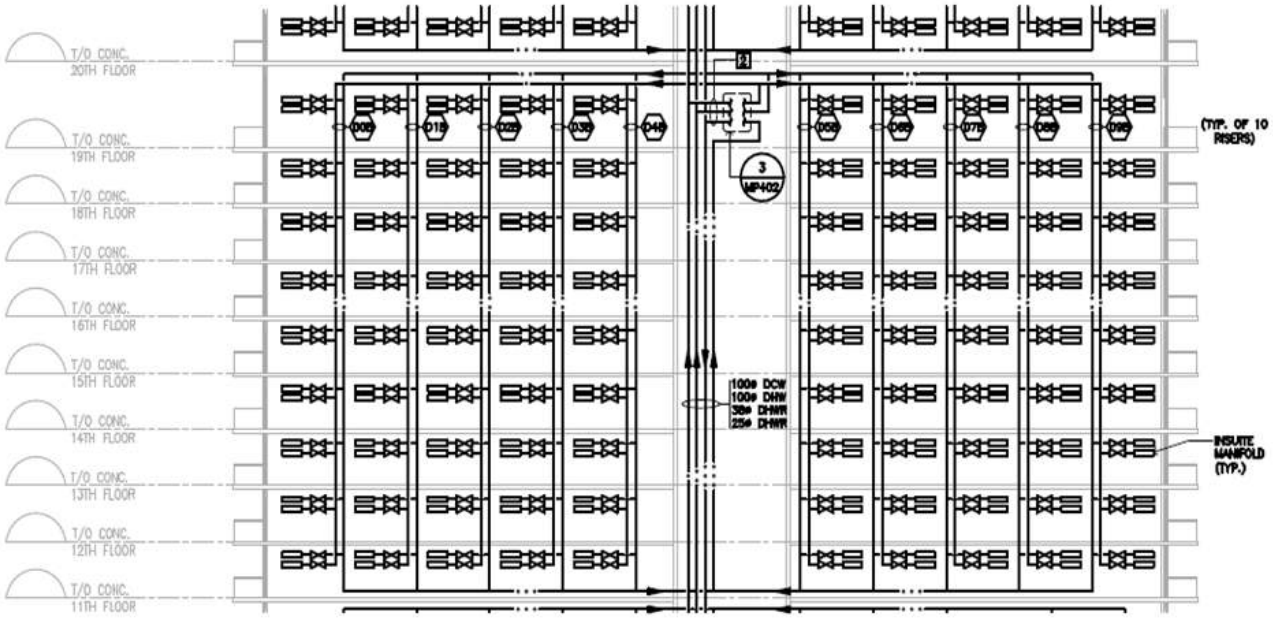

a)

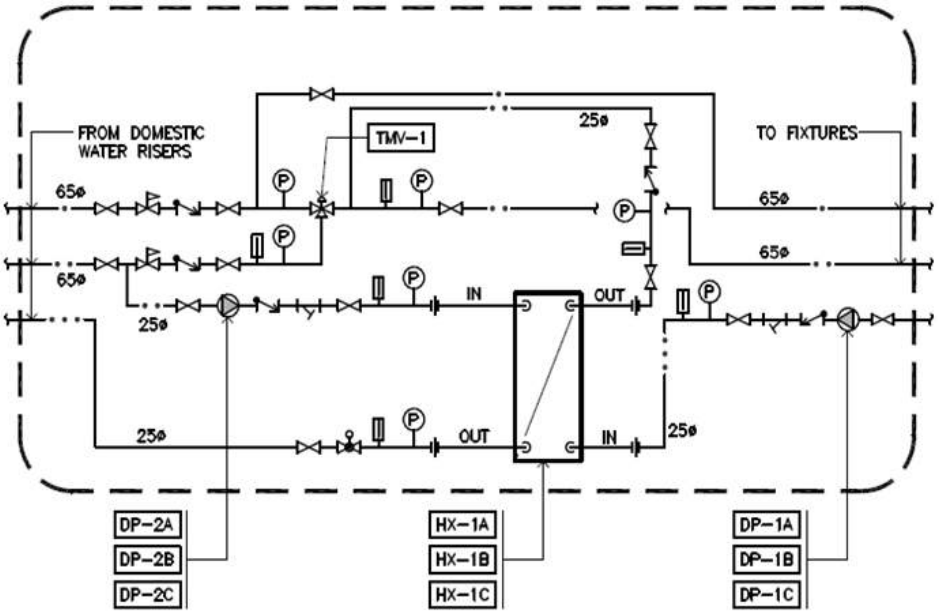

b)

Fig. 4. Proposed recirculation system
a) Capture of Domestic Water Riser Schematic, b) DHWR Zone Heat Exchanger Schematic

4. Design Phase Selection and Calculation

Bellow there is a short presentation of domestic cold water (DCW) and domestic hot water (DHW) systems design including the booster pumps [7, 8, 9, 10]:

- First it was found out what specific engineering codes, standards, and regulations are applicable
- In order to determine the size for the main water entry line it was calculated the domestic water load (both hot and cold water) based on the total number of the fixture units. Having the total fixture units and using the codes and standards it can be determined the total water demand in gallons per minute (GPM) and sized the main entry domestic line.
- Being a high-rise building (i.e., 27 floors) both DCW and DHW required booster pumps. It was calculated booster pumps capacity and head loss. For DCW calculation: First, it was determined the total pressure loss, which is based on total static height of the building, residual pressure at the most remote point (i.e., 275.7KPa (40psi), piping and fitting head losses (e.g., backflow preventer head loss = 89kpa (30ft)) and the received city water pressure (i.e., 241KPa (35psi). It was sized the pipes for a velocity less than 2.4 m/s (8 fps). Next, it was calculated the flow rate: Being a building with multiple apartments (i.e., 242 apartments), the diversity factor plays an important role in determining the total flow rate. For this calculation it was used three different sources: the method Frenkel Conversion [8], and Armstrong Pressure Booster System Chart for 242 suits [9]. For DHW booster pump calculation, it was followed the same procedure. It was designed pumps complete with variable frequency drives (VFDs). The design package for both cold and hot water consisted of two pumps connected in parallel that alternate on a weekly basis (i.e., LEAD and LAG system). The system was complete with hydropneumatic pressure tanks. The tanks were located in the mechanical penthouse and their role is to keep booster pumps off during very low demand at night time.
- Because the building has 27 stories (92.96-meter height (305 feet height) the static pressure is high and the Code states that maximum static pressure at the fixtures cannot exceed 550kPa~79,77PSI (1psi=2.31ft).

In this case the building was separated in three different zones for both cold and hot water:

- *Zone 1*: Ground Floor to 10th Floor- residual pressure 241.3 KPa (35 psi) and total static pressure 528.68 KPa (76.68psi);

- *Zone 2*: 11th Floor to 19th Floor- residual pressure 241.3 KPa (35 psi) and total static pressure 503.3KPa (73psi);
- *Zone 3*: 20th Floor to 27th Floor residual pressure 275.7KPa (40psi) and total static pressure 524KPa (76psi).

Each zone was complete with pressure reducing valves (PRVs) to avoid excessive pressures at plumbing fixtures.

The domestic hot water (DHW) was supplied by the two storage tanks via booster pumps. The domestic water storage tanks were fed from the main loop via a heat exchanger. From domestic storage water tanks, the DHW at 60°C (140ºF) is sent to the thermostatic mixing valve (TMV). The thermostatic mixing valve mixed domestic hot water (140ºF) from storage tank, with cold water 4.4°C (40ºF) from the City, and with recirculation water ~43.3 °C (~110ºF) from the building; the resulting domestic hot water that goes to the fixtures is 48.8°C (120ºF). (The send out temperature is low enough to help prevent accidental scalding; for public safety controlling temperature is very important). For DHW storage tanks calculation it was used two sources: ASHRAE Handbook - Service Water Heating - for 200 or more apartments, (Figure 5) [10], considering usable storage capacity per apartment = 30 liters/apartment (8 gallons/apartment) and recovery capacity = 13.2 liter/hour/apartment (3.5 gallons/hour/apartment) and Alfred Steel, hot water required per person= 75 liters/day (20 gal/day) [8, 9, 10].

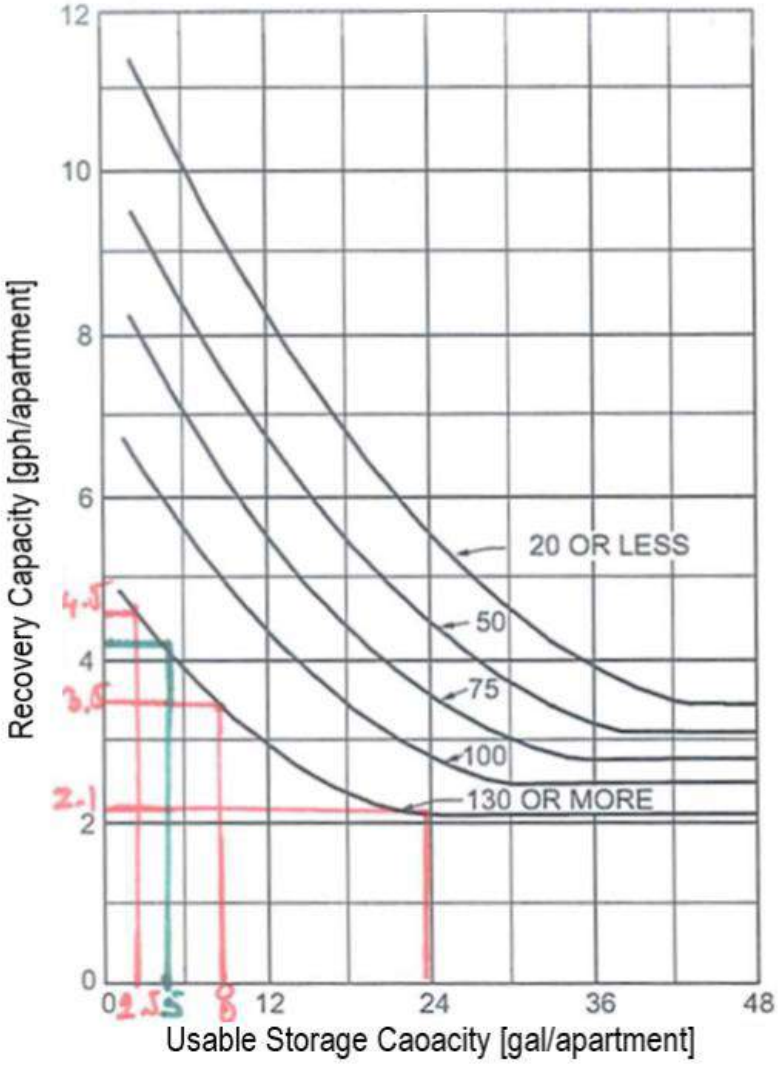

a)

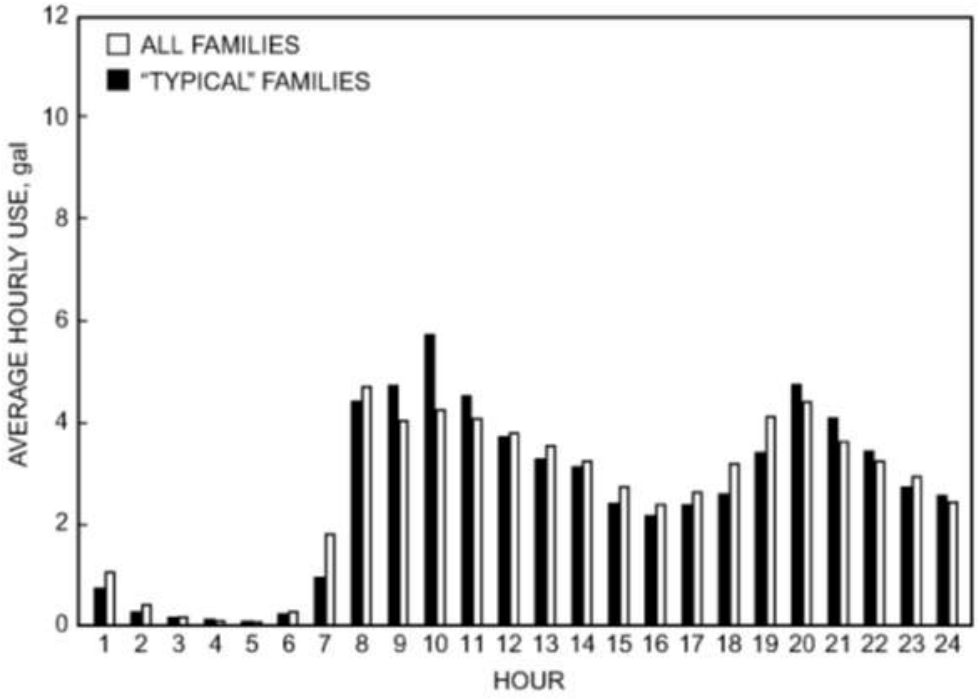

b)

Fig. 5. Diagram for DHW calculation
a) Calculation nomograms (Source: ASHRAE Handbook -Service Water Heating), b) Domestic Hot Water Profile (Source: ASHRAE Application Handbook)

6. Conclusion

As it can be seen, lower head zone pumps and smaller local heat exchangers can be used successfully. By using a low head pump instead of a high head pump it can be saved the operating cost, even though the initial cost of a small double wall plate heat exchanger and low head pump is comparable to the cost of a high head pump.
As technology advanced, we should be focusing on both efficiency and energy conservation. De-coupled recirculation provides benefits for both mentioned above.

References

[1] Tokar, A., D. Foriș, D. Tokar, and S. Popa-Albu. "Solutions for the Reuse of Rainwater in Indoor Plumbing." *Hidraulica Magazine*, no. 4 (2020): 51-58.
[2] Pantsios, A. "8 Shocking facts about water consumption", 2014. Accessed December 18, 2020. https://www.ecowatch.com.
[3] U.S. Geological Survey (USGS). "Summary of the Water Cycle." Accessed December 18, 2020. https://water.usgs.gov.
[4] World Wildlife Fund (WWF). "Freshwater: What's at stake, what we're missing, what we're losing, what it's worth." Accessed December 18, 2020. http://wwf.panda.org.
[5] Avram, N. "Hot water immediately after opening the tap by recirculating the hot water." Accessed December 17, 2020. https://www.trust-expert.ro.
[6] U.S. Department of Energy (U.S.DOE). "World Energy Usage and Consumption." Accessed December 17, 2020. https://www.energy.gov.
[7] The Authoritative Source for Plumbing, Hydronics, Fire Protection and PVF. *Plumbing Engineer* 2010 Edition, p. 60.
[8] Steele, A. *Engineered Plumbing Design 2 - Frenkel Conversion-Table - Maximum Probable Flow and Armstrong Pressure Booster System*. Miramar Publishing Company, p. 381, 1977.
[9] ***. *Armstrong Ltd. Installation and operating instructions*. Accessed December 18, 2020. https://www.pumpexpress.com.
[10] American Society of Heating, Refrigerating, and Air-Conditioning Engineers. *ASHRAE Handbook – Fundamentals*, 2017.

A New Type of Fine Bubble Generator Used to Water Aeration

PhD Std. **Nicoleta Dorina ALBU**[1], Prof. Dr. Eng. **Nicolae BĂRAN**[1],
Șl. Dr. Eng. **Mihaela CONSTANTIN**[1]*

[1] University Politehnica of Bucharest

* i.mihaelaconstantin@gmail.com

Abstract: *The paper presents a fine air bubble generator made by micro-drilling with a special KERN Micro machine. The perforated plate of the generator has 152 orifices with a diameter of 0.1 mm. The scheme of the installation, the researches methodology and the experimentally obtained results are presented.*

Keywords: *Fine bubble generator, water aeration, oxygen transfer*

1. Introduction

Aeration of water by means of pneumatic installations (or diffusion aeration) is defined by the process of insufflating atmospheric air or oxygen-enriched atmospheric air, under pressure, under the surface of a liquid. Oxygen transfer takes place through the contact surface between the air bubble and the surrounding liquid.
Air is introduced under pressure into the aeration system and is released by it in the form of columns of air bubbles. Thus, pneumatic water aeration systems can be classified according to the size of the bubble they produce [1] [2]:
• Aeration installations that produce large and coarse bubbles (with a bubble diameter> 3 mm);
• Aeration installations that produce medium bubbles (with a bubble diameter between 1-3 mm);
• Aeration installations that produce fine bubbles (with a bubble diameter between 0.1 mm and 1 mm);
According to the size of the diameter of the air bubbles, the bubbles can be classified as follows (figure 1):

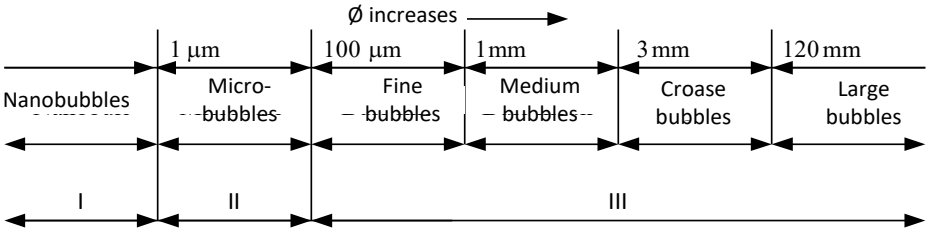

Fig. 1. Classification of gas bubbles according to their diameter [3]

According to the way the bubbles are obtained, the aeration installations fall into three categories [3] [4] [5]:
a) Aeration installations with drilled pipes;
b) Aeration installations provided with porous diffusers;
c) Aeration installations with fine bubble generators.
In recent years, researches on water aeration have focused on obtaining fine bubble generators in which the air supply orifices to the water have a diameter Φ <1 mm. Fine bubble generators have been built, the perforated plate being made by an unconventional technological process (spark-erosion); this process ensures a uniform distribution of the holes on the plate surface and an equal diameter of the holes [3] [4].
Fine bubble generators have applicability in several fields due to the efficiency of the aeration process and the low consumption of electricity, such as environmental protection (wastewater treatment), agriculture (rehabilitation of aquatic systems), health, food industry, chemical industry, etc. [6].

2. Installation scheme for introducing atmospheric air into water

The experimental installation is composed of (figure 2):
- Electro compressor with air tank (1), for the production of compressed air with the following functional parameters: maximum discharge pressure p = 8 bar, suction flow rate $\dot{V} = 600\ dm^3/h$, operating temperature t = (- 10 ÷ 100) ºC, electric motor power P = 1,1 kW, speed n = 2850 rpm, tank volume V = 24 dm^3. The electric compressor is equipped with a differential pressure manometer in the range 1 ÷ 16 bar to display the air pressure in the compressor tank and a pressure reducer (2), to determine the pressure in the system pipes.
- Plastic compressed air pipes, with inside diameter Ø 15 mm and a wall thickness of 2 mm; it supplies the microbubble generator with air and ensure the evacuation of the surplus air delivered by the compressor to the atmosphere.
- Aeration tank made of plexiglass plates with a thickness of 5 mm, measuring 0.5 x 0.5 x 1.6.
- The microbubble generator (MBG). This type of MBG was subjected to tests in an experimental installation built in the laboratories of the University POLITEHNICA of Bucharest. The orifices in the plate with d_0 = 0.1 mm were made using a C.N.C. (Computer Numerical Control) which has a special micro processing machine KERN Micro type.
- Oxygenometer probe actuation mechanism.

The scheme of the installation used to carry out the experimental researches is presented in figure 2.

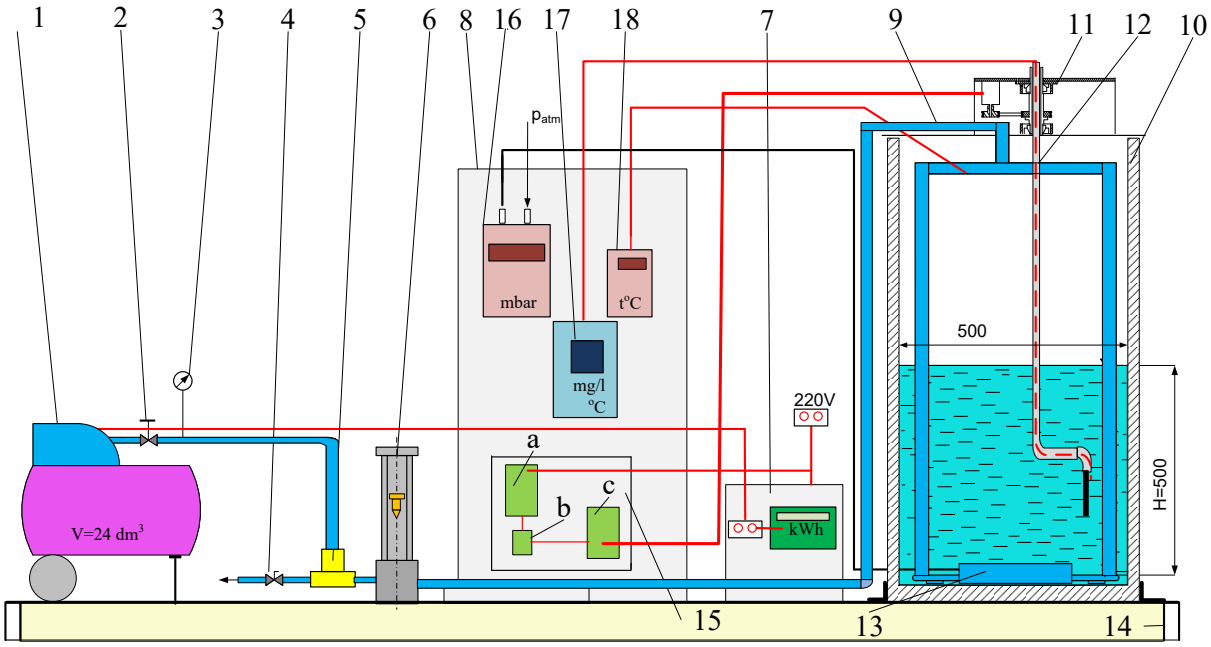

Fig. 2. Scheme of the experimental installation for research on water oxygenation
1 - electro compressor with air tank; 2 - pressure reducer; 3 - manometer; 4 - connection for evacuating air into the atmosphere; 5 – T-joint; 6 - rotameter; 7 - electrical panel; 8 - panel with measuring devices; 9 - pipe for transporting compressed air to the microbubble generator; 10 - water tank; 11 - mechanism of actuation of the probe; 12 - oxygenometer probe; 13 - microbubble generator; 14 - support for installation; 15 - control electronics: a - power supply, b - switch, c - control element, 16 - digital manometer; 17 - oxygenometer; 18 - digital thermometer

Figure 2 shows that, after compressing the air, the air temperature, pressure and flow rate are measured; subsequently it is introduced in MBG with the parameters: $\dot{V} = 600\ dm^3/h$, p = 573 mm H_2O.
The duration of the experiments is 2 hours, during which time the dissolved oxygen concentration in the water increases from C_0 to C_s.
Taking into account the volume flow of the gas, an air velocity results through the MBG supply line [7].

$$\dot{V} = A \cdot w \tag{1}$$

$$w = \frac{\dot{V}}{A} = \frac{\dot{V}}{\frac{\pi \cdot d_i^2}{4}} = \frac{600 \cdot 10^{-3}}{3600} \cdot \frac{1}{0.785 \cdot (0.012)^2} \tag{2}$$

$$w = 1.474 \ \ m/s \tag{3}$$

As a result, the Reynolds number is $Re = \frac{w \cdot d_i}{\upsilon} = \frac{1.474 \cdot 0.012}{16 \cdot 10^{-6}} = 1105.5$, so the theoretical flow regime is laminar.

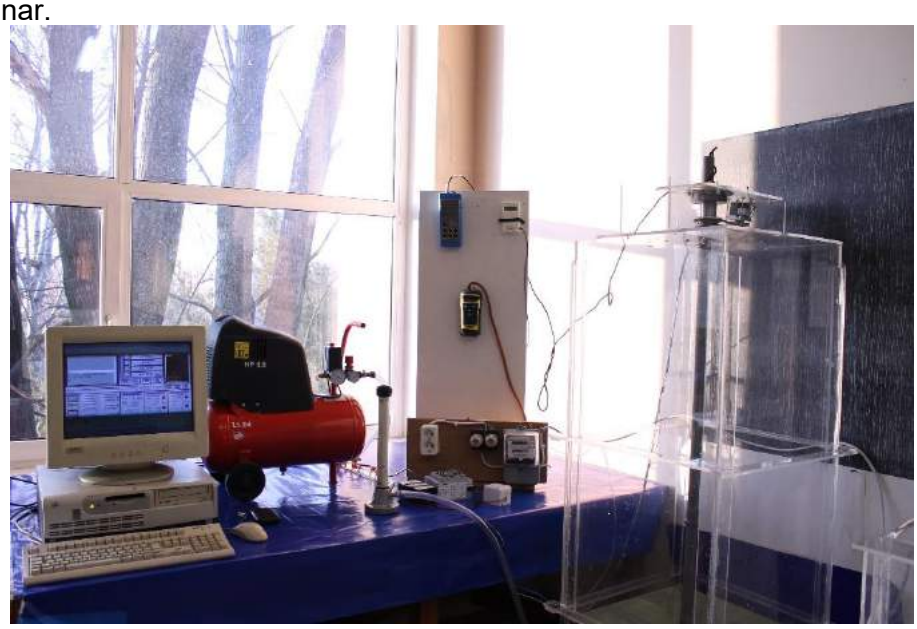

Fig. 3. Overview of the experimental installation for the introduction of atmospheric air

The installation for the introduction of atmospheric air into water is shown in figure 3.

3. Experimental researches

The experimental researches carried out in the laboratory of the Department of Thermotechnics, Engines, Thermal and Refrigeration Equipment's aimed the experimentally determination of the variation of the dissolved oxygen concentration in water as a function of time.
For each measurement stage, the following phases follow one another:
-The pressure test of the fine bubble generator is performed;
-Fill the tank with water up to H = 0.5 m;
-Measure the initial concentration of dissolved oxygen in water C_0 (mg / dm^3);
-Measure the water temperature in the tank and the air temperature;
-Introduce the fine bubble generator into the water and note the time of beginning the experiment;
-The flow rate and the pressure of the compressed air are measured and kept constant with the help of the control valves;
-After 15 minutes, the oxygenation of the water is stopped and the oxygenometer probe is inserted in the water;
- The electro-mechanism of actuating the probe is started, which ensures a speed of 0.3 m / s; when the value of the oxygen concentration on the oxygenometer screen stabilizes, it means that the measurement has been completed;
-The oxygen meter probe is lifted from the tank;
-Restart the oxygenation system and note the time.
From previous researches [8][9][10][11][12] it was found that by blowing an air flow $\dot{V} = 600 \ \ dm^3/h$ in the water tank with hydrostatic load of H = 0.5 m with a volume of water (0.5 x 0.5 x 0.5 =

0.125m^3), the dissolved oxygen concentration in water approaches the value of the saturation concentration after a time τ = 2 h.
The dissolved oxygen concentration in water was measured at equal time intervals: τ = 0 min; τ = 15 min; τ = 30 min; τ = 45 min; τ = 60 min; τ = 75 min; τ = 90 min; τ = 105 min; τ = 120 min.

4. Experimental obtained results

The operation of the MBG of rectangular shape with 152 orifices with a diameter of Ø 0.1 mm is shown in figure 4.

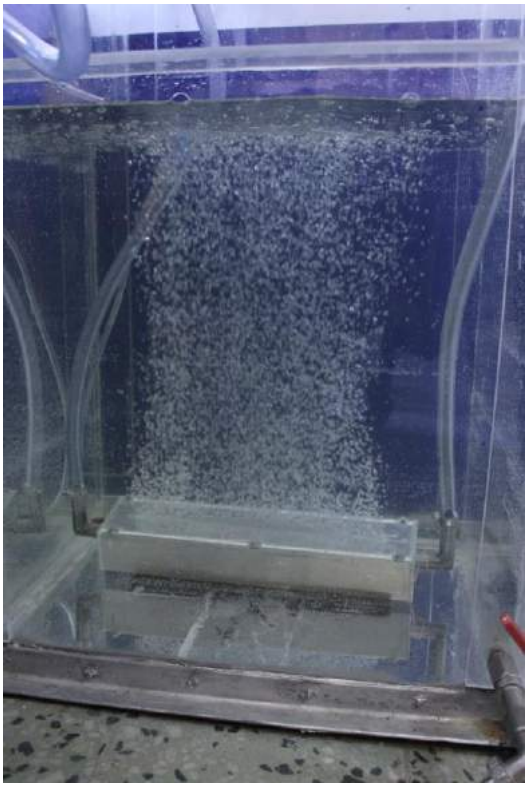

Fig. 4. Microbubble generator with 152 orifices Ø 0.1 mm in operation

Following the performed measurements, the data in Table 1 were obtained.

Table 1: Values of the concentration as a function of time

τ [min]	0	15	30	45	60	75	90	105	120
$\dot{V}_{air}\,[dm^3/h]$	600	600	600	600	600	600	600	600	600
$\dot{V}_{IO_2} = 0.21 \cdot 600 = 126\ [dm^3/h]$	126	126	126	126	126	126	126	126	126
$\dot{V}_{O_2}$ from other sources	0	0	0	0	0	0	0	0	0
t_{H2O} [°C]	23.7	23.7	23.7	23.7	23.7	23.7	23.7	23.7	23.7
t_{air} [°C]	24.1	24.1	24.1	24.1	24.1	24.1	24.1	24.1	24.1
C_0 [mg/dm^3]	5.84	5.84	5.84	5.84	5.84	5.84	5.84	5.84	5.84
C_s [mg/dm^3]	8.4	8.4	8.4	8.4	8.4	8.4	8.4	8.4	8.4
C [mg/dm^3]	5.84	6.89	7.65	8.01	8.10	8.26	8.31	8.35	8.39

Based on the data in table 1, the graph in figure 5 was drawn.

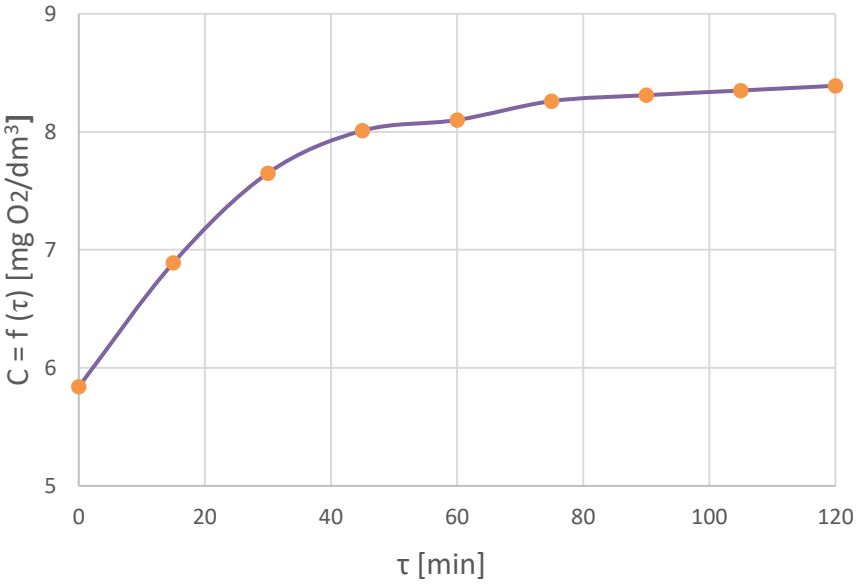

Fig. 5. Variation in the dissolved oxygen concentration in water

These results are in good agreement with those obtained theoretically, contained in similar papers [13] [14].

5. Conclusions

For the aforementioned researches, a microbubble generator (MBG) was used which is provided with a perforated plate with 152 orifices of Ø 0.1 mm made by micro-drilling.
During the experimental researches, the following values are kept constant: gas pressure at the entrance to the MBG, the gas flow rate and the hydrostatic load.
At an interval of 15 minutes the air supply to the MBG is stopped and the oxygenometer probe is inserted; the signal taken from the probe is processed in the microcomputer and digitally displayed on the microcomputer screen. There is a good correspondence between the theoretical data and the data experimentally obtained.

References

[1] Călușaru, I. *The influence of the physical properties of the liquid on the efficiency of the oxygenation processes/Influenţa proprietăţilor fizice ale lichidului asupra eficienţei proceselor de oxigenare*. Doctoral thesis. University Politehnica of Bucharest, Faculty of Mechanical and Mechatronics Engineering, 2014.
[2] Pătulea, Al. S. *The influence of the functional parameters and the architecture of fine bubble generators on the efficiency of aeration installations/Influenţa parametrilor funcţionali şi a arhitecturii generatoarelor de bule fine asupra eficienţei instalaţiilor de aerare*. Doctoral thesis. University Politehnica of Bucharest, 2012.
[3] Stoianovici, S., and D. Robescu. *Processes and equipment for water treatment and purification /Procedee și echipamente pentru tratarea și epurarea apei*. Bucharest, Technical Publishing House, 1982.
[4] Rajendren, R. "Water Treatment, Aeration." *Kirk-Othmer Encyclopedia of Chemical Technology*. John Wiley & Sons, Inc., Published Online: 2007.
[5] Ionescu, Gh. C-tin. *Wastewater treatment systems/Sisteme de epurare a apelor uzate*. Bucharest, MatrixRom Publishing House, 2010.
[6] Stenstrom, M. K., S. Y. Leu, and P. Jiang. *Theory to Practice: Oxygen Transfer and the New ASCE Standard*. Water Environment Foundation, 2006.
[7] Stoianovic, S., D. Robescu, and D. Stamatoiu. *Calculation and development of water oxygenation equipment /Calculul şi construcţia echipamentelor de oxigenare a apelor*. Bucharest, CERES Publishing House, 1985.
[8] Tănase, B., N. Băran, M. Constantin, and R. Cusma. "Hydrostatic Load Influence on Water Oxygenation Process." *Energy Procedia* 74 (August 2015): 44-50.

[9] Băran, N., M. Vlăsceanu, M. Băran, and E. B. Tănase. ″Increasing the performance of oxygenation installations." *Termotehnica,* no.1 (2014): 16-21.
[10] Tănase, E. B., N. Băran, and R. Mlisan. ″An Efficient Solution for Water Oxygenation." *Asian Engineering Review* 1, no. 3 (2014): 36-40.
[11] Constantin, M., N. Băran, B. Tănase, and R. Mlisan (Cusma). ″Research regarding the free surface water aeration." *Termotehnica*, no. 2 (2014): 82-86.
[12] Tănase, B., D. Besnea, R. Mlisan (Cusma), N. Băran, and M. Constantin. ″Researches regarding the pressure losses on fine bubble generators." *The Romanian Review Precision Mechanics, Optics & Mechatronics*, no. 48 (2015): 155-157.
[13] Băran, Gh., I. Pincovschi, G. Oprina, and F. Bunea. ″Performance of fine bubble generators /Performanţe ale generatoarelor de bule fine.″ *Revista Hidrotehnica* 53, no. 3-4 (2008): 27-32.
[14] Tănase, E. B., N. Băran, and M. Vlăsceanu (Banu). ″Reduction of energy consumption in water aeration plants.″ *IJISET - International Journal of Innovative, Enginnering & Technology* 1, no. 5 (2014): 522-524.

Drying of Biomass in an Infrared Tunnel with Conveyor Belt

PhD Stud. Eng. **Ioan PAVEL[1*],** PhD Eng. **Gheorghe ȘOVĂIALĂ[1],**
Dipl. Eng. **Alina Iolanda POPESCU[1],** Tech**. Kati PAVEL[1],** Dipl. Eng. **Dragoș PREDA[2],**
Dipl. Eng. **Bogdan DURAN[2]**

[1]Hydraulics and Pneumatics Research Institute INOE 2000-IHP

[2] S.C. ROLIX IMPEX SERIES S.R.L

* pavel.ihp@fluidas.ro

Abstract: *The article addresses the drying of cellulosic vegetable waste from fruit growing, and viticulture in an infrared tunnel dryer with conveyor belt. Data are presented regarding the average mass resulting from cutting, energy efficiency, calculation of drying speed and drying rate. Also, are presented some of the results of the dryer test according to the test methodology.*

Keywords: *Dryers, infrared, biomass, wood moisture*

1. Introduction

At present, in order to reduce pollution and increase the quality of combustion or to use biomass in processing processes (briquettes, pellets), biomass drying is practiced. Plant biomass, used as a raw material, is hygroscopic material, so it has the ability to exchange moisture with the atmosphere, and as a result has the property to change its calorific value, durability, stability during transportation and storage.
The most representative categories of combustible wood materials are: firewood, tree bark, branches from forest exploitation, chopped branches from the maintenance of tree orchards, vine ropes, sawdust, wood chips, small pieces of timber and other residues from wood processing.
Cellulosic vegetable waste from fruit and viticulture can be a source of biomass, the dryer and greenhouse are direct users of thermal and electrical energy, and ash can be used as an important component of mineral fertilizers used on farms. As an example, the wood biomass obtained from the annual cuttings from orchards and dried up to 20% represents an average mass of 1,500 kg / ha from which a gas energy of 4.5 MWht can be obtained with which it can be dried, with a yield 35% drying, about 8,500 kg of apples. Another example: from one hectare of vineyard on which 4000-5000 logs are in production, 0.65 kg of ropes are obtained at the annual cuttings from each log, so at least 3000 kg / ha of ropes cut with a relative humidity of about 40%. By natural drying or in dryers the cut ropes reach 20% humidity and a mass of very good quality cellulosic fuel of about 2200 kg / ha is reached. From this fuel by gasification can produce a quantity of 4800 m^3 of gas with which can produce a thermal energy of 6.60 MWht. In our country, for wood waste from cutting down trees in orchards, logging, sawmills, etc., it can be estimated that the price of fuel that is introduced into gas is on average 10 € / t, a similar value for other areas in Europe for which similar case studies have been performed. The result is a price for primary energy of maximum 0.6 € / GJ. Dryers are high heat consumers, which leads to high production costs for their products. Reducing thermal energy costs leads to lower overhead costs and increased competitiveness of dehydrated products. The use of locally available biomass can ensure a significant reduction in production costs and an increase in energy independence [1].
One ton of dry biomass has an energy potential of 15.530 GJ / t.bm or 4.3 MWhth. From the published data, for Europe, results an average cost of gathering, chopping and transport for a ton of cuts of about 40 € / t. Taking into account the costs for drying and a profit of 20%, it results that a ton of biomass usable for the production of thermal energy can be sold for about 80 € / t. The specific price for the primary energy of biomass is in the case studied of 5.2 € / GJ or 18.6 € / MWhth, values much lower than those for diesel of 33.22 € / GJ or for LPG of 21.52 € / GJ [2]. The researchers showed that for the artificial drying of biomass from 35% to 15%, 70% of the energy consumed is used for processing, while for the actual pelletizing of pellets - only 7%. Regarding the

moisture of biomass for pelletizing, Li, Yadong and Liu, Henry [3], stated that it should be between 6-12%, and Obernberger, I. and Thek, G [4] recommend values of 8-12%. It should be noted that the moisture content of the biomass at harvest can far exceed the required level. Humidity after maintenance cuttings in orchards or vines is up to 50%. For economic reasons, the reduction of the high humidity of the harvested biomass is recommended to be achieved in natural conditions, using solar energy or atmospheric air [5].

2. Biomass drying

Drying is the operation by which water from solid materials (in our case biomass) is removed with the help of air which has the role of bringing the heat necessary to vaporize moisture and to evacuate the resulting water vapor. The speed of the drying process is defined by the amount of moisture removed from the surface unit of the material to be dried in the unit of time. The factors that influence the drying in the case of biomass are:

• Quantity (flow);
• Shape: powder, granules, sheets, etc.;
• Humidity and the form in which it is found;
• Thermal and oxygen (air) sensitivity;
• Bulk density.

Wood moisture (U) is related to dry mass. This value describes the relationship between the mass of water included, compared to the dry mass. Moisture can therefore be transformed into water content, respectively can be calculated from it. In conclusion, wood moisture can be described as a relationship between water and dry biomass. Wood moisture is a common notion in wood management. Instead, in the practice of wood energy use is calculated only with the water content.

$$M = \frac{G_u - G_0}{G_u} \cdot 100, (\%) \quad (1)$$

$$U = \frac{G_u - G_o}{G_u} \cdot 100, (\%) \quad (2)$$

Where:
• M - Water content;
• U - Wood moisture;
• G_u- Fresh weight;
• G_o - Dry weight.

In the energy use of wood, the caloric value of the biomass used in addition to the essence and dimensions of the pieces has an essential importance. Because biomass without water does not exist in nature, larger or smaller amounts of water must evaporate during combustion. The energy (heat) required for this decreases the net energy efficiency.

The influence of water content on the caloric value of the biomass used can be calculated with the following equation:

$$q_{p,net,ar} = q_{p,net,d} \cdot \frac{(100 - M_{ar})}{100} \cdot 0{,}02443 \cdot M_{ar} \quad (3)$$

Where:
• $q_{p,\,net,\,ar}$ - Caloric value of wood at a certain water content [MJ / kg];
• $q_{p,\,net,\,d}$ - Calorific value of dry wood mass in waterless state [MJ / kg];
• M_{ar} - Water content in delivery condition [%];
• 0.02443 - Constant for water vaporization heat at 25 ° C [MJ / kg].

It follows that the caloric value of wood (approx. 18.5 MJ / kg) decreases linearly with increasing water content [6].

Transforming biomass into thermal energy by burning imposes certain moisture values of fuel as follows [6]:
- the maximum humidity of biomass for burning in conventional combustion plants= 25 %;
- the maximum humidity of biomass for burning in specific combustion plants = 60 %;
- optimum humidity of biomass for burning = 7 – 10 %;
- maximum humidity of biomass for gasification = 35 %;
- the maximum humidity of biomass for transformation into pellets or briquettes = 10 %.

Analyzing the data on the humidity values that appear for the use of biomass by combustion, it is necessary to dry it. The high humidity of the biomass at the time of combustion negatively influences the technical condition of the combustion plant [7].

3. Dryers with infrared radiation

Infrared (IR) radiation is electromagnetic radiation whose wavelength is longer than that of visible light (400 - 700 nm), but shorter than that of terahertz radiation (100 μm - 1 mm) and microwaves (~ 30000 μm). Most of the thermal radiation emitted by objects at room temperature is infrared.
Infrared energy is emitted or absorbed by molecules when the rotational-vibrational movements change. Infrared energy excites modes of vibration in a molecule through a dipole change, making it a useful frequency range for studying these energy states for molecules of corresponding symmetry. Infrared spectroscopy examines the absorption and transmission of photons in the infrared energy range.
IR heating power is used in IR infrared dryers. Electromagnetic radiation with a wavelength of 0.76 μm - 1 mm is called infrared. Depending on the wavelength of the radiation, they can be SIR dryers (short IR radiation), MIR dryers (medium radiation) and LIR dryers (long radiation) [4].
The firm S.C. ROLIX IMPEX SERIES has developed, following a subsidiary contract of type D, contract in collaboration with a research organization, INOE 2000, within the contract on structural funds POC, a new solution of infrared dryer.
It is shown in figure 1, and in figure 2 is its practical realization.

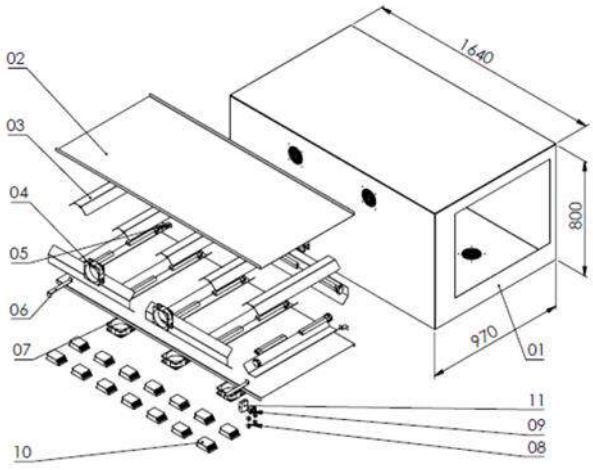

Fig. 1. Infrared biomass dryer

Fig. 2. Physical realization of ME of infrared biomass dryer

The infrared dryer consists of a tunnel housing (1), lamp holder (2), reflector holder (3), IR lamps (4), brackets (5) and (6), fans (7), lamp switches (8), display control module (9), IR lamp holders (10), wireless controller (11).
IR lamps (4) are installed inside the tunnels housing (1) which are mounted on the supports (10). The heat is directed to the chopped biomass fragments by the targeting plate sheets (3).
The drying tunnel enclosure is traversed by the belt-chopped biomass conveyor, driven by its own variable speed electric motor (via frequency converter) and a chain transmission.

The brackets (5, 6) provide the necessary distance between the tunnel housing (1) and the outer jacket of the dryer, for mounting the belt conveyor motor and the 10 fans (7): four on the sides of the outer jacket, two on the lower support plate sheet and four on the top plate sheet.
The operation of the IR lamps is done from the four switches (8), located in the upper part of the front panel of the drying tunnel and the operating of the fans from the control and display module (9), located in the lower part. The fans create inside the dryer the air current for the evacuation of water vapor resulting in the drying process.

4. Testing the IR dryer with conveyor belt

4.1 Measurement / recording of the working speed of the conveyor belt (fig.3)

The IR dryer has variable speed on the conveyor belt.
The process speed of the drying process can be determined with the formula:

$$w = \frac{dW}{A \cdot dt} \tag{4}$$

In which:
- w - speed of the drying process;
- dW - the amount of moisture removed;
- A - the unit of surface of the material subjected to drying;
- dt - unit of time.

When the drying speed is known, the drying time is determined by integrating the equation:

$$w = \frac{dW}{A \cdot dt} \Rightarrow \int \frac{dW}{A \cdot w} \tag{5}$$

Knowing the data regarding the drying time, the speed of the conveyor belt can be adjusted in such a way that the material to be dried remains inside the dryer for the calculated duration.
During the test, using the Lutron VT-8204 [8], the rotational speed at the drive shaft of the device in contact with the drive chain of the conveyor belt was measured. The measured rotational speeds (fig. 3) for the preset gears in the control panel were: minimum of 35 rpm and then with the settings in the control panel it was measured: 59.9 rpm, 90.8 rpm, 123.6 rpm, 159.8 rpm, 185.7 rpm, 216.6 rpm, 245.1 rpm and max. 286.3 rpm.

Fig. 3. Measuring the rotational speed of the conveyor belt

After calculating the drying speed, the speed of the conveyor belt is established and adjusted.

4.2 Measurement / recording of vacuum vibration level with Lutron VT-8204 apparatus [8] (fig. 4)

The measured min. value of was 0.130 Hz and max measured value was 0.145 Hz:

Fig. 4. Measurement / recording of vacuum vibration level with Lutron VT-8204

4.3 Measurement / recording of vacuum vibration level with sound level meter model RS-232:SL-4012 (fig.5)

Using the sound level meter model RS-232: SL-4012 [9], the noise level was measured at a minimum speed of 70 db and that at a maximum speed of 79 db.

Fig. 5. Measurement / recording of vacuum vibration level with sound level meter model RS- 232:SL-4012

4.4 Temperature measurement in the drying tunnel (fig.6)

The measurement was made empty with the Fluke Ti20 Imager [10] which is a last generation thermal imaging unit, pistol type.

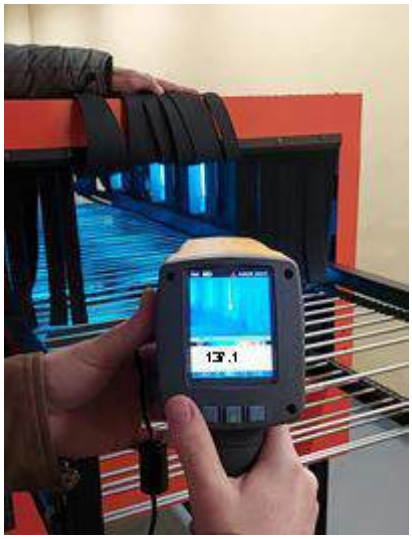

Fig. 6. Temperature measurement in the drying tunnel

The temperature measured in the tunnel, without material, was 137.1 °C.

5. Conclusions

1. The cellulosic vegetable waste from orchards and viticulture can be a source of green energy from biomass.
2. The infrared radiation loses the least energy in contact with air. It does not heat the air but the objects it comes in contact with. Almost all the energy is transmitted to the object we want to dry.
3. The infrared tunnel dryers with conveyor belt are often combined with conventional dryers for efficiency and short drying time.
4. The infrared tunnel dryers with conveyor belt are more economical than conventional ones in terms of energy consumption.
5. The continuous adjustment of the conveyor belt displacement and temperature in the drying tunnel.
6. Drying with infrared lamps and convection fans to make drying more efficient.
7. It saves 30% of electricity compared to similar equipment.

Acknowledgments

This paper has been developed in INOE 2000-IHP, as part of a project co-financed by the European Union through the European Regional Development Fund, under Competitiveness Operational Programme 2014-2020, Priority Axis 1: Research, technological development and innovation (RD&I) to support economic competitiveness and business development, Action 1.2.3 – Partnerships for knowledge transfer, project title: Eco-innovative technologies for recovery of biomass wastes, project acronym: ECOVALDES, SMIS code: 105693-594, Financial agreement no. 129/23.09.2016.

References

[1] Murad, Erol. *Modelarea şi Simularea Proceselor Ecologice /Modeling and Simulation of Ecological Processes.*https://www.academia.edu/9767599/BIOMASA_SURSA_DE_ENERGIE_REGENERABILA_SI_ECOLOGICA. Accessed March 3, 2021.
[2] Pavel, Ioan, Gabriela Matache, Alexandru-Polifron Chiriță, Alina-Iolanda Popescu, and Cristian Diaconu. "Biomass Processing from Agricultural Residual Production and Maintenance Operations when Cutting Trees and Vines". *Hidraulica Magazine*, no. 4 (2020): 93-97.
[3] Li, Y., and L. Henry". "High-pressure densification of wood residues to form an upgraded fuel". *Biomass and Bioenergy* 19 (2000): 177-186.
[4] Obernberger, I., and G. Thek. "Physical characterization and chemical composition of densified biomass fuels with regard to their combustion behaviour". *Biomass and Bioenergy* 27 (2004): 653-669.
[5] Ericsson, K., and S. Werner. "The introduction and expansion of biomass use in Swedish district heating systems". *Biomass Bioenergy* 94, (2014): 57-65.

[6] http://www.biomasstradecentre2.eu/data/intranet/D5.4_Biomass_manual_Romania.pdf. Accessed March 8, 2021.
[7] Voicea, I., A. Danciu, M. Matache, G. Voicu, and V. Vladut. "Biomass and the thermo-physical-chemical properties of this related to the compaction process." *Annals of Faculty Engineering Hunedoara-International Journal of Engineering* 11 (2013): 59-64.
[8] https://www.manualslib.com/manual/1218778/Lutron-Electronics-Vt-8204.html. Accessed March 5, 2021.
[9]http://www.lutron.com.tw/ugC_ShowroomItem_Detail.asp?hidKindID=1&hidTypeID=60&hidCatID=&hidShowID=345&hidPrdType=&txtSrhData=. Accessed March 5, 2021.
[10] https://dam-assets.fluke.com/s3fs-public/Ti20____umeng0000.pdf. Accessed March 3, 2021.

A Critical Review of Combustion Noise in Combustion Engines

Dr. **Sunny NARAYAN**[1], Dr. **Aman GUPTA**[2]

[1] Indus University, India, sn2008@rediffmail.com

[2] Indus University, India

Abstract: *Combustion noise generated mainly depends upon the rate of in cylinder pressure developed during ignition delay period. Overall design of combustion chamber as well as variations in various fuel injection parameters e.g., injection pressure, amount of fuel injected and its timings also play a crucial role in contributions of combustion noise emissions from engines. The present work issues various factors effecting combustion base noise and analysis its generation using a mathematical model.*

Keywords: *Piston secondary motion, liner system*

1. Introduction

Depending upon the type of engine as well as various operational parameters, overall noise emissions from a typical diesel engine may be in range 80-110dBA [1,2, 3]. Split injection using electronic control unit (E.C.U.) may help to shortens the period of premixed phase of combustion and hence help to reduce the overall noise emissions by about 5-8dBA [4]. Head and Wakes have shown that during transient operational conditions, overall noise levels are about 4-7dBA higher as compared to steady state operations [5]. Cold starting conditions may lead to higher ignition delay period which in turn causes increase in the premixed period of combustion [6]. Quality of fuel injected inside combustion chamber also affects the magnitude of combustion noise. It has been observed that a reduction of Cetane number of fuel from 50 to 40 causes a rise of up to 3 dBA in combustion based noise emissions [7]. For a naturally aspirated engine, the combustion-based noise depends upon the quantity of fuel that mixes with air charge during the course of delay period and hence the compression ratio of engines also plays a vital role [7]. In case of gasoline engines, the delay period is longer due to lower compression ratio which may lead to lower temperature of charge and hence more noise emissions [7].

2. Background

Due to high efficiency, diesel engines have been a favourite choice in case of heavy-duty automobiles including trucks [8]. However, they suffer from major drawbacks of high noise, weight and vibrations. These engines may be further classified into following two major types:

1. Direct injection (D.I.) engines

2. Indirect injection (I.D.I.) engines

In case of D.I. engines, the fuel is injected directly inside the combustion chamber and as a consequence of it, lesser time is available for formation of fuel and air mixture. Hence a heterogeneous mixture consisting of both rich as well as lean parts is formed inside the chamber.

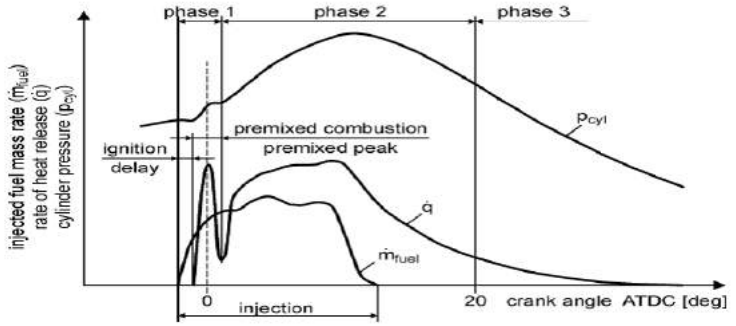

Fig. 1. Various phases of Diesel engine combustion [8]

Figure no 1 shows various phases of combustion as observed during course of operation of a typical diesel engine. The delay phase starts with onset of injection process and ends with beginning of premixed phase of combustion. The injection of fuel inside combustion chamber begins a few degrees before TDC position depending on the various injection conditions of engine. As soon as the cold jet of fuel penetrates the chamber, it mixes up with hot compressed air already present inside. The droplets thus formed vaporize, forming layers of fuel-air mixture around the periphery of jet. As the temperature rises to about 750K, the first break down of Cetane fuel takes place. Further propagation of various chemical reactions produces C2H2, C3H3, C2H4, CO2 as well as water vapours [9]. Resulting rise in temperatures causes a complete combustion of fuel-air mixture formed. This sudden period of combustion further leads to rise in the heat release rate as well as high pressure gradient (dP/dθ). This further enhances temperatures in the pre-mixed zone leading to conditions favourable for production of NOx. Once the premixed phase consumes all mixture formed, oxygen available for combustion is consumed around the inner regions wherein the temperatures in ranges of 1600-1700K are reached [8]. Now various partially burnt particles diffuse towards outer layers and begin to burn within a thin region of reaction formed around the periphery of spray leading to formation of a diffusion flame. This phase of combustion is known as diffusion-controlled combustion and is depicted by region 2 and 3 in figure no 1. Higher temperatures along with lack of oxygen provides an ideal condition for the formation of soot.

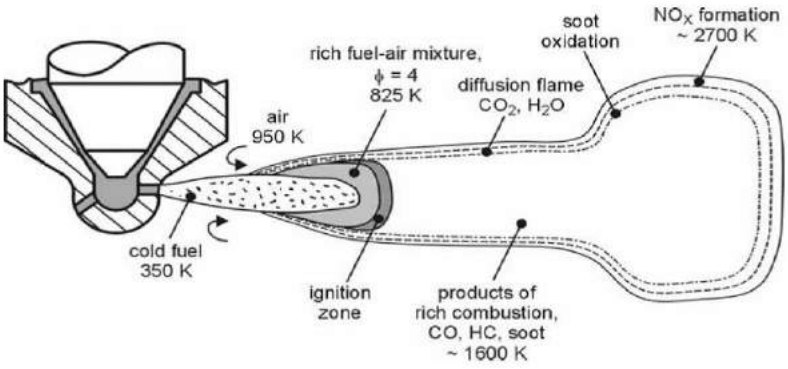

Fig. 2. Conventional diesel engine spray formation [8]

The diffusion flame thus formed then uses rest of oxygen available from surrounding environment resulting in high temperatures of order 2700K which consumes all the soot formed. At outer zone of flame there is enough oxygen content for formation of NOx. Figure no 3 shows the rate of soot formation as a function of crank angle. Most of soot that is formed during earlier stages is later consumed and hence final exhaust emissions may have only a fraction of initial soot emissions. As seen from figure no 1, the diffusion-controlled combustion can be divided into further three phases. During the second phase, the burning rate is dependent on rate of mixing of fuel fragments formed and air and hence rate of reaction is faster. During the third phase, oxidation of remaining unburnt particles and soot takes place, however due to decreased temperature of end gas formed during the expansion stroke as well as lesser oxygen content available, slower reaction rates are observed.

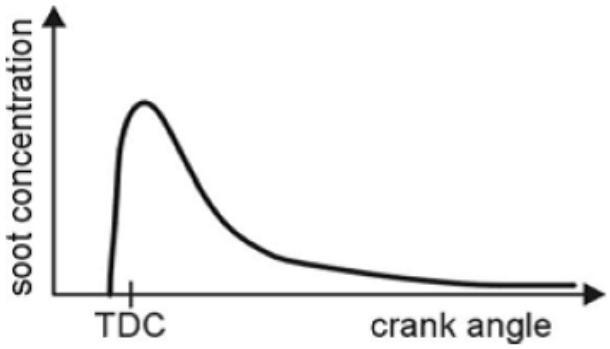

Fig. 3. Rate of soot formation [8]

Process of NOX and soot formation in combustion engines has shown an opposite trend as shown in figure no 4. In order to reduce the NOx formation rate it is necessary that local temperatures must not rise beyond 2000K [8]. A possible way to do so is to inject fuel late inside combustion chamber which further shifts the combustion phase towards expansion phase resulting in significant reduction of chamber temperatures. However, rate of consumption of fuel and soot formation increases due to late combustion.

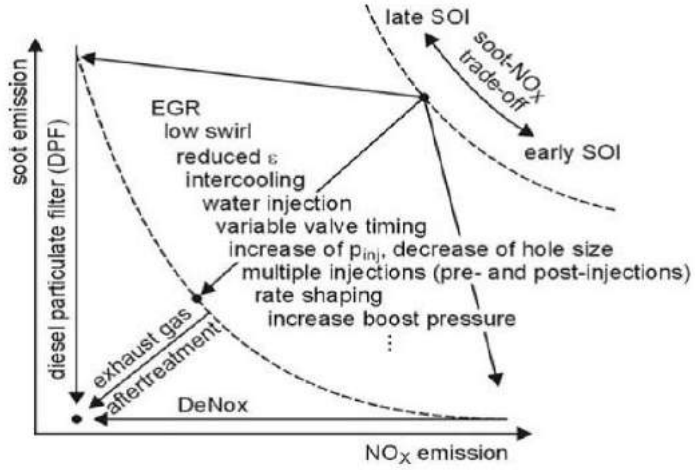

Fig. 4. Soot & NOx trade off [8]

Hence modern systems utilize multiple injection techniques in order to control both NOx as well as soot formation rate [8, 9, 10, 11].

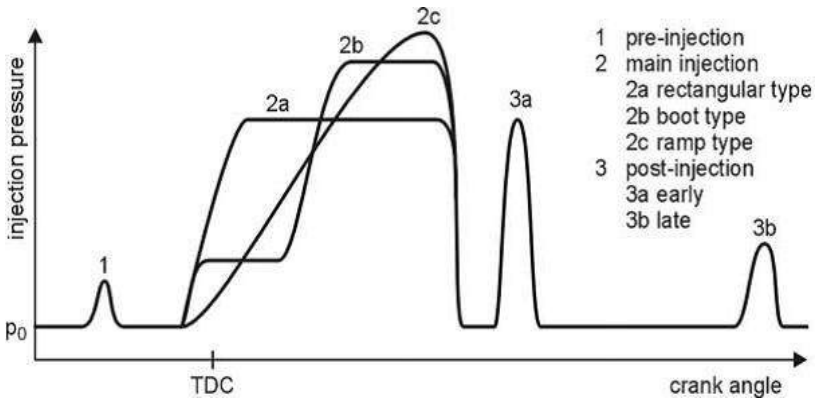

Fig. 5. Multiple injection methods adopted for modern diesel engines [8]

There are generally three phases of injection process used, namely pre-injection period, main-injection period & post injection period. There is a delay period between instant at which fuel is injected inside the combustion chamber and actual start of ignition process. Greater this delay period, more is the temperature achieved during course of combustion and hence better conditions exist for NOx formation. In order to shorten this delay period, a small amount of fuel is pre-injected before main injection occurs during the phase of pre-mixed combustion. Torque and power produced in engine mainly depends on the duration of main injection period. It is advantageous to vary the injected fuel mass with time in order to reduce the specific consumption of fuel. This is achieved by rate shaping as seen in figure no 5. Rate shaping curve may be rectangular, step or boot type in shape. Post-injection of fuel is done in order to reduce the soot emissions and in some cases may be useful for exhaust gas recirculation treatment [12]. It has been reported that post injection may reduce the rate of soot formation by about 70% without increasing the fuel consumption [13].

3. Factors effecting combustion noise [20]

The rate of pressure (which mainly depends on the ignition delay period) and quantities of combustion gas formed during this period is a key parameter to analyze combustion-based noise. A shorter delay period means lesser amount of combustible gas formed and hence lesser combustion noise. Hence delay period must be reduced as much as possible for effective reduction of combustion noise. Structure and layout of engine also plays a significant role [14-20]. Between 300Hz-2000Hz they were related to first derivative of in cylinder pressure, whereas above 2000Hz were related to second derivative of cylinder pressure. Increase in the compression ratio and chamber temperature may shorten this delay period. However, an increase in compression ratio can cause a rise in noise due to slapping motion of skirt. Various parameters of fuel injection system like instance of fuel injection, injection pressure, number of nozzles and fuel supply rate also effects the combustion noise. Increasing the pressure of injection or engine speed leads to an increase in the amount of fuel accumulated during the delay period resulting in rise of combustion noise.

There are many approaches to control combustion noise. One of these includes reducing cylinder pressure spectrum typically in middle and high frequency ranges. Other include reducing ignition delay period or amount of combustible gases formed during this period. Increasing the stiffness of parts, use of turbo charging process and use of split injection methods have also proved to be other effective methods.

4. Effects of heat release rate

Previous works have shown a relationship between peak of combustion noise and overall heat release rate [4,5]. It was observed that higher slopes of rate of heat release curves led to higher combustion noise irrespective of fuel injection timings [2]. There is a tradeoff between combustion efficiency and the noise generated due to combustion [7]. Efficient combustion leads to higher heat release rate near top dead center position which further gives rise to high frequency components in noise spectrum. Late release of heat release leads to lower pressures and subsequent lower frequencies in spectrum.

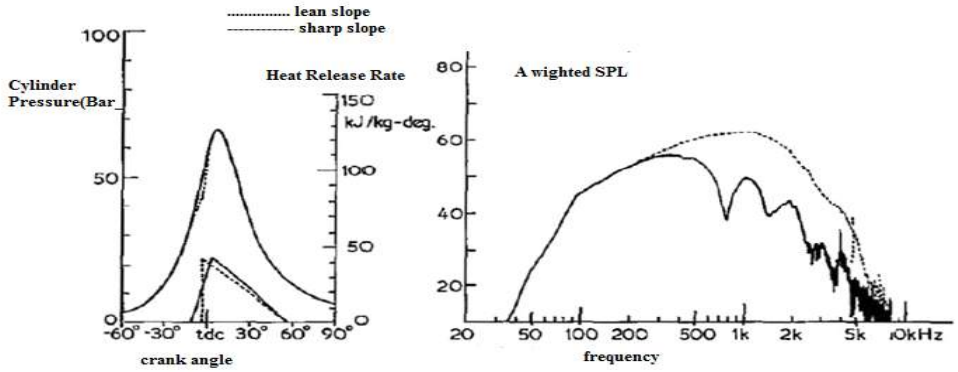

Fig. 6. Effects of heat release rate on combustion noise

It has been observed that up to a 10dB reduction in sound pressure levels were possible without change in fuel consumption as shown in figure no 4.66. However, there is a fall in efficiency of cycle and smoke emissions increase if ROHR is not terminated 50° after TDC position (ATDC) [7].

5. Effects of cyclic variations

Combustion process in diesel engines varies from cycle to cycle which may lead to variations in noise emissions from engines [28]. These variations may be attributed due to different fuel injection rates, compression ratios as well as difference in fuel spray process, mixture formation and flame propagation. Torregrosa has studied these cyclic variations as shown in figure 7 [9]. These variations were attributed to resonance phenomenon occurring in combustion chamber.

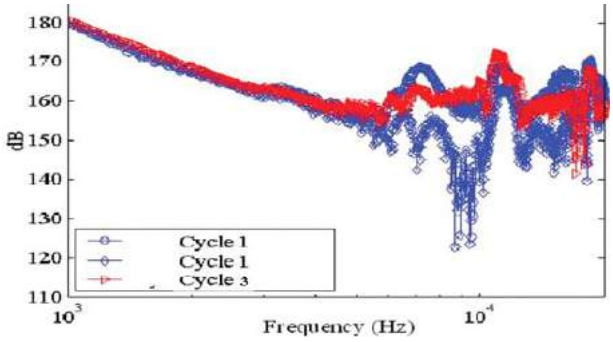

Fig. 7. Cyclic variations in combustion noise

6. Resonance phenomenon

Resonance taking place inside combustion chamber effects the noise emissions. Grover observed high peaks in the noise spectrum which may be attributed to this phenomenon [3]. Hickling found peaks of higher amplitude by filtering data in range 20Hz-1500Hz which showed increased with engine load [2]. The amplitude of oscillations due to resonance is dependent on the geometry of bowl as well as temperature of gas [3]. Resonance phenomenon can be considered as an unsteady process as it changes continuously during course of combustion process [4].
The frequency of resonance (f_r) may be defined in terms of cylinder bore(B), axial length(L) and speed of sound(C) as:

$$f_r=\sqrt{(\frac{C}{2L})^2+(\frac{q_{m,n}}{B})^2} \quad (1)$$

Where m,m,k determines the circumferential, axial and radial modes as shown in figure no 8.

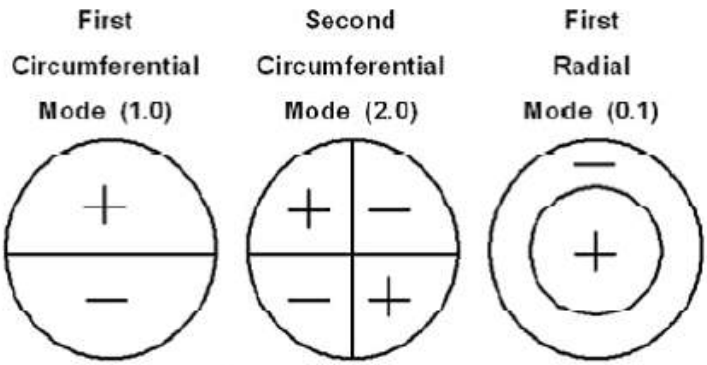

Fig. 8. Various modes of combustion chamber cavity

7. In cylinder pressure decomposition method

A methodology to decompose the total in cylinder pressure signals was first proposed by Payri [5]. In this method the cylinder pressure was decomposed into three parts namely: combustion pressure, resonance pressure and compression pressure. The combustion part was dependent on injection process and hence resulting ROHR. Using suitable cutoff frequencies, the motored part of pressure can be isolated from excessive part (which is sum of compression and resonance part. Figure no 9 shows results of this methodology as applied to in cylinder pressure [5].

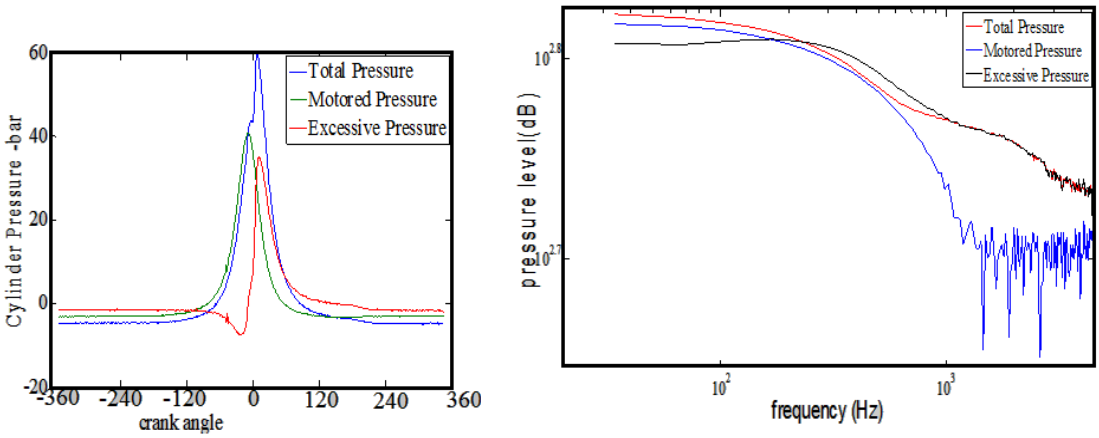

Fig. 9. Decomposition of cylinder pressure signal

As evident from these figures, motored part dominated at low frequency ranges. Resonance portion is clearly visible with fluctuating peaks. This portion can be isolated by filtering excessive pressure part using a high pass filter. The contribution due to combustion process can be obtained by subtracting resonance portion from excessive portion. These contributions dominated in mid frequency ranges, whereas the resonance phenomenon dominated at high frequency ranges [5].
The decomposed signals thus obtained can be further used to calculate various indices defined in terms of ideal engine speed (N_{ideal}) as:

$$I_n = \log\left[\frac{N}{N_{ideal}}\right] \quad (2)$$

$$I_1 = \left[\frac{N}{N_{ideal}}\right]\left[\frac{\left(\frac{dp}{dt}\right)_{pilot}+\left(\frac{dp}{dt}\right)_{main}}{\left(\frac{dp}{dt}\right)_{motored}}\right] \quad (3)$$

$$I_2 = 10*\log(10^6 \int (\frac{P_{residual}^2}{P_{motored}^2})dt \quad (4)$$

Where $(\frac{dP}{dt})_{pilot}$ is maximum pressure gradient during pilot injection period, $(\frac{dP}{dt})_{main}$ is maximum pressure gradient during main injection, $P_{residual}$ is residual pressure and $(\frac{dP}{dt})_{motored}$ is maximum pressure gradient in motored pressure signal. These indices can be further used to express overall noise (ON) emitted from engine given by:

$$ON = C_0+C_1I_1+C_2I_2+C_nI_n \quad (5)$$

Where constants C_0,C_1,C_2 and C_n depend upon size of engine.

9. Mathematical Model of Generation of Combustion Noise [7]

In this part of work a transient model of generation process of combustion noise has been discussed. For this purpose, aMorlet wavelet was defined in terms of its central frequency f_c and bandwidth fb as:

$$\psi(t) = \frac{1}{\sqrt{\pi f_b}} e^{i2\pi f_c t} e^{\frac{-t^2}{f_b}} \quad (6)$$

Figure no 10 shows real and imaginary parts of this wavelet having f_b = 1.5 and f_c = 1

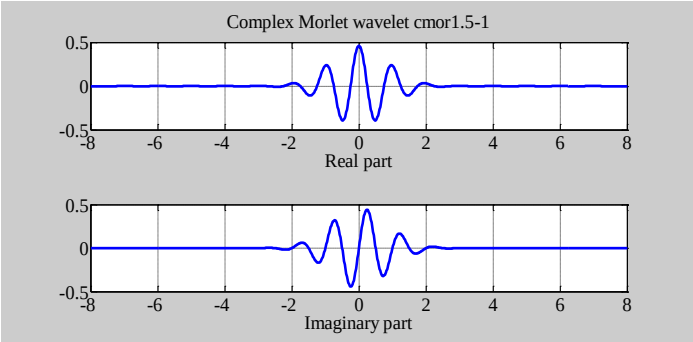

Fig. 10. Complex Morlet Wavelet

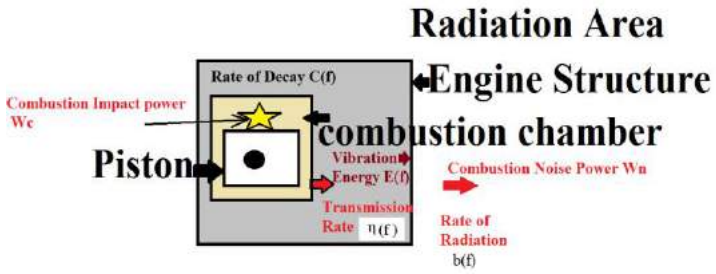

Fig. 11. Noise generation model

Further a transient model of combustion noise generation is discussed in Figure no 11. This model can be analyzed by following three processes: generation of vibrational energy inside chamber due to combustion process, transmission and decay of this energy and finally its radiation around the engine surface.

The combustion process inside engines generates combustion impact power (W_c) which is related to in cylinder pressure(p), impedance of medium (ρc) and cylinder surface area(A) as:

$$W_c = \frac{P^2}{\rho c} A \quad (7)$$

The available energy at engine surface can be written in terms of transmission rate coefficient η(f) as:

$$E(f) = \eta(f)\int_0^t W_c dt \tag{8}$$

Differentiating both sides of this equation we have:

$$\frac{d}{dt}\big(E(f)\big) = \eta(f) W_c \tag{9}$$

Taking into account the decay rate C(f) this equation gets modified as:

$$\frac{d}{dt}(E(f)) = \eta(f) W_c - C(f)E(f) \tag{10}$$

Where the decay constant C(f) may be defined as:

$$C(f) = -\frac{d[\log(Wn))]}{dt} \tag{11}$$

$$\frac{d}{dt}(W_n) = b(f)\eta(f) W_c - C(f) W_n(f) \tag{12}$$

10. Conclusions

This part of work investigated use of various experimental data for diagnosis of combustion-based noise. Further a transient model of combustion noise generation was also analyzed. High levels of correlations observed between various indices, show the applicability of vibration signals from engine as an input feedback parameter in case of a closed loop control system as depicted in figure no 12 [6]. This process can help to achieve an effective control over combustion noise by controlling optimal MBF50/MBF100/ fuel injection timings [7].

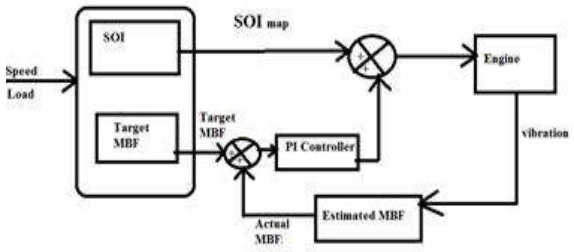

Fig. 12. Use of vibration signals as a feedback

References

[1] Abubakar, S., F.O. Anafi, M.U. Kaisan, S. Narayan, S. Umar, and U.A. Umar. "Comparative analyses of experimental and simulated performance of a mixed-mode solar dryer." *Proceedings of the Institution of Mechanical Engineers, Part C: Journal of Mechanical Engineering Science* 234, no. 7 (2020): 1393 - 1402.

[2] Kaisan, Muhammad Usman, Latifat Ovaiyoza Yusuf, Ibrahim Umar Ibrahim, Shitu Abubakar, and Sunny Narayan. "Effects of Propanol and Camphor Blended with Gasoline Fuel on the Performance and Emissions of a Spark Ignition Engine." *ACS Omega* 5, no. 41 (October 2020): 26454-26462.

[3] Narayan, S. "Wavelet analysis of diesel engine noise." *Journal of Engineering and Applied Sciences*, 8 no. 8 (2013): 255-259.

[4] Mahroogi, Faisal O., and Sunny Narayan. "A recent review of hybrid automotive systems in Gulf Corporation Council region." *Proceedings of the Institution of Mechanical Engineers, Part D: Journal of Automobile Engineering* 233, no. 14 (March 2019): 3579 -3587.

[5] Narayan, S., S. Milojevic, and V. Gupta. "Combustion monitoring in engines using accelerometer signals." *Journal of Vibroengineering* 21, no. 6 (2019): 1552 -1563.

[6] Narayan, Sunny, Ali Sulaiman Alsagri, and Vipul Gupta. "The design and analysis of hybrid automotive suspension system." *International Journal of Mechanical and Production Engineering Research and Development* 9, no. 4 (2019): 637-642.

[7] Kaisan, M.U., S. Abubakar, B. Ashok, Dhinesh Balasubramanian, S. Narayan, Ivan Grujic, and Nadica Stojanovic. "Comparative analyses of biodiesel produced from jatropha and neem seed oil using a gas chromatography–mass spectroscopy technique." *Biofuels* (December 2018): 1-12.

[8] Narayan, Sunny, and Vipul Gupta. "Numerical Analysis of Secondary Motion of Piston Skirt in Engines." *International Journal of Acoustics and Vibration* 23, no. 4 (2018): 1-10.
[9] Mahroogi, Faisal O., S. Narayan, and Vipul Gupta. "Acoustic transfer function in gasoline engines." *International Journal of Vehicle Noise and Vibration* 14, no. 3 (2018): 270 - 280.
[10] Grujic, I., N. Stojanovic, R. Pesic, A. Davinic, and S. Narayan. "Numerical analysis of IC engine operation with high pressure hydrogen injections." *Transactions of FAMENA* 44, no.1 (2020): 55-66.
[11] Narayan, Sunny. "A review of diesel engine acoustics." *FME Transactions* 42, no. 2 (2014): 150-154.
[12] Narayan, S. "Analysis of piston slap motion." *International Journal of Applied Mechanics and Engineering* 20, no. 2 (2015): 445- 450.
[13] Narayan, Sunny. "Modeling of Noise Radiated from Engines." SAE Tech paper 2015-01-0107, 2015. Paper presented at The 11th International Conference on Automotive Engineering (ICAE 11), Bangkok, Thailand, March 30 - April 1, 2015.
[14] Narayan, Sunny. "Effects of various parameters on piston secondary motion." SAE Tech paper 2015-01-0079, 2015. Paper presented at 18th Asia Pacific Automotive Engineering Conference (APAC 18), Melbourne, Victoria, Australia, March 10-11, 2015.
[15] Stojanovic, Nadica, Nouby M. Ghazaly, Ivan Grujic, Jasna Glisovic, and S. Narayan. "Influence of size of ventilated brake disc ribs on air flow velocity." *International Journal of Advanced Science and Technology* 29, no. 1 (2020): 637-647.
[16] Narayan, S. "Analysis of Piston Slap Motion." *International Journal of Applied Mechanics and Engineering* 20, no. 2 (May 2015): 445-450.
[17] Narayan, Sunny. "Piston Slap Noise in engines." *International Journal of Applied Engineering Research* 8, no.14 (2013): 1695-1700.
[18] Narayan, Sunny. "Effect of dwell time on noise radiated from diesel engine." *International Journal of Applied Engineering Research* 8, no.11 (2013): 1339-1347.
[19] Abubakar, S., F. Anafi, M. Kaisan, S. Narayan, S. Umar, and U. Umar. "Comparative analysis of experimental and simulated performance of a mixed mode solar dryer." *Proceedings of institute of mechanical engineers Part C: Journal of Mechanical engineering* 234, no. 7 (2019): 1393-1402.
[20] Kaisan, Muhammad Usman, Shitu Abubakar, Muhammed Mustapha M., and S. Narayan. "Determination of Wear Metals Debris Concentration in Aircraft Engines." *International Journal of Recent Technology and Engineering (IJRTE)* 8, no. 2 (2019): 1289-1292.

Upgrading a Digital Hydraulic Switching Valve to Become an Intelligent Hydraulic Equipment

PhD. Stud. Eng. **Bogdan-Alexandru TUDOR**[1*], PhD. Stud. Eng. **Mihai-Alexandru HRISTEA**[1], PhD. Eng. **Marian BLEJAN**[1], PhD. Stud. Eng. **Ștefan-Mihai ȘEFU**[1]

[1] INOE 2000 – Subsidiary Hydraulics and Pneumatics Research Institute (INOE 2000-IHP)

[*] btudor.ihp@fluidas.ro

Abstract: *Digital hydraulics is a recently introduced concept in the field of hydraulics. Some of the solutions used in digital hydraulics have been used for a long time in classical hydraulics, but not at the level at which they can be applied now. The development of the field of digital hydraulics was possible due to the technological advances that the field of electronics has experienced. At present, digital hydraulics intends to offer simpler devices, with less demanding requirements than those of servovalves and with a high reliability and energy efficiency.*
An intelligent system implies a system that is equipped with various sensors and transducers, connected to a Programable Logic Controller (PLC) that gathers all the information and transmits it to a software interface, from where the user can remotely monitor system parameters, can change their values and generate various reports. Another feature of an intelligent system is the fact that an automatic adjustment loop can be made, which allows it to adapt its own parameters according to needs.
In the present paper, the authors started from a digital hydraulic switching valve that they upgraded to become an intelligent hydraulic equipment, which can be controlled, tracked and parameterized remotely via a PLC with Ethernet port and application software.

Keywords: *Digital hydraulics, intelligent, hydraulic switching valve*

1. Introduction

The digital hydraulics [1] is defined by the active control of the system outputs of a hydraulic component (directional valve, pump, actuator). Digital hydraulics is not limited to digital control of analog components, but is based on intelligent control using PWM (pulse width modulation) signals and obtaining flow and speed adjustments, using on/off directional valve, encoded either PNM (Pulse Number Modulation), or PCM (Pulse Code Modulation). [2]
In the realization of the concept described in this paper, we started from a normally closed digital hydraulic switching valve presented in figure 1. Also, in order to realize the concept, flow and pressure transducers and a PLC were used to gather all this information and transmit it to the intelligent system control interface.
Digital hydraulic switching valves are 2-way and two-position on/off directional valves, and the switching signal is a PWM signal [3]. By switching at high frequencies between the closed and the open position of the directional valve, the flow regulation is performed. The flow at the exit of the directional valve is the sum of the closed and open periods.
Intelligent systems are systems that contain sensors and transducers for measuring all the main process parameters, but also process control equipment of PLC type provided with Modbus TCP communication, with the help of which the connection between the system and the software interface is made, where the process parameters can be viewed, the evolution of the system over time can be monitored, but one can also make changes and generate graphs.
With the help of the data obtained from a dedicated software interface, an analysis of the state of the system can be performed in order to be able to consider its introduction during the maintenance period or not. Due to the fact that the main parameters of the process can be viewed at any time, we can also talk about predictive maintenance.
Predictive maintenance refers to the fact that, based on the data collected from the software application, an analysis can be performed to show if the system needs maintenance in order to operate at optimal parameters, thus trying to avoid situations where the equipment fails randomly,

thus unscheduledly stopping the process in which it was involved, which can result in loss of time and money.

2. Hydraulic switching directional valve

The symbol of a digital hydraulic switching valve is represented in figure 1.

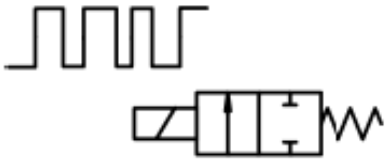

Fig. 1. Hydraulic switching directional valve - symbol

Figure 2 shows a section through the normally closed digital switching valve.
What is of interest to this digital hydraulic switching valve compared to a directional valve, is the fact that its spool switches between the closed and the open position with a frequency of over 100 Hertz and implicitly in order to achieve this both the electromagnet and the spool are made of special materials.

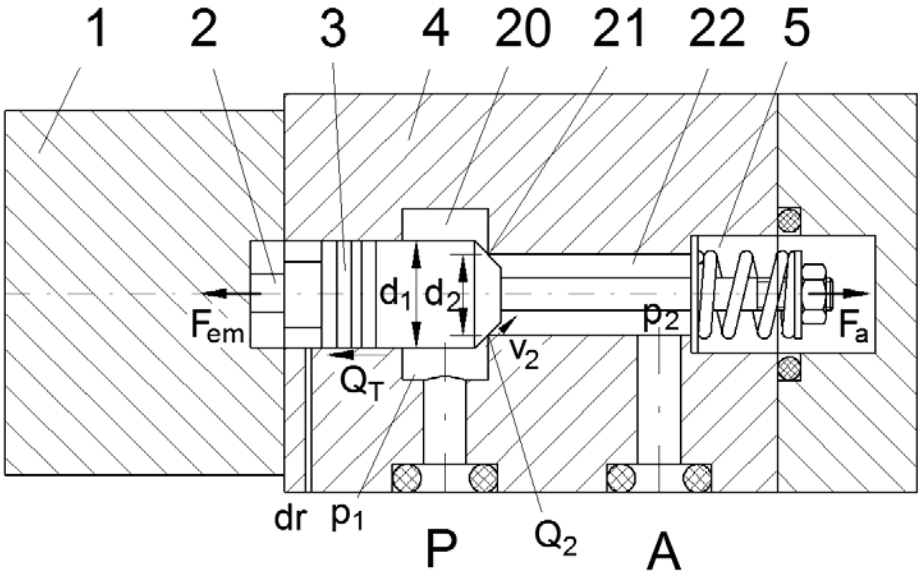

Fig. 2. Normally closed switching valve [4]

The components of interest are:

- High frequency electromagnet (1)
- The electromagnet shaft attached to the spool (2)
- Distribution spool (3)
- Valve body (4)
- Closing spring (5)
- Admission chamber (20)
- Crossing section (21)
- Discharge chamber (22)

When the electromagnet (1) is electrically operated, the distribution spool (3) opens the crossing section 21, so that the hydraulic connection is made between ports P and A. When the signal to the electromagnet is stopped, the closing spring (5) brings the distribution spool (3) in the closed position, so that the hydraulic connection between ports P and A is interrupted. [5]

An example of a step PWM signal can be found in figure 3.

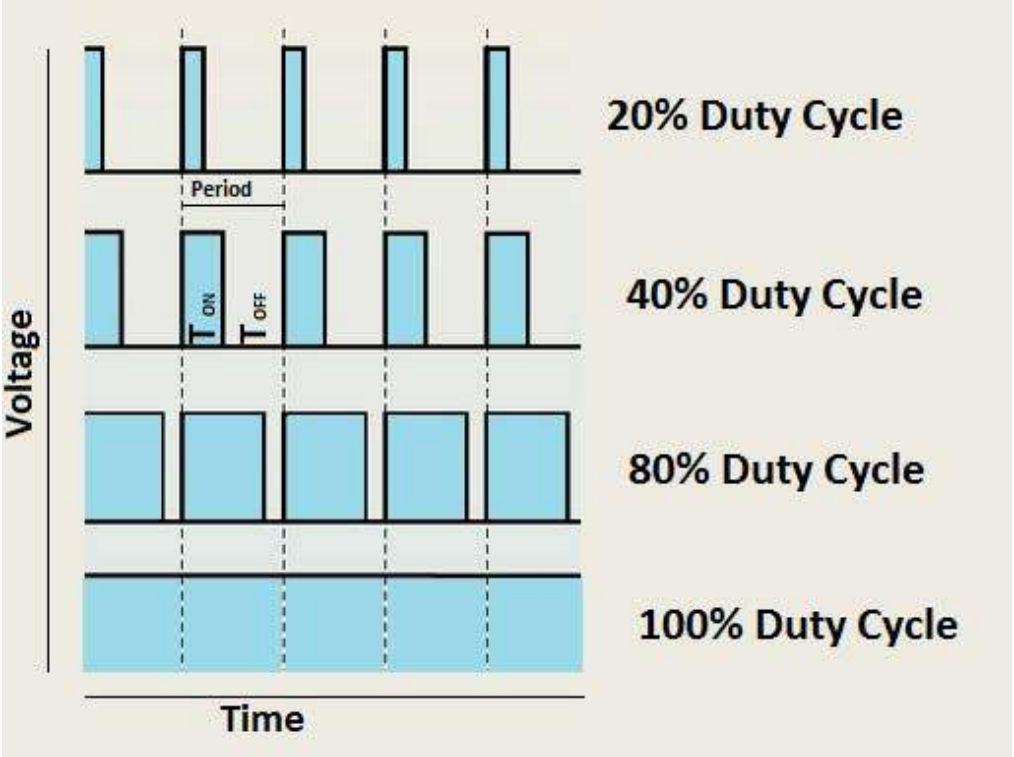

Fig. 3. Example o the PWM signal

The figure above is a graphical representation of a step type PWM signal, and as one can see, 4 actuation variants are represented, modifying the time in which the digital hydraulic switching valve is open and the time in which the digital hydraulic switching valve is closed. The open type, together with the closed type, forms a period. The average between the closing and opening periods of the digital hydraulic switching valve is equal to the flow at the exit of the digital hydraulic switching valve.

3 Electrohydraulic scheme of the system

The software architecture client/server configuration was used; thus, the PLC being configured as a server using the *MODBUS TCP / IP* protocol.
Using the system one can monitor the pressure and flow at the entrance of the hydraulic motor and the digital hydraulic switching valve can be controlled via Modbus TCP IP on the intranet using a specific application and can connect to the internet through a router for remote control and parametrization.
The hydraulic system consists of constant pressure and flow source, digital normally closed digital hydraulic switching valve (DHSV), directional valve normally open (DV), Pressure transducer, hydraulic accumulator, hydraulic motor, flow transducer and tank.
When the hydraulic motor has to start, the directional valve is actuated which closes the circuit to the tank and starts operating the digital hydraulic switching valve, so that the flow supplied by the pump is no longer directed to the tank, but enters the system through the digital hydraulic switching valve. The hydraulic accumulator is placed in this system to attenuate the flow pulses produced by the digital hydraulic switching valve. The pressure and flow transducer record the flow and pressure values and send them to the PLC to be displayed in the software application.

The developed client applications are: test signal generator, the parameterization and control application of the digital hydraulic switching valve and motor and the monitoring and data management application.
The control and monitoring scheme of the digital hydraulic switching valve is presented in fig. 4.

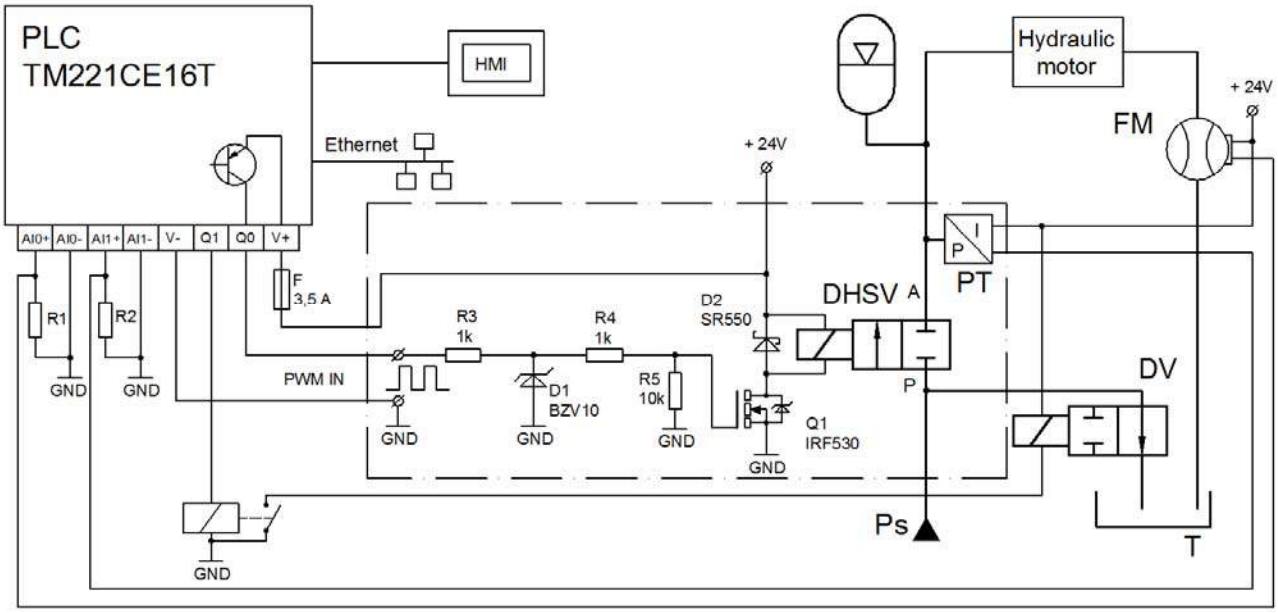

Fig. 4. Switching valve monitoring and control diagram using the PLC

The diagram contains a Mosfet transistor as a driver for the valve solenoid and the connection of the flow and pressure transducer signals to the analog inputs of the PLC. The pressure transducer is positioned before entering the hydraulic motor, and the flow transducer is positioned at the outlet. For the PWM signal control of the digital hydraulic switching valve, the output on transistor Q0 is used. A Human machine interface (HMI) console is used for local monitoring and possible parameterizations. The PLC connection to the network is made through the RJ45 connector located on the front panel of the PLC.

Fig. 5. PLC TM221CE16T from Schneider Electric

The PLC in figure 5 is from the Modicon M221 series, it has 9 discrete inputs where local commands can be connected (buttons, switches), two 0-10V analog inputs where the two pressure and flow transducers are connected, 7 outputs discrete with transistors of which two fast outputs (PWM) where it connects the Digital Hydraulic Switching Valve and Directional valve.

Basically, this PLC in the system is the one that monitors and controls all the process that this system has to perform.
An example of a software application related to the digital intelligent switching system is shown in figure 6. This type of application can be installed on most existing PCs at this time and can work with minimal hardware and software requirements of the operating system on which it is installed.

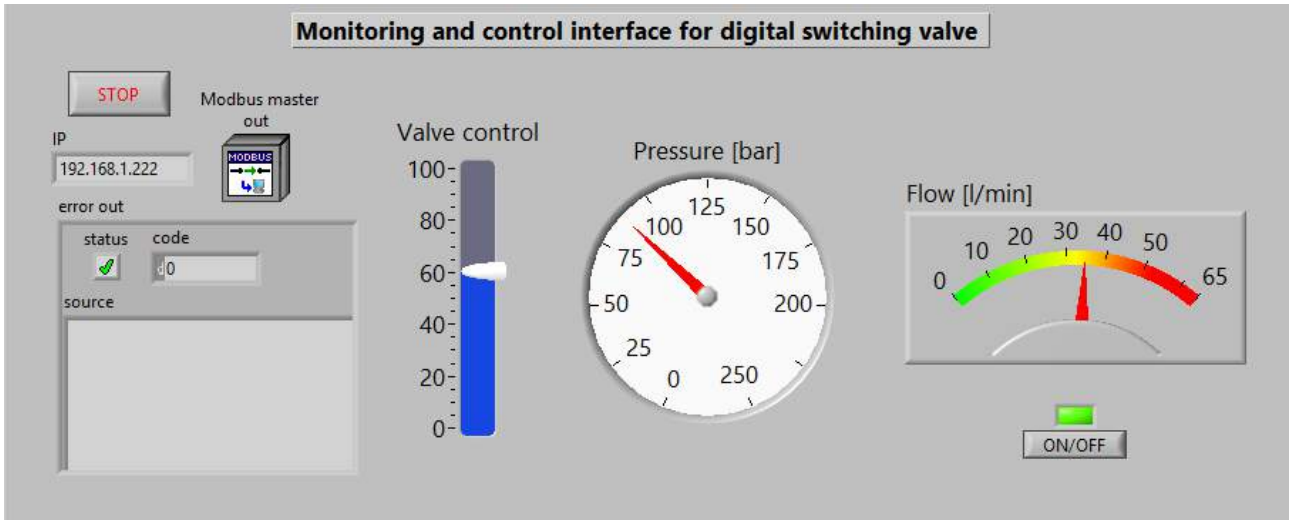

Fig. 6. Software application for intelligent digital switching system.

From the window in fig. 6 of the control software application of the intelligent digital hydraulic switching system, it is possible to monitor the pressure in bars, the flow in liters per minute and the bar (slider) for manual control of the switching valve.
Also, in the application there is the STOP button that closes the application, but also the on/off button which, when activated (the indicator above it is green) activates the manual control bar (valve control) of the digital hydraulic switching valve. When the button is off (the indicator has the LED off) the manual control bar cannot be changed and the system works automatically in the set parameters.

4. Conclusions

The system consisting of a constant pressure and flow source, a digital hydraulic switching valve, a flow transducer, a pressure transducer, a hydraulic accumulator, a hydraulic motor, a PLC for driving the whole process and a software application, becomes an intelligent digital hydraulic system, so that the parameters of the process can be followed remotely and can be modified to optimize the process.
Intelligent systems also bring with them the concept of predictive maintenance, which is very beneficial both for the life of hydraulic components and for the one who exploits the systems.
Intelligent systems are equipment with great prospects for the future and both production technologies and much easier interconnection of more such equipment.
For the system described in this paper, simulations will be made and later an experimental model will be developed on which laboratory tests will be performed, and this will be the subject of a new paper.

Acknowledgments

This paper has been funded by the Romanian Ministry of Research and Innovation under NUCLEU Programme, Financial Agreement no. 18N/2019, Ad 11/2020, Project code PN 19-18.01.01, Phase 17 "Comparative study of energy losses between current hydraulic systems, with classical and proportional equipment, and digital hydraulic systems". European funding has also been granted, under Competitiveness Operational Programme POC 2014-2020, call POC-A1-A.1.1.3-H-2016, Financial agreement no. 253/02.06.2020, signed between INOE 2000 and the Ministry of Education and Research for the project

titled “Horizon 2020 Support Center for European project management and European promotion PREPARE”, MYSMIS2014 code 107874.

References

[1] Drumea, Petrin, Radu Rădoi, Bogdan Tudor, and Ilare Bordeașu. “Digital Hydraulics Solutions.” Paper presented at Hervex 2016 International Conference on Hydraulics and Pneumatics, Baile Govora, Romania, November 9-11, 2016.

[2] Linjama, Matti. “Digital Fluid Power – State of The Art.” Paper presented at the Twelfth Scandinavian International Conference on Fluid Power, Tampere, Finland, May 18-20, 2011.

[3] Scheidl, Rudolf, Helmut Kogler, and Bernd Winkler. “Hydraulic Switching Control – Objectives, Concepts, Challenges and Potential Applications.” Paper presented at Hervex 2012 International Conference on Hydraulics and Pneumatics, Calimanesti-Caciulata, Romania, November 7-9, 2012.

[4] Rădoi, R.I., M. Blejan, I. Ilie, and P. Drumea. *Hydraulic directional control valve with electric control, high frequency switching and low flow rates / Distribuitor hidraulic cu comanda electrica, comutațional de înaltă frecvență și debite mici.* Patent application no. A/00432, 2016.

[5] Drumea, Petrin, Radu Radoi, Bogdan Tudor, Alexandru Hristea, and Ioan Balan. “Normally closed switching valve for high frequency.” Paper presented at Hervex 2016 International Conference on Hydraulics and Pneumatics, Baile Govora, Romania, November 9-11, 2016.

A Critical Review of Piston Motion Noise in Combustion Engines

Dr. **Sunny NARAYAN**[1], Dr. **Aman GUPTA**[2]

[1] Indus University, India, sn2008@rediffmail.com

[2] Indus University, India

Abstract: *Piston skirt contact is caused as the force in connecting rod changes its direction resulting in slapping noise. This is a major source of noise and also leads to wear of liners [1]. Major factors that affect piston slap include [1]:*
a) Cylinder Bore Temperature
b) Lubrication Oil Film Thickness
c) Oil Viscosity
d) Engine speed
e) Skirt Profile
f) Skirt Roughness
g) Skirt Waviness
i) Skirt Size
j) Wrist pin offset
k) Piston-Liner gap.
Piston slap takes occurs mainly near top dead center (TDC) positions.
Motion of crankshaft picks up the lubrication oil from sump. This oil is then transported along cylinder bore due to motion of piston skirt, piston rings and gravity. Oil is consumed either inside the combustion chamber or it returns back to sump, or is blown away by residual gases.
This work presents secondary motion of skirt considering tribological facts.

Keywords: *Piston secondary motion, liner system*

1. Introduction

According to Stribeck curve, various lubrication zones may be classified into following three major types: boundary zone, hydrodynamic zone and mixed zone [2]. In the boundary lubrication zone, the asperities in mating parts come into contact, whereas in hydrodynamic zone there is no direct contact and hence the film of lubricant separates mating surfaces. The function of piston rings of skirt assembly is to seal pressure inside the combustion chamber and prevent leakages of oil from crankcase into combustion chamber. Type of lubrication zone changes with variations in operational conditions of engine. As piston reaches towards dead center positions, its speed approaches zero and hence boundary lubrication zone dominates. At mid strokes, where piston speed is at its maximum values, the hydrodynamic zone dominates as seen in figure no 1.

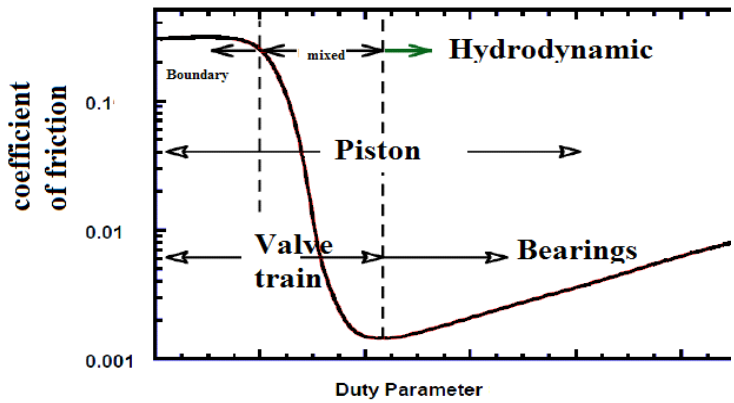

Fig. 1. Stribeck lubrication curve [1]

2. Background

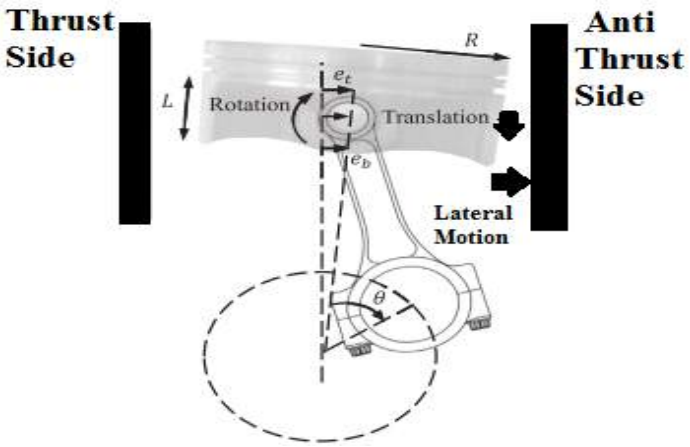

Fig. 2. Piston secondary motion [2]

Increasing demand for noise, vibration and harness comfort levels have led to detailed study of dynamic motion of skirt as skirt-liner contact plays an important role in various frictional losses occurring in engines [2]. Piston dynamics is a key concept to understand lateral motion of skirt as depicted in figure no 2 [3]. Piston may impact either on thrust side (TS) or anti-thrust side (ATS) of liner. These contacting motions cause vibrations in liner which are further transmitted from various surfaces of engine. In general, three major approaches have been identified to locate instances of skirt-liner contact during this motion [3]. First one includes study of piston secondary motion without taking into consideration lubrication effects of oil and rotatory motion of skirt. This approach is known as static method. In second one, piston side force is analyzed by taking into lubrication pressure distribution as represented by Reynolds equations [3].

Oil film thickness is the third parameter to analyze the lateral motion of skirt. Skirt -liner contact may occur if this thickness is minimum which may occur either towards thrust or anti thrust side [4]. As the slope of film thickness changes, the squeezing action is initiated indicating a possible instance of piston slap. Other methods to study slapping motion includes energy transfer method and angular duration method [4]. Instances at which the maximum energy is transferred to liner wall can indicate a possible location of skirt-liner contact [4]. The angular duration method includes study of crank angle duration starting from initiation of squeezing action of oil film and terminating at occurrence of minimum oil thickness [5]. Up to 6-10 instances of actual skirt-liner contacts have been practically observed [5]. In order to validate various possible instances of slap, block vibration data from accelerometers mounted at various locations on engine block has been analyzed [6]. However, this data may include contributions due to other sources of noise such as combustion-based noise [6]. Pruvost has used spectro filters to separate the above-mentioned sources [7]. Liu and Randall used blind source separation (BSS) algorithm to achieve effective source separation [8]. Chen analyzed the concept of pseudo angular acceleration to study phase and frequency variations of slapping noise of skirt [9].

3. Reynolds equation for lubrication oil pressure distribution

The tribology of lubricating oil plays an important role in mechanical losses occurring in assembly of piston. About 3-5% of the total energy losses take place in the piston skirt assembly [10]. Figure no 3 shows a typical breakdown of various losses for a typical diesel engine, wherein it is clear from the figure that share of piston assembly accounts for about 20% -30% [11, 12].

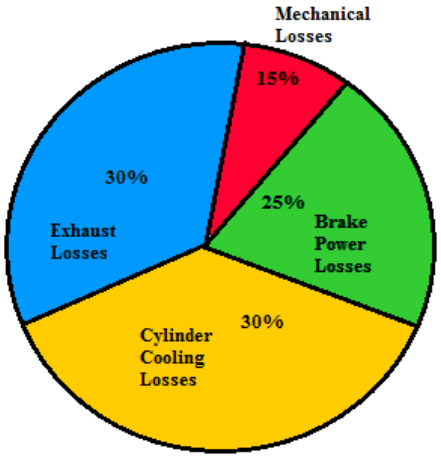

Fig. 3. Break up of total dissipation of fuel energy [10]

In 1886, Osborne Reynolds studied hydrodynamic pressure generated between two sliding surfaces. For an incompressible fluid with constant density, he proposed the Reynolds equation given by [13]:

$$\frac{\delta}{\delta x}\left(\frac{h^3}{12\eta}\frac{\delta P}{\delta x}\right)+\frac{\delta}{\delta z}\left(\frac{h^3}{12\eta}\frac{\delta P}{\delta z}\right)=\frac{1}{2}\frac{\delta(U_2-U_1)h}{\delta x}+(V_2-V_1)+\frac{1}{2}\frac{\delta(W_2-W_1)h}{\delta z} \quad (1)$$

In this relationship, the left-hand side terms are called pressure terms, whereas the right-hand side terms are known as source terms. The terms of $\frac{\delta U}{\delta x}$&$\frac{\delta U}{\delta z}$ depict stretching action, whereas $\frac{\delta h}{\delta x}$,$\frac{\delta h}{\delta z}$ depicts the wedging action. The velocity difference term (V_1 - V_2) is known as squeezing action as shown in figure no 4 [13].

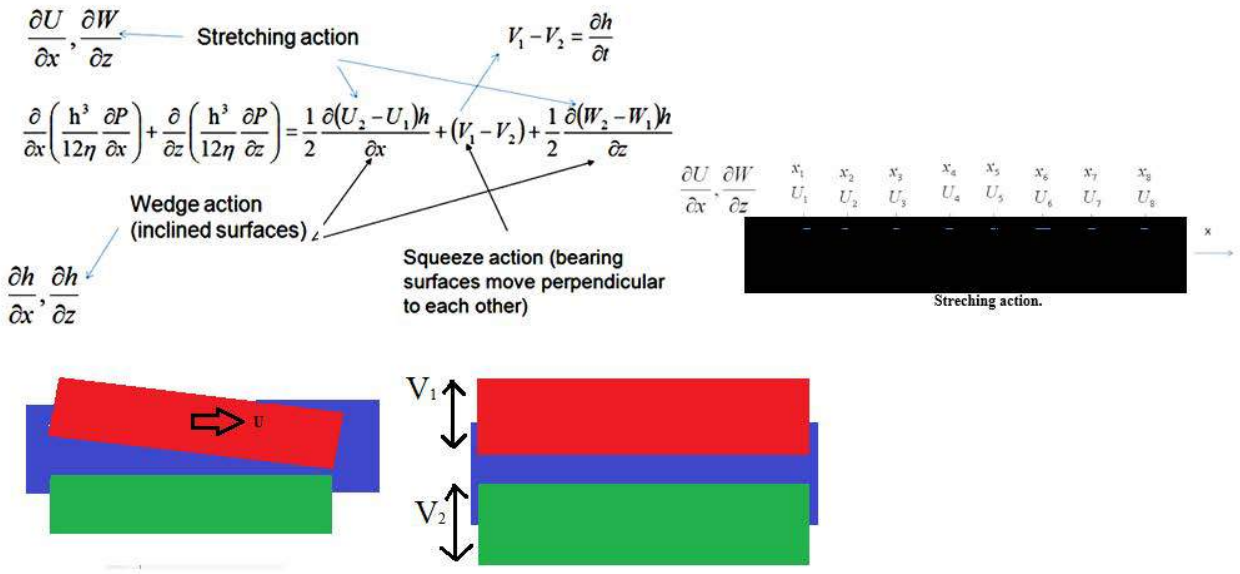

Fig. 4. Interpretation of terms in Reynolds equation [14]

Assuming that the lubrication oil used is a Newtonian fluid, flow is incompressible, value of viscosity is constant and neglecting various effects e.g., inertial forces, slip, angle of inclination, pressure gradient and stretching action, the Reynolds equation may be simplified as:

$$\frac{\delta}{\delta x}\left(h^3\frac{\delta p}{\delta x}\right)+\frac{\delta}{\delta z}\left(h^3\frac{\delta p}{\delta z}\right)=6\eta\frac{\delta(U_2-U_1)h}{\delta x}+12\eta\frac{\delta h}{\delta z} \quad (2)$$

In order to estimate the oil pressure distribution, this equation needs to be solved. One way to do this, is by considering pressure variations in one direction as shown in figure no 5. The piston may be assumed to be as a kind of short bearing and circumferential pressure gradient was neglected as compared to axial one. Using these assumptions, the Reynolds equation discussed above gets modified as:

$$[\frac{\delta}{\delta z}\left(h^3 \frac{\delta p}{\delta z}\right)] = 6\eta \frac{\delta h}{\delta x} \tag{3}$$

Using boundary conditions of P (θ,z= $\pm\frac{L}{2}$) = 0,the closed form of pressure distribution P can be expressed as:

$$P= \frac{-3\eta\omega}{c^2} (x^2 - \frac{L^2}{4}) \frac{\xi \sin\theta}{(1+\xi\, cos\theta)^3} \tag{4}$$

Where c is skirt-liner gap and ξ is skirt-liner eccentricity.
The density of lubricant is dependent on the generated oil pressure (P) and density at mean liner temperature (ρ_0) as expressed from following equation [6]:

$$\rho = \rho_0[1+\frac{0.6\times10^{-9}\times P}{1+1.7\times10^{-9}\times P}] \tag{5}$$

Table no F of presents values of various coefficients for different grades of SAE oils. The oil used for lubrication in present study was of SAE30W grade type for which viscosity may be expressed as [15]:

$$\eta = 0.1531*9.8 * 10^4 * a * e^{\left(\frac{b}{c}\right)} \tag{6}$$

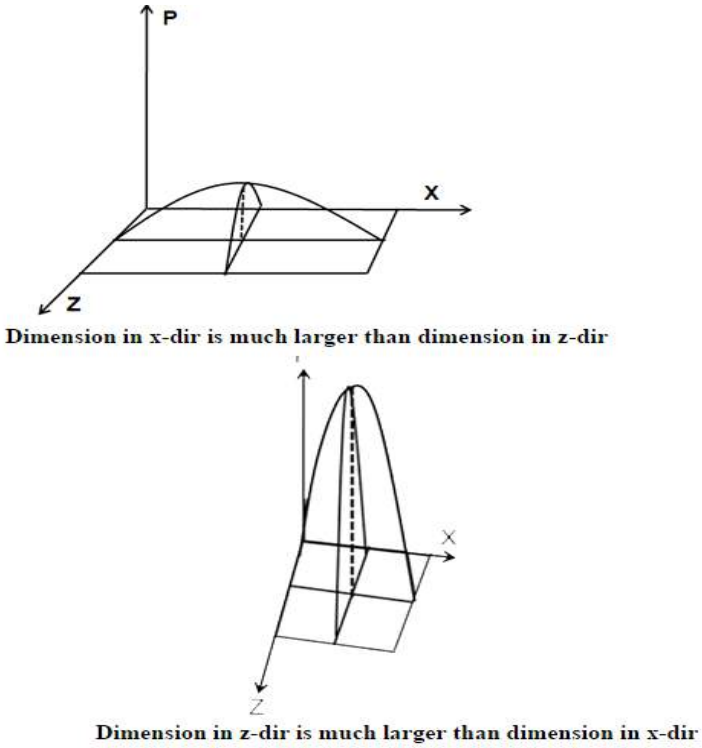

Fig. 5. Variation of pressure along one direction [14]

Since pressure terms have magnitude of order MPa and the oil film thickness are in microns, there may be some inconsistencies while solving the Reynolds equation.

This may be sorted out by considering the Nondimensionalization in which space coordinates may be written as:

$$\left.\begin{aligned} \bar{x} &= \frac{x}{X} \\ \bar{y} &= \frac{y}{Y} \\ \bar{z} &= \frac{z}{Z} \\ \bar{h} &= \frac{h}{C} \\ \bar{p} &= \frac{pC^3}{6\eta UX^2} \\ \bar{t} &= \frac{tU}{C} \end{aligned}\right\} \quad (5.7)$$

Substituting these non-dimensional values, the new equation gets modified as:

$$\frac{\delta}{\delta \bar{x}}\left(\bar{h}^3 \cdot \frac{\delta \bar{p}}{\delta \bar{x}}\right) + \frac{X^2}{Z^2}\frac{\delta}{\delta \bar{z}}\left(\bar{h}^3 \cdot \frac{\delta \bar{p}}{\delta \bar{z}}\right) = \frac{C}{X}\frac{\delta \bar{h}}{\delta \bar{x}} \quad (8)$$

In order to solve this equation, finite element analysis (FEA) method was used for which the mating surfaces were analyzed into number of nodes as shown in figure no 6 [14]. A mesh was made so that nodes on the lubrication zone of skirt correlates with those used in finite element analysis (FEA) in order to analyze the pressure distribution of lubricating oil.

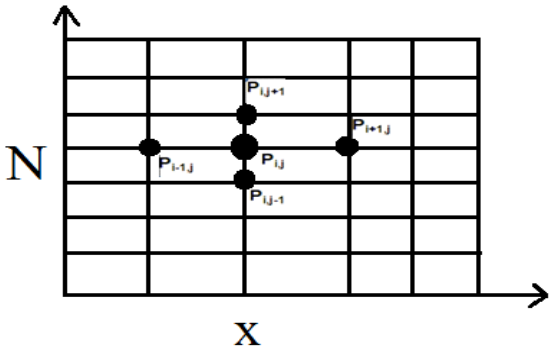

Fig. 6. Nodal representation of surface [14]

Various gradient terms of Reynolds relationship can be solved using Taylors approximation which yields following results [14]:

$$\bar{h}^3 \cdot \frac{\delta \bar{p}}{\delta \bar{x}} = \frac{\bar{h}_{i,j+0.5}^{\ 3}\, \bar{p}_{i,j+1} + \bar{h}_{i,j-0.5}^{\ 3}\, \bar{p}_{i-1,j} - (\bar{h}_{i,j+0.5}^{\ 3} + \bar{h}_{i,j-0.5}^{\ 3})\bar{p}_{i,j}}{\Delta \bar{x}^{-2}} \quad (9)$$

$$\bar{h}^3 \cdot \frac{\delta \bar{p}}{\delta \bar{z}} = \frac{\bar{h}_{i,j+0.5}^{\ 3}\, \bar{p}_{i,j+1} + \bar{h}_{i,j-0.5}^{\ 3}\, \bar{p}_{i-1,j} - (\bar{h}_{i,j+0.5}^{\ 3} + \bar{h}_{i,j-0.5}^{\ 3})\bar{p}_{i,j}}{\Delta \bar{z}^{-2}} \quad (10)$$

$$\frac{\delta \bar{h}}{\delta \bar{x}} = \frac{\bar{h}_{i+1,j} - \bar{h}_{i-1,j}}{2\,\Delta \bar{x}} \quad (11)$$

Substituting these relationships and rearranging them we have:

$$P_{i,j} = A_{i,j}\, P_{i,j+1} + B_{i,j}\, P_{i,j-1} + C_{i,j}\, P_{i+1,j} + D_{i,j}\, p_{i-1,j} + E_{i,j} \quad (12)$$

Most of values of nodal pressure ($P_{i,j}$) are unknown so an iterative loop must be used with suitable convergence limits (£) to get values of pressure. i.e.

$$\frac{(\sum_{i=1}^{n}\sum_{j=1}^{m} \bar{p}_{i,j})_{iteration\ k} - (\sum_{i=1}^{n}\sum_{j=1}^{m} \bar{p}_{i,j})_{iteration\ k-1}}{(\sum_{i=1}^{n}\sum_{j=1}^{m} \bar{p}_{i,j})_{iteration\ k}} \leq £ \quad (13)$$

4. Results and discussions

A MATLAB code was used to analyze the lubrication behavior of oil between piston skirt and liner considering its motion of skirt analogous to that of a journal inside the bearing [14].
Plots of oil pressure distribution on the piston skirt plane were next analyzed for each 90° crank angle rotation of skirt in case of a single cylinder of engine for a compete cycle as shown in figure no 7-10. Rotation operating speed of engine was 2000 RPM with nominal skirt-liner gap of 0.05mm.

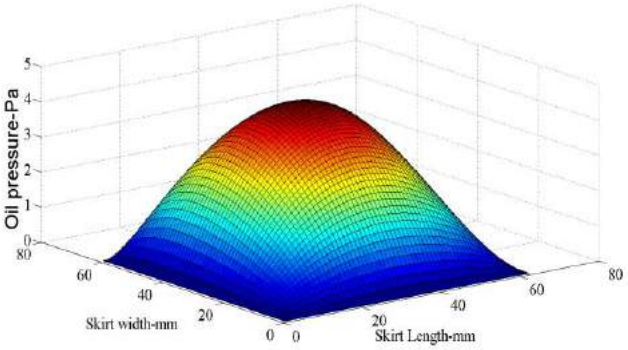

Fig. 7. Oil pressure distribution (180° crank angle)

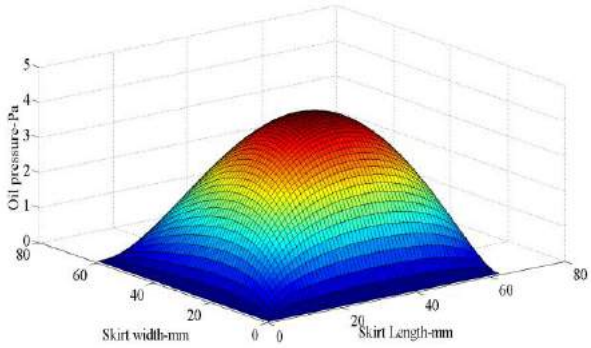

Fig. 8. Oil pressure distribution (360° crank angle)

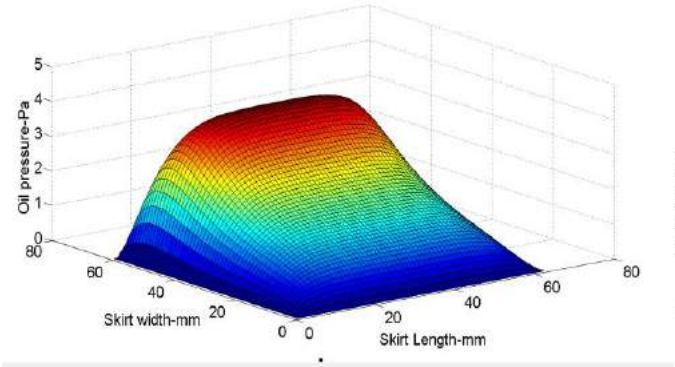

Fig. 9. Oil pressure distribution (540°crank angle)

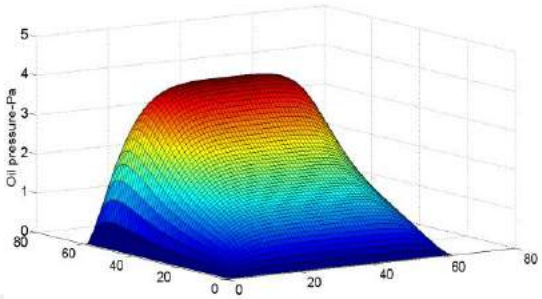

Fig. 10. Oil pressure distribution (720°crank angle)

At 180° crank angle towards the end of intake stroke, peak pressures were observed towards the midpoint of skirt. At 360° crank angle position, as the end of compression stroke approaches, the slopes of pressure curves starts shifting slightly towards right hand side. At 540° crank angle, the peak values of oil pressures were seen to shift towards the bottom part of skirt. During the exhaust stroke peak of slopes shifted slightly towards right side. There is a lag between positions corresponding to peak cylinder pressure developed and peak hydro dynamic oil pressure developed.

The energy transferred to liner due to impacts may be analyzed by taking various grid points on the liner. Energy at each point ($W_{I,J}$) can be calculated using average of local force ($\tilde{F}_{I,J}$) between two time steps as [12]:

$$W_{I,J} = \tilde{F}_{I,J} \left(h_{2I,J} - h_{1I,J}\right) \quad (14)$$

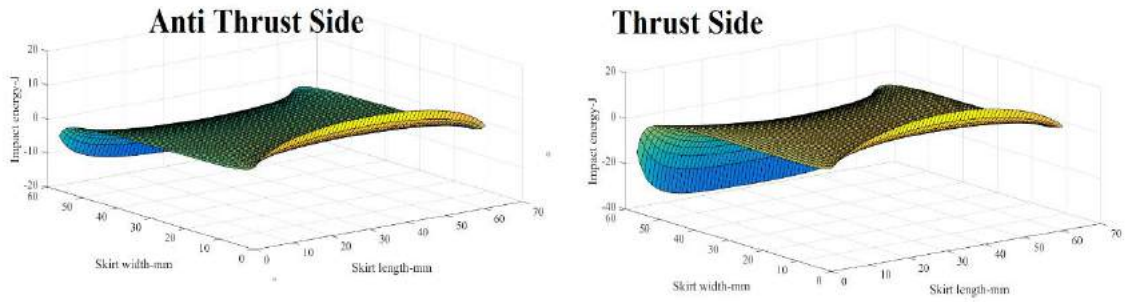

Fig. 11. Impact Energy (720°crank angle)

Figure no 11 shows variations in the impact energy transferred to liner walls at 2000 RPM at 720˚ crank angle position. It is clear that energy is transferred both on thrust as well as anti -thrust sides at the same time. When value of $W_{I,J}$ is positive, lubricant is squeezed and oil film absorbs the impact energy. Otherwise, this energy is utilized in skirt deformation.
The acoustic power available at surface of engine (P_a) may be expressed in terms of radiation efficiency (σ), density of air (ρ_a), wave speed(c_a), area of noise radiating surface (A_r)and surface velocity(v_r) as [3]:

$$P_a = \sigma * \rho_a * c_a * v_r^2 A_r \quad (15)$$

The impact power (P_v) can be expressed in terms of impedance (Z) and impact velocity V_v by the following relationship:

$$P_v = Z V_v^2 \quad (16)$$

Hence overall transmission efficiency (η_t) can be written in terms of these responses and expressed as:

$$\eta_t = \frac{Pa}{Pv} = \frac{\sigma V^2{}_r \rho_a C_a A_r}{Z V_v^2} \quad (17)$$

Using law of conservation of energy, it may be assumed that impacting energy is transmitted without any loss to outer surface of skirt and may be expressed in terms of thickness of structure (h), area (A), velocity (V) and density (ρ). i.e. [12]

$$\frac{1}{2}\rho_v h_v A_v V_v^2 = \frac{1}{2}\rho_R h_R A_R V_R^2 \quad (18)$$

Where subscript v denotes liner structure and R denotes engine block.

Hence the transmission efficiency at each node (i,j) at both thrust and anti -thrust side may be expressed by [12]:

$$\eta_t(i,j) = \frac{\sigma \rho_v \rho_a h_V C_a A_v(i,j)}{Z_{i,j} \rho_R h_R} \quad (19)$$

Where $Z(i,j) = \frac{F_v(i,j)}{V_v(i,j)}$

The SPL at each node can be estimated taking reference pressure level P_{ref} ($2*10^{-6}$ Pa) and expressed in terms of distance of microphone from engine block (R) as [12-20]:

$$SPL_{i,j} = L_{i,j} + 10\log\left(\frac{S^-}{4\pi R^2}\right) \quad (20)$$

Where $L_{i,j} = 10\log\left(\frac{P_a\, i,j}{P_{ref}}\right)$

10. Conclusions

Piston slapping motion is a major cause of noise and vibrations in engines. The dynamic equations of piston secondary motion may be solved to see effects of various skirt design issues.

References

[1] Abubakar, S., F.O. Anafi, M.U. Kaisan, S. Narayan, S. Umar, and U.A. Umar. "Comparative analyses of experimental and simulated performance of a mixed-mode solar dryer." *Proceedings of the Institution of Mechanical Engineers, Part C: Journal of Mechanical Engineering Science* 234, no. 7 (2020): 1393 - 1402.

[2] Kaisan, Muhammad Usman, Latifat Ovaiyoza Yusuf, Ibrahim Umar Ibrahim, Shitu Abubakar, and Sunny Narayan. "Effects of Propanol and Camphor Blended with Gasoline Fuel on the Performance and Emissions of a Spark Ignition Engine." *ACS Omega* 5, no. 41 (October 2020): 26454-26462.

[3] Narayan, S. "Wavelet analysis of diesel engine noise." *Journal of Engineering and Applied Sciences*, 8 no. 8 (2013): 255-259.

[4] Mahroogi, Faisal O., and Sunny Narayan. "A recent review of hybrid automotive systems in Gulf Corporation Council region." Proceedings of the Institution of Mechanical Engineers, Part D: Journal of Automobile Engineering 233, no. 14 (March 2019): 3579 -3587.

[5] Narayan, S., S. Milojevic, and V. Gupta. "Combustion monitoring in engines using accelerometer signals." Journal of Vibroengineering 21, no. 6 (2019): 1552 -1563.

[6] Narayan, Sunny, Ali Sulaiman Alsagri, and Vipul Gupta. "The design and analysis of hybrid automotive suspension system." International Journal of Mechanical and Production Engineering Research and Development 9, no. 4 (2019): 637-642.

[7] Kaisan, M.U., S. Abubakar, B. Ashok, Dhinesh Balasubramanian, S. Narayan, Ivan Grujic, and Nadica Stojanovic. "Comparative analyses of biodiesel produced from jatropha and neem seed oil using a gas chromatography–mass spectroscopy technique." *Biofuels* (December 2018): 1-12.

[8] Narayan, Sunny, and Vipul Gupta. "Numerical Analysis of Secondary Motion of Piston Skirt in Engines." *International Journal of Acoustics and Vibration* 23, no. 4 (2018): 1-10.

[9] Mahroogi, Faisal O., S. Narayan, and Vipul Gupta. "Acoustic transfer function in gasoline engines." *International Journal of Vehicle Noise and Vibration* 14, no. 3 (2018): 270 - 280.

[10] Grujic, I., N. Stojanovic, R. Pesic, A. Davinic, and S. Narayan. "Numerical analysis of IC engine operation with high pressure hydrogen injections." *Transactions of FAMENA* 44, no.1 (2020): 55-66.

[11] Narayan, Sunny. "A review of diesel engine acoustics." *FME Transactions* 42, no. 2 (2014): 150-154.

[12] Narayan, S. "Analysis of piston slap motion." *International Journal of Applied Mechanics and Engineering* 20, no. 2 (2015): 445- 450.

[13] Narayan, Sunny. "Modeling of Noise Radiated from Engines." SAE Tech paper 2015-01-0107, 2015. Paper presented at The 11th International Conference on Automotive Engineering (ICAE 11), Bangkok, Thailand, March 30 - April 1, 2015.

[14] Narayan, Sunny. "Effects of various parameters on piston secondary motion." SAE Tech paper 2015-01-0079, 2015. Paper presented at 18th Asia Pacific Automotive Engineering Conference (APAC 18), Melbourne, Victoria, Australia, March 10-11, 2015.

[15] Stojanovic, Nadica, Nouby M. Ghazaly, Ivan Grujic, Jasna Glisovic, and S. Narayan. "Influence of size of ventilated brake disc ribs on air flow velocity." *International Journal of Advanced Science and Technology* 29, no. 1 (2020): 637-647.

[16] Narayan, S. "Analysis of Piston Slap Motion." *International Journal of Applied Mechanics and Engineering* 20, no. 2 (May 2015): 445-450.

[17] Narayan, Sunny. "Piston Slap Noise in engines." *International Journal of Applied Engineering Research* 8, no.14 (2013): 1695-1700.

[18] Narayan, Sunny. "Effect of dwell time on noise radiated from diesel engine." *International Journal of Applied Engineering Research* 8, no.11 (2013): 1339-1347.

[19] Abubakar, S., F. Anafi, M. Kaisan, S. Narayan, S. Umar, and U. Umar. "Comparative analysis of experimental and simulated performance of a mixed mode solar dryer." *Proceedings of institute of mechanical engineers Part C: Journal of Mechanical engineering* 234, no. 7 (2019): 1393-1402.

[20] Kaisan, Muhammad Usman, Shitu Abubakar, Muhammed Mustapha M., and S. Narayan. "Determination of Wear Metals Debris Concentration in Aircraft Engines." *International Journal of Recent Technology and Engineering (IJRTE)* 8, no. 2 (2019): 1289-1292.

FLUIDAS

NATIONAL PROFESSIONAL ASSOCIATION OF HYDRAULICS AND PNEUMATICS IN ROMANIA

fluidas@fluidas.ro